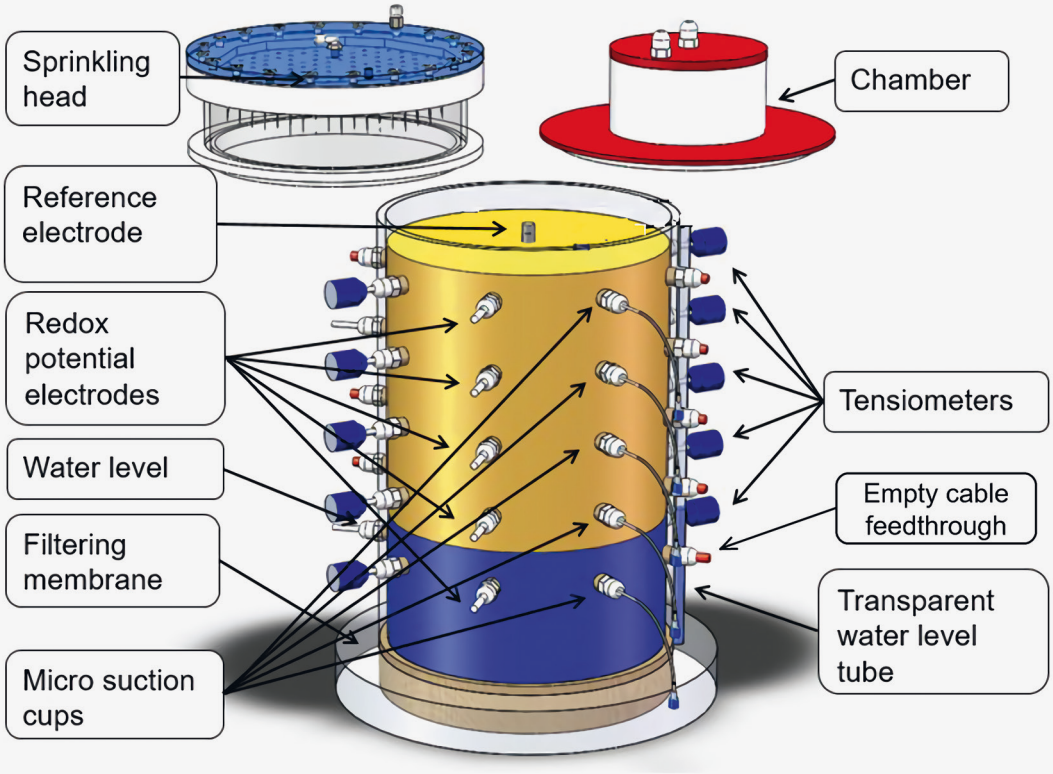

Characterisation of the effect of redox potential on the emission of greenhouse gases using wireless sensing techniques

Jihuan Wang

Energie & Umwelt / Energy & Environment
Band / Volume 554
ISBN 978-3-95806-581-9

Mitglied der Helmholtz-Gemeinschaft

JÜLICH
Forschungszentrum

Schriften des Forschungszentrums Jülich
Reihe Energie & Umwelt / Energy & Environment Band / Volume 554

Forschungszentrum Jülich GmbH
Institut für Bio- und Geowissenschaften
Agrosphäre (IBG-3)

Characterisation of the effect of redox potential on the emission of greenhouse gases using wireless sensing techniques

Jihuan Wang

Schriften des Forschungszentrums Jülich
Reihe Energie & Umwelt / Energy & Environment Band / Volume 554

ISSN 1866-1793 ISBN 978-3-95806-581-9

Bibliografische Information der Deutschen Nationalbibliothek.
Die Deutsche Nationalbibliothek verzeichnet diese Publikation in der
Deutschen Nationalbibliografie; detaillierte Bibliografische Daten
sind im Internet über http://dnb.d-nb.de abrufbar.

Herausgeber und Vertrieb:	Forschungszentrum Jülich GmbH Zentralbibliothek, Verlag 52425 Jülich Tel.: +49 2461 61-5368 Fax: +49 2461 61-6103 zb-publikation@fz-juelich.de www.fz-juelich.de/zb
Umschlaggestaltung:	Grafische Medien, Forschungszentrum Jülich GmbH
Druck:	Grafische Medien, Forschungszentrum Jülich GmbH
Copyright:	Forschungszentrum Jülich 2021

Schriften des Forschungszentrums Jülich
Reihe Energie & Umwelt / Energy & Environment, Band / Volume 554

D 5 (Diss. Bonn, Univ., 2021)

ISSN 1866-1793
ISBN 978-3-95806-581-9

Vollständig frei verfügbar über das Publikationsportal des Forschungszentrums Jülich (JuSER)
unter www.fz-juelich.de/zb/openaccess.

Table of contents

Acknowledgments

First, I want to express my thanks to all of the people around for they gave me lots of help; without them, the preparation of this thesis would not be finished. At foremost, I want to thank my supervisor Prof. Nicolas Brüggermann for all the support in the past years for his guidance, excellent ideas, and constructive criticism. Besides, constructive discussions during experiments help me to overcome the difficulties and stay focus. I also appreciate Heye Bogena, my second supervisor, and the first examiner who give me opportunities to research the TERENO project. In IBG-3, he taught me the knowledge about hydrology in the soil; give me helpful suggestions during the experiment. When my experiments were frustrated, I got support from them, and then I can have the possibility to finish the papers in the Ph.D.

I am also thankful to Harry Vereecken, the director of the Agrosphere Institute, for the half-yearly discussion, the seminar, and give me many suggestions. Many thanks extend to the Chinese Scholarship Council for the supported project on the finance that gives me that funding me to finish my work. Besides, the TERENO project financed by the Helmholtz Association of German Research Centers. For helping me in the setup of the lysimeter experiments, field sensors installation, and technical support, I would like to thank Ansgar Weuthen and Bernd Schilling. I am sincerely grateful to Franz Leistner and Holger Wissel for their help on the gas and chemical analysis. Moreover, I would want to thank Thomas Süß for the help in the FTIR system maintain in for the field experiment for half a year. A special thanks to Zhen Zhou and Cheng Sheng for the good lunching time in Jülich, and want to thank Qunce Shao and Yu Liu for their support. Last but not least, I would like to thank my family and all my friends, for their strong support in my research work and never questioned my decisions regardless of the physical distance.

Abstract

Soils act as both a source and sink of greenhouse gases (GHGs) and are widely considered to contribute to global warming. Soil N_2O emissions originate from microbial nitrification and denitrification processes. Reducing conditions in soils alter the biogeochemical processes and result in large emissions of N_2O and CH_4. Soil redox potential (Eh) measurements are a promising way to differentiate the major source mechanism in soil N_2O production and evaluate their functions within the N cycle and may contribute to the development of N_2O emission mitigation strategies.

While soil GHG emissions have been studied in the recent past, the relationship between GHG production and Eh has not been systematically studied in detail. Eh monitoring can improve the assessment of soil chemical potential variations and GHG emissions, especially for CH_4 emissions, which mainly occur when soil is in highly reduced conditions as a result of the soil submerged below the water table (WT) continually, and for N_2O emissions, that have two distinct source processes at different Eh, i.e. nitrification at high Eh, and denitrification at intermediate Eh values. The change between oxidizing and reducing conditions in soil can be monitored and quantified by soil platinum (Pt) electrodes in combination with a reference electrode and a datalogger system with high temporal resolution (less than 1 min).

The objectives of this thesis were to systematically investigate soil surface GHG emissions and their relationship with the spatial distribution and temporal variation of Eh. Because it is challenging to establish controlled conditions in natural soils, this study is based on a series of step-by-step laboratory experiments, exploring the effects of soil water content, N fertilization, and Eh on GHG emissions, followed by long-term measurements of Eh and GHG emissions in the field.

In laboratory experiments, soil was exposed to varying WT levels to evaluate the utility of Eh monitoring for interpretating soil GHG emissions. To quantify soil GHG emissions, the static chamber method was used, in which gas samples were collected manually and analyzed by gas chromatography (GC). These measurements opened the possibility to interpret the long-term monitoring Eh data and to evaluate their influence on soil GHG emission under controlled soil moisture conditions.

The Eh decreased steadily after the soil was submerged under water. It was found that CO_2 emissions had no clear relationship with Eh variations, but were closely related to soil water potential. In addition, soil Eh variations showed different ranges of values at different depths. N_2O emission peaks occurred at different Eh ranges and were influenced by WT level changes or fertilization events. In order to obtain more accurate information on N_2O emission sources in cropland, we used an irrigation system in combination with the stable isotope labeling technique using a ^{15}N-labeled fertilizer. This isotope tracer method provided better insight into N_2O source partitioning and provided an independent validation of the Eh-based N_2O source partitioning. It was found that the changes in soil Eh and N_2O emissions were induced by irrigation and fertilization events, and were also related to the vertical distribution of dissolved NO_3^- and NH_4^+ in the soil profile. Soil Eh values proved to be a suitable basis for identifying the two dominant N_2O sources, i.e. hydroxylamine oxidation (during nitrification) and nitrite reduction (during denitrification). It can be concluded from the laboratory experiments that measurements of Eh with high spatial and temporal resolution can make an important contribution to the study and interpretation of the temporally and spatially diverse N turnover processes in soils.

As an application of the approach developed and tested in the laboratory to field conditions, we conducted continuous automated monitoring of the soil redox status along a transect in the riparian zone of a deforested Norway spruce forest for over a year. We found that the variability of soil Eh values increased during the transition from dry to wet conditions, while it decreased with soil depth. Most of the changes in soil Eh dynamics could be attributed to fluctuating WT depths. The GHG emissions from the study area were dominated by CO_2 and were mainly controlled by soil temperature and soil humidity. Only few N_2O emission events were observed, mainly at mid-slope position, and originated from both nitrification and denitrification. CH_4 emission was only observed at the position closest to the stream after the soil reached extremely reducing conditions (Eh < -150 mV). It could also be concluded from the field measurements that simultaneous monitoring of Eh and GHG emissions improves the understanding of soil biogeochemical processes and captures their dynamic variations in riparian zones.

Overall, soil Eh monitoring with redox electrodes improved our understanding of the temporal and spatial distribution of oxidizing and reducing conditions within the soil profile and at different locations in the riparian ecosystem. In addition, continuous measurement of Eh variations has increased our understanding of soil biogeochemical process control of soil GHG production in soils and proved to be a valuable method for N_2O source partitioning. This work also suggests that Eh measurements could help improve the understanding of inorganic N turnover in soil. Therefore, we recommend the installation of redox sensors as standard components in long-term monitoring programs in critical zone observatories to assess the effects of climate or environmental changes on soil biogeochemical processes and GHG fluxes.

Zusammenfassung

Böden fungieren sowohl als Quelle als auch als Senke für Treibhausgase (THGs) und werden allgemein als Mitverursacher der globalen Erwärmung angesehen. Die N_2O-Emissionen des Bodens stammen aus mikrobiellen Nitrifikations- und Denitrifikationsprozessen. Die Verringerung des Redoxpotentials in Böden verändert die biogeochemischen Prozesse und kann zu hohen N_2O- Emissionen führen. Messungen des Bodenredoxpotentials (Eh) sind auch ein vielversprechender Weg, um den Hauptquellenmechanismus bei der N_2O-Produktion im Boden zu differenzieren und ihre Funktionen innerhalb des N-Zyklus zu bewerten, und können an der Entwicklung von Strategien zur Minderung der N_2O-Emissionen beitragen.
In der jüngeren Vergangenheit sind die Treibhausgasemissionen im Boden untersucht worden, aber der detaillierte Zusammenhang zwischen der Treibhausgasproduktion und Eh wurde noch nicht systematisch untersucht. Das Eh-Monitoring kann die Bewertung der chemischen Potenzialschwankungen des Bodens und der Treibhausgasemissionen verbessern, insbesondere bei CH_4-Emissionen. Der Wechsel zwischen oxidierten und reduzierenden Bedingungen im Boden kann durch Pt-Elektroden in Kombination mit einer Referenzelektrode und einem Datenloggersystem langfristig in hoher zeitlichen Auflösung (weniger als 1 min) erfasst und quantifiziert werden.
Ziel dieser Arbeit war es, die THG-Emissionen aus Böden und die räumlich Verteilung von Eh in Zeitreihen systematisch zu untersuchen. Da es schwierig ist, kontrollierte Bedingungen in natürlichen Böden zu etablieren, basiert diese Studie auf einer Reihe von Laborexperimenten zur Untersuchung der Auswirkungen von Bodensättigungsgrad, N-Düngung und Eh auf die THG-Emissionen sowie einem Experiment im Feldmaßstab.
In den Laborexperimenten befand sich der Boden unter kontrollierten Wasserständen, um den Nutzen der Eh-Messungen für die Interpretation der THG-Emissionen im Boden bei verschiedenen Bodensättigungsgraden zu bewerten. Zusätzlich wurde die statische Kammermethode zur Erfassung der Emissionraten verwendet, wobei Gasproben aus einer luftdichten Kammer entnommen und die Gaskonzentration mittels Gaschromatographie (GC) gemessen wurden und auf deren Basis die THG-Emissionen berechnet werden konnten. In den Experimenten wurden die durch die Veränderungen des Bodenwasserpotentials induzierten Schwankungen der Eh- und Treibhausgasemissionen gemessen. Das langfristige Eh-Monitoring unter kontrollierter Bodenbedingungen erlaubte es, den Einfluss der Redoxbedingungen auf die THG-Emissionen aus dem Boden zu untersuchen. Es wurde festgestellt, dass die CO_2-Emissionen keinen eindeutigen Zusammenhang mit den Eh-Werten zeigten, sondern eng mit den Änderungen des Bodenwasserpotentials zusammenhängen. N_2O-Emissionspeaks traten in verschiedenen Eh-Bereichen auf und wurden durch Wasserstandsänderungen oder Düngungsmaßnahmen hervorgerufen.
In einem weiteren Laborexeriment sollten die Bedingungen, die die N_2O-Emission eines Ackerbodens beeinflussen, besser nachvollzogen werden. Hierzu wurde ein Bewässerungssystem sowie die stabile Isotopentechnik unter Verwendung eines ^{15}N-markierten Düngemittels eingesetzt. Der ^{15}N-Tracer lieferte weitere Einblicke in die Verteilung der N_2O-Quellen. Es wurde festgestellt, dass die Änderungen der Eh- und N_2O-Emissionen des Bodens durch Bewässerungs- oder Düngemaßnahmen hervorgerufen wurden und von der vertikalen Verteilung von gelöstem NO_3^- und NH_4^+ abhingen. Der Versuchsaufbau war eine geeignete Methode zur Bewertung der dominanten N_2O-Quellen, nämlich Hydroxylaminoxidation (während der Nitrifikation) und Nitritreduktion (während der Denitrifikation). Aus den Laborexperimenten

konnte gefolgert werden, dass Messungen von Eh mit hoher räumlicher und zeitlicher Auflösung einen wichtigen Beitrag zur Untersuchung und Interpretation der zeitlich und räumlich vielfältigen N-Umsatzprozesse in Böden leisten können.

Darüber hinaus wurde ein Feldexperiment durchgeführt, bei dem entlang eines Transektes in der Uferzone eines abgeholzten Fichtenwaldes über ein Jahr ein kontinuierliches automatisches Monitoring des Redoxzustandes im Boden durchgeführt wurde. Es wurde festgestellt, dass die Variabilität der Eh-Werte des Bodens mit dem Übergang von trockenen zu feuchten Bedingungen zunahm, wohingegen die Eh-Variabilität mit der Bodentiefe abnahm. Die dynamischen Eh-Änderungen des Bodens konnten größtenteils auf Grundwasserschwankungen zurückgeführt werden. Das dominierende Treibhausgas, das aus diesem Gebiet emittiert wurde, war CO_2 dessen Emission hauptsächlich von der Bodentemperatur und der Bodenfeuchte gesteuert wurde. Es wurden nur wenige N_2O-Emissionsereignisse beobachtet, hauptsächlich in mittlerer Hanglage, und entstammten sowohl aus der Nitrifikation als auch aus der Denitrifikation. CH_4-Emission wurden nur beobachtet, nachdem der Boden extrem reduzierenden Bedingungen ($Eh < -150$ mV) ausgesetzt war.

Das Feldexperiment zeigte, das ein Langzeit-Monitoring von Eh und THG-Emissionen das Verständnis der die THG-Emissionen steuernden biogeochemischen Prozesse im Boden und deren dynamischen Variationen in Uferzonen verbessern kann, z.B. zur Bewertung der Verteilung von N_2O-Quellen in Bodenzonen mit häufiger Bodenfeuchtesättigung. Diese Arbeit legt auch nahe, dass Eh zum besseren Verständnis des anorganischen N-Umsatzes im Boden beitragen könnte. Daher wird die Messung des Redoxpotentials in Böden in langfristigen Monitoringprogrammen in Critical-Zone-Observatorien empfohlen, z.B. zur Bewertung der Auswirkungen von Klima- oder Umweltveränderungen auf biogeochemische Prozesse im Boden und der von ihnen verursachten THG-Emissionen..

List of Figures

List of tables

List of abbreviation

Ag	silver
AgCl	chloride
Ah	humic mineral topsoil horizon
ANOVA	Analysis of variance
BD	soil bulk density
C	carbon
C/N	carbon-to-nitrogen ratio
$CaCl_2$	Calcium chloride
CH_4	methane
CO_2	carbon dioxide
CV	coefficient of variation
e^-	electron
Eh	soil redox potential
Fe^{2+}	ferrous iron
Fe^{3+}	ferric iron
FTIR	Fourier-transform infrared spectroscopy
H^+	proton
H_2O	water
IPCC	Intergovernmental Panel on Climate Change
IRMS	isotope ratio mass spectrometer
LoRa	Long Range Digital Wireless Data Communication Technology
Mn^{2+}	manganese ion
Mn^{III}/Mn^{3+}	manganese (III) ion
Mn^{IV}/Mn^{4+}	manganese (IV) ion
N	nitrogen
N_2	nitrogen gas
N_2O	nitrous oxide
NH_2OH	hydroxylamine
NH_3	ammonia
NH_4^+	ammonium
$(NH_4^+)_2SO_4$	ammonium sulfate
NO	nitric oxide
NO_2^-	nitrite
NO_2	nitrogen dioxide
NO_3^-	nitrate
N_{tot}	total nitrogen

O_2	oxygen gas
pH	power of hydrogen or potential for hydrogen
Pt	Platinum
PVC	polyvinyl Chloride
S	sulfur
SD	standard deviation
SE	standard error
SMP	soil matrix potential
SO_4^{2-}	sulfate ion
SRP	soil redox potential
ST	soil temperature
SWC	soil water content
SWP	soil water potential
TERENO	Terrestrial Environmental Observatories
TOC	total organic carbon
WFPS	water-filled pores space
δ	isotope ratio relative to standard isotope ratio
$\delta^{15}N$	isotopic ration of ^{15}N relative to a standard
$\delta^{15}N^{bulk}$	average $\delta^{15}N$ of N_2O
$\delta^{15}N^{\alpha}$	$\delta^{15}N$ of the central position of N_2O
$\delta^{15}N^{\beta}$	$\delta^{15}N$ of the terminal position of N_2O
$\delta^{18}O$	isotopic ration of ^{18}O relative to a standard

Chapter 1

Introduction

1.1 Greenhouse gas emission

The 2015 Paris agreement proposed that the global temperature increase should be maintained within 2 °C from the pre-industrial level (Rogelj et al., 2016). However, according to the IPCC (IPCC, 2018), the global temperature is expected to rise by 1.5°C above pre-industrial levels between 2030 and 2052. This increase in global temperature is mainly caused by greenhouse gases (GHGs), i.e., carbon dioxide (CO_2), methane (CH_4), nitrous oxide (N_2O) and other climate-relevant trace gases.

The impact of soil emissions should not be underestimated or overlooked in discussions of global temperature increases, as 35% of CO_2, 47% of CH_4, and 53% of N_2O of the annual emissions can be attributed to soil degassing (IPCC, 2007). Although the most common emitted GHG is CO_2, Both CH_4 and N_2O have more potent greenhouse effects. For example, CH_4 and N_2O have an around 23 and 300 times higher infrared absorption potential than CO_2, respectively (Ramaswamy et al., 2001). CH_4 is highly chemically reactive and related to many changes in the chemical composition of the atmosphere (Cicerone and Oremland, 1988). Furthermore, Thompson et al. (2019) found that global N_2O emissions have increased significantly since 2009. They estimated a global emission factor of 2.3 ± 0.6% in N_2O by their inversion-based emissions, and a value which is significantly larger than the IPCC default (1.375%). The temperrature increases resultant from GHG effects will increase soil microbial metabolism and thus in higher GHG emissions, thus propelling a positive feedback loop which exponentially perpetuates greenhouse gas concentration increases (Bond-Lamberty and Thomson, 2010; Butterbach-Bahl and Dannenmann, 2011; Heimann and Reichstein, 2008). Although new agricultural practices (e.g., increasing artificial fertilizer application) satisfied the demands of an ever-increasing population demand, it boosted soil N_2O emissions over the course of the last 100 years (FAO, 2017; Pachauri et al., 2014). Moreover, a large amount of fertilizer applied in the soil caused N to leach into groundwater, and N_2O were present in both water and soil as a consequence (Davidson E.A., 2009). Agriculture accounts for 60% of global anthropogenic N_2O emissions, mainly from organic and mineral nitrogen (N) fertilizers, and the widespread use of legumes as crops or green coverings (Davidson E.A., 2009; IPCC, 2013). De Klein et al. (2006) estimated that 1 kg of the N in N_2O is from the added N-input per 100 kg N fertilizer. To better understand soil GHG emissions processes and reduce GHG emissions, a detailed study of the soil GHG production models for developing mitigation of GHG emissions strategies is required.

1.2 Rationale

1.2.1 The main influence factors of soil GHG emissions

The study of soil GHG emissions is a key step in carbon and nitrogen cycling, and researching these emissions is essential for understanding the carbon cycle in the soil-atmosphere. The main factors

affecting the emission rate of soil GHG emissions include soil temperature, soil moisture, substrate availability, and soil pH (Ludwig et al., 2001). These parameters are affected by soil structure, weather, and topography (Oertel et al., 2016). Land use, land-use change, and management practices will change the steady-state of soil organic C and N in soils (Poeplau and Don, 2013; Sainju et al., 2008). Soil conditions affect the level of soil carbon dioxide emission from the heterotrophic organisms. Soils are CH_4 sinks under aerobic conditions, and thus seasonal or permanently flooded systems are strong CH_4 sources (Dutaur and Verchot, 2007; Fiedler et al., 2005). Under anaerobic conditions, the CH_4 is produced by methanogenesis and consumed in aerobic conditions by methanotrophic microorganisms (Dutaur and Verchot, 2007).

Increased soil temperatures ultimately lead to increased soil microbial metabolism and soil respiration, and CO_2 emissions exponentially increase with temperature (Fang and Moncrieff, 2001). Moreover, the increase of soil microbial metabolism led to a decrease of O_2 concentrations in soil and increase CH_4 and N_2O emissions (Butterbach-Bahl et al., 2013). Soil humidity is the single most important soil parameter which should be considered in control soil GHG emissions (Oertel et al., 2016). Soil water controls the residual oxygen in the soil pores and controls bacterial activities, such as the nitrification of bacteria requiring O_2 for N_2O emissions. Soil with lower water content illustrates that the bulk of N_2O emissions originates from nitrification (Ludwig et al., 2001). CH_4 emissions require strictly anaerobic conditions with high soil humidity (Smith et al, 2003). Lowered water level will increase the surface CO_2 emission and cause low CH_4 emissions due to subsurface CH_4 oxidation (Fielder et al., 2005).

After long dry periods, the birch effect will cause the burst emission of CO_2 after precipitation (Barnard et al., 2020). Subsequent soil distribution, though grain-sized, will influence soil moisture. Soil with fine pores will support high CO_2 emissions (especially sandy soils in warm and dry conditions), and CH_4 and N_2O emissions will increase under anaerobic conditions (Dilustro et al., 2005; Dutaur and Verchot, 2007; Gu et al., 2013). Nutrient availability is essential for soil microbial activities as well as the respiration process. Emissions of CO_2 and CH_4 are positively correlated with the C/N-ratio, but soil N_2O emissions are negatively correlated with the C/N-ratio (Pilegaard et al., 2006; Shi et al., 2014; Weslien et al., 2009). In the reduced soil, the electron donors such as Fe^{3+}, Mn^{4+}, SO_4^{2-} and NO_3^- will limit the CH_4 production in soils under aerobic conditions (Oertel et al., 2016). The application of N fertilizer (NO_3^- or NH_4^+) leads to an increase in soil N_2O emissions as they are the important substrates for the nitrification or denitrification process.

1.2.2 Soil microbial N_2O emission and consumption process

Nitrous oxide is a relatively stable GHG which contributes to atmospheric photochemical reactions, and eventually leads to ozone destruction within the stratosphere (Chapuis-Lardy et al., 2007). The emission of N_2O gases in agricultural or forest soil is the result of several concurrent processes. Most soil N_2O emissions are related to the biological processes of nitrification (i.e., during NH_3 oxidation to nitrate (NO_3^-)) and denitrification (i.e., during NO_3^- reduction to N_2 (Bremner J.M., 1997). Autotrophic aerobic nitrification (by ammonia oxidizing bacteria and nitrite-oxidizing bacteria) and anaerobic denitrification (mediated by denitrifying bacteria) are the primary processes in the N cycle in soils (Signor et al., 2013). Microbial nitrification and the denitrification process in the soil contribute

approximately 70% to the global N_2O budget (Braker and Conrad, 2011). In the nitrification process that starts with NH_3 as a substrate, the N_2O is the byproduct of this process, and N_2O is the intermediate product during this denitrification process (Baggs et al., 2011; Thomson et al. 2012). In general, the nitrification process can be summarized as the following reactions:

$2NH_4^+ + 3O_2 \rightarrow 2NO_2^- + 2H_2O + 4H^+ +$ energy (Nitrosomonas, Comammox) (1.1)

$2NO_2^- + O_2 \rightarrow 2NO_3^-$ + energy (Nitrobacter, Nitrospira, Comammox) (1.2)

OR

$2NH_3+3O_2 \rightarrow 2NO_2^-+2H^++2H_2O$ (1.3)

$NO_2^- + H_2O \rightarrow NO_3^- + 2H^+ + 2e^-$ (1.4)

The denitrification process can be summarized in the following reactions:

$NO_3^- + 2H^+ + 2e^- \rightarrow NO_2^- + H_2O$ (Nitratereductase) (1.5)

$NO_2^- + 2H^+ + e^- \rightarrow NO + H_2O$ (Nitrite reductase) (1.6)

$2NO + 2H^+ + 2e^- \rightarrow N_2O + H_2O$ (Nitric oxide reductase) (1.7)

$N_2O + 2H^+ + 2e^- \rightarrow N_2 + H_2O$ (Nitrous oxide reductase) (1.8)

Although the NH_4^+ and NO_3^- concentrations are important for the nitrification or denitrification reactions, these processes are also governed by other soil characteristics, like the O_2 content, temperature pH, water content, C/N ratio and even microbial diversity (Bremner, 1997; Butterbach-Bahl et al., 2013; Pärn et al., 2018; Signor et al., 2013). The nitrification process is the dominant process for N_2O production when the soil is dry and well-aerated, and, alternatively, denitrification occurs when the soil is in condition featuring limited oxygen levels. It is critical to partition the specific contribution of the different pathways of N_2O production, and the results may provide process-oriented N_2O mitigation practices in soil management.

1.2.3 Soil redox potential

Microbial or chemical reduction-oxidation (redox) involves the transfer of electrons between reactants and products (DeLaune and Reddy, 2005). The tendency of a pair of compounds to accept or donate electrons is defined as the redox potential (Eh) (DeLaune and Reddy, 2005). Different soil microbial community responses to environmental changes will result in changes in both community composition and population, which will subsequently alter soil biochemical processes (Picek et al., 2000; Nygaard and Ejrnæs, 2009). The metabolic activities of suitable microorganisms in the soil are increased and the activities of unsuitable microorganisms are inhibited. Consequently, the different tolerance of microorganisms causes a variety of Eh ranges and are influenced by fluctuations in soil moisture (Fiedler et al., 2007). Therefore, the redox probes can measure the redox state to explain these changes in the long-term process, and these data can analyze the changes in the substrate and microbial functions in space and time (Peralta et al., 2014). For most soil, the production or consumption of the three major greenhouse gases in the oxidation and reduction processes is regulated by interactions between the carbon and the electron acceptors (e.g., O_2, Mn^{4+}, Fe^{3+}, NO_3^-) (Husson, 2013; Li, 2007). The Eh can improve the knowledge of soil biogeochemistry, and Pt-electrodes and a reference cell can be applied to study the soil 'functional' heterogeneity to distinguish the soil microenvironment difference (Fiedler et al., 2007; Wanzek et al., 2018). Gillespie

(1920) was the first to measure Eh by Pt electrodes successfully. The reference cell can provide a defined and constant virtual grounding potential and be stable against the outer electrolyte composition (Fiedler et al., 2007). The Ag/AgCl single-junction reference electrode is a common reference type, and the most common versions consist of a tube with a 4-M solution of KCl saturated with AgCl (Fiedler et al., 2007). Additionally, the oxidation and reduction processes in soils regulate biogeochemical reactions, providing knowledge of soil microenvironments via the presence or absence of oxidants and reductants (DeLaune and Reddy, 2005). The inorganic oxidants, including O_2, NO_3^-, Mn^{4+}, Fe^{3+}, SO_4^-, and CO_2, can serve sequentially as alternative electron acceptors when the Eh decreases from oxic to highly reduced conditions (DeLaune and Reddy, 2005; Ponnamporuma, 1972).

The soil Eh can rapidly change and ranges from -300 to +800 mV in natural environments (DeLaune and Reddy, 2005). Soil Eh conditions can be classified in four different levels: oxidizing (Eh > 400 mV), with O_2 as the predominant electron acceptor in the soil; weakly reducing (400 > Eh > 200 mV), with NO_3^- as main electron acceptor; moderately reducing (200 > Eh > -100 mV), with $Mn^{III,IV}$ and Fe^{III} as electron acceptors; and strongly reducing (Eh < -100 mV), with SO_4^{2-} and CO_2 as the main electron acceptors (DeLaune and Reddy, 2005). Furthermore, soil Eh can be a good indicator to quantify soil aeration or reduction intensity, which governs GHG production (Yu and Patrick, 2003). The change of Eh depends on the intensity of biogeochemical oxidation or reduction activities, and Eh is related to groundwater level and oxygen diffusion (van Bochove et al., 2002), temperature (Husson et al., 2016), soil water content (Karathanasis et al., 2003; Wang et al., 2018) and pH value (Husson et al., 2016; Yu et al., 2013). Due to the coexistence of oxic and anoxic environments, the wetland or the riparian zone is widely considered to be the area that is that features both the production and consumption of CH_4 and N_2O (Reddy et al., 1989; Pfeifer-Meister et al., 2018).

Many researchers have studied the relationship between changes in soil Eh and greenhouse gas emissions (Flessa and Beese, 1995; Hou et al., 2000; Minamikawa and Sakai, 2007; Minick et al., 2016; Rubol et al., 2012; Włodarczyk et al., 2002; Yu et al., 2003; Yu et al., 2006) and found that the soil Eh has the potential for a better understanding of soil GHG emissions. However, the detailed relationship between s oil GHG production and Eh has not been systematically studied in the past.

1.3 State of the art

1.3.1 Measurements of soil Eh and GHG emissions

The Eh measurement is a promising way to better understand the different hydrological controls on biogeochemical processes that govern GHG emissions (Rubol et al., 2012). The lysimeter is an important tool for soil water and matter fluxes, and is normally equipped with sensors to monitor the soil physical and chemical parameters of soil (soil water content, temperature and chemical contents) (Wanzek et al., 2018). Under controlled water conditions, the lysimeters become suitable tools to study the changing water table elevations and associated changes in soil Eh variations in detail in relation to greenhouse gas emission.

Several researchers have already studied soil Eh variations using lysimeters (Yagi et al., 1998; Yaduvanshi et al., 2010); some studied the characterization of Eh and GHG emission using soil columns (Flessa and Beese et al., 1995; Reth et al., 2008), while others focused on nutrient leaching (Rubol et al., 2012). However, they did not study the relationship between Eh and GHG changes systematically and did not do similar field soil measurements afterward. The Eh measurement should have duplicate electrodes in each layer to ensure the Eh value is credible (Fiedler et al., 2007). In the event of high Eh values (> 400 mV) nitrification dominates within the soil (e.g., Masscheleyn et al., 1993), while denitrification takes place in oxygen-deficient environments (200 mV and lower) (Fiedler et al., 2007; Marin et al., 2016). CH_4 emissions typically occur under highly reduced conditions (-150 mV and lower) (Masscheleyn et al., 1993). Therefore, soil Eh measurements from controlled lysimeters to field conditions are a suitable method and increase our understanding of the effects of Eh variations on soil GHG emissions, especially for N_2O and CH_4.

1.3.2 Stable isotope techniques for N_2O source partitioning in soils

The analysis of N_2O isotopocule abundances (the $\delta^{15}N$, $\delta^{18}O$, and ^{15}N site preference) can be applied to identify the main production process of N_2O (Ibraim et al., 2019; Sutka et al., 2006). The isotopic signature of N_2O is the difference of ^{15}N abundance at the central (α) and terminal 15 (β) and the position in the N_2O molecule called SP values ($SP = \delta^{15}N^{\alpha} - \delta^{15}N^{\beta}$) (Heil et al. 2015). Toyoda and Yoshida (2019) found that even if the $\delta^{15}N$ and $\delta^{18}O$ values of the original substrate change, the SP value of N_2O from the same source remains constant. Therefore, SP becomes an effective and sensitive indicator to distinguish different sources of N_2O. The SP (site preference) measurements were conducted in several studies for N_2O sources in the mixed culture systems, and they confirmed the End-map area of different microbial pathways for N_2O production (Sutka et al., 2006; Toyoda at al., 2017; Toyoda at al., 2019; Verhoeven et al., 2019; Wei et al., 2017). The end-member map (SP, $\delta^{15}N$ and $\delta^{18}O$) of ^{15}N of N_2O allows one to differentiate the N_2O production and consumption processes (Heil et al., 2015). Furthermore, after using the ^{15}N labeled ammonium fertilizer, it is possible to quantify the sources of N-N_2O (Guardia et al., 2018; Linzmeier et al., 2001). The combination of ^{15}N-N_2O methods with redox conditions measurements provides a more comprehensive information on the analysis of N_2O sources and the involved N_2O production process.

1.3.3 Soils GHG and Eh measurements in the riparian ecosystem

Riparian zones play a vital role in the C and N sink and regulating the C and N exported from the catchments (Poblador et al., 2017). Because of the large amount of substance and energy exchange in this ecotone area between aquatic and terrestrial ecosystems, the riparian zone has been regarded as a hot point for GHG sources (Gilliam, 1994; Naimanand and Décamps, 1997). Riparian soil biogeochemistry is affected by temperature and water variability. Soil water variations thus influence GHG emissions, and thus the effects of climate change differ in various hydrologic regimes, resulting in a multitude of soil microbial processes (Poblador et al., 2017). Furthermore, riparian hydrology and the water table variations controls the substrate levels and the redox conditions of riparian soils (Jacinthe et al., 2015;

Vidon, 2016). The riparian soil biogeochemistry is affected by temperature and water variability (Jacinthe et al., 2015; Poblador et al., 2017; Vidon, 2016). Finally, these activities will influence the soil microbial processes and GHG emissions. The spatial and temporal shifts in biogeochemical processes with broad Eh ranges include highly reducing conditions and high soil water content also suitable for N_2O emissions by denitrification processes as well as CH_4 emissions (Yu et al., 2001). However, we have limited knowledge of the dynamics of GHG in the riparian zone. Poblador et al. (2017) have studied the CO_2 and N_2O emissions in Mediterranean riparian zones which undergo spatial and temporal shifts. Although Eh measurements were taken, their analysis did not offer a satisfying conclusion regarding the relationship between GHGs and Eh in the soil. Wanzek et al. (2018) have established Eh electrodes array for detailed analysis of the Eh variations in the field scale under different drained conditions. Therefore, Eh electrodes array opened the possibility for detailed analyses of the relationships between GHG emissions and Eh within riparian zones. The recently developed wireless sensor network SoilNetLoRa can help us to collect soil physical properties (e.g., the soil temperature, soil Eh, and soil water content) and upload the data to the server in near real-time (Forschungszentrum Jülich GmbH, Jülich, Germany). The Eh and other relevant soil parameter measurements may help to create a working hypothesis in GHG production and in related areas to aid in better understanding the global GHG budget.

1.4 Objectives and outline of the thesis

This thesis aimed to explore the relationship between soil Eh changes at varying water levels as a result of irrigation and precipitation, soil mineral N dynamics, and N_2O, CO_2 and CH_4 emissions. The experiments described within this thesis utilized instruments ranging from a laboratory lysimeter to an automated Eh and GHG monitoring system (SoilNetLoRa network) at field scale, and were designed to explore the possibility of the relationship between Eh and GHG emissions at different water conditions in homogenous soil. For the laboratory experiments, a vegetation-free soil lysimeter system was used, thereby avoiding competition between microorganisms and plants for mineral N, and ensuring an unambiguous attribution of soil mineral N dynamics and N_2O emission to microbial processes only. Variations of soil Eh value and GHG emissions were measured at different water table heights and moisture conditions. The field experiment was implemented in a small headwater catchment zone to explore and verify the relationships between Eh and GHG emissions in undisturbed soil. This thesis also focused on soil N_2O emission and identification of the related pathways, i.e. nitrification and denitrification, by Eh measurements and with isotope-aided analysis.

The main research questions of this thesis were the following:

1) Do changes in soil Eh induced by water table variations affect GHG emissions?
2) Is it possible to determine the influence of precipitation and N fertilizer application on soil Eh and N_2O emissions?
3) Is it possible to interpret changes in dissolved inorganic N (NH_4^+ and NO_3^-) with changes in soil Eh?

4) Does the application of ^{15}N-labeled fertilizer in combination with Eh measurments help to improve the knowledge of the soil N_2O production pathways?
5) Can the newly developed wireless SoilNetLoRa network capture long-term soil Eh variations in a riparian zone?
6) Is it possible to transfer the findings of the laboratory lysimeter experiment regarding the relationship between GHG emissions and Eh to a natural riparian zone?

Chapter 2

Characterizing redox potential effects on greenhouse gas emission induced by water-level changes

Based on:

Wang, J., H.R. Bogena, H. Vereecken, and N. Brüggemann. (2018) Characterizing redox potential effects on greenhouse gas emissions induced by water-level changes. *Vadose Zone J. 17:170152.*

2.1 Introduction

The greenhouse gases CO_2, CH_4, and N_2O are recognized as the most important contributors to global warming. Large amounts of C and N are stored in the top soil layer (1 m) of the Earth, accounting for about 1500 Pg C (Batjes, 1996; Bruce et al., 1999; Johnson and Henderson, 1995) and an estimated 133 to 140 Pg N (Batjes, 1996; Post et al., 1985). Thus, soil comprises the largest terrestrial C and N pools (Kutsch et al., 2009; Nieder and Benbi, 2008; Schaufler et al., 2010; Schlesinger and Andrews, 2000). According to the Intergovernmental Panel on Climate Change, total GHG emissions in agriculture, forestry, and other land uses (e.g., cropland, grassland, and biomass burning) contribute about 25% of global GHG emissions using 100-yr global warming potential metrics (Pachauri et al., 2014). Furthermore, agricultural N_2O emissions contributed about 60% of total anthropogenic N_2O emissions in 2005 (Reay et al., 2012) and amounted to 4% of global GHG emissions in 2010 (Olivier and Janssens-Maenhout, 2012). Therefore, the study of biogeochemical processes in soils is critical to better understand the controlling factors of soil GHG fluxes and to more effectively reduce soil GHG emissions.

Many studies have investigated GHG emissions from soils under natural conditions (Dalal et al., 2003; Le Mer and Roger, 2001; Martikainen et al., 1993; Moore and Knowles, 1989; Šimůnek and Suarez, 1993; Weihermüller et al., 2009) or under controlled soil temperature and soil moisture conditions (del Prado et al., 2006; Ruser et al., 2006; Schaufler et al., 2010) but usually without measurements of soil redox conditions (Eh). Under field conditions, soil moisture and temperature are covaried or interact, which may complicate the discrimination of the controlling mechanisms of GHG emission (Fang and Moncrieff, 2001).

Although redox potential measurements have shown to be useful to better understand the hydrological control on biogeochemical processes that govern GHG emissions (Rubol et al., 2012), few studies have focused on the effects of soil redox conditions on soil GHG emissions. Flessa and Beese (1995) showed that N_2O emissions increased after application of N in the form of sugar beet residues during low redox potential conditions, and Yu and Patrick (2003) found higher emission rates of N_2O and CH_4 during moderately reducing to reducing conditions for paddy soils. Nitrous oxide can be produced by nitrification at high redox potentials (400 mV) or by denitrification processes in O_2-deficient environments (200 mV and lower), whereas CH_4 emissions typically occur under extended anaerobic conditions (-150 mV and lower) (Masscheleyn et al., 1993). Rezanezhad et al. (2014) performed laboratory column experiments with fluctuating water tables and showed that induced redox potential changes between -100 and 700 mV affected CO_2 emission as well as the distribution of nutrients. The above studies indicated that the different controlling factors of GHG emissions are interrelated in a complex way and that more information on the interplay of O_2 availability, redox potential, and GHG emission is needed to improve the accuracy of GHG emission models (Rubol et al., 2012).

In environmental science, the redox potential is often used as a criterion for the oxidation-reduction status of water bodies, sediments, and soils (Fiedler et al., 2007) that governs the production and consumption of GHG (Yu and Patrick, 2003). For instance, frequent fluctuations of soil water content may favor N_2O production and its emission to the atmosphere because N_2O efflux was found to be greatest at moderately reducing conditions (Smith et al., 2003). In this respect, oxidation is defined as removal of electrons from

a chemical compound, and reduction is defined as the uptake of electrons by a chemical compound (Bhaumik and Clark, 1948; Delaune and Reddy, 2005). A high redox potential favors the oxidation of reduced compounds, whereas a low redox potential promotes reduction of oxidized compounds.

The soil microbial community is highly sensitive to soil aeration conditions. In the case of a sufficient O_2 concentration, the aerobic microorganism populations thrive, whereas the activity of anaerobic microorganisms is suppressed (Porter et al., 2004). The decline of redox potential during conditions of insufficient supply of O_2 is caused by microbial consumption of O_2. This decreasing trend in redox potential indicates that certain populations of microbes continue to utilize the free energy from easily decomposable organic compounds despite the reduced O_2 availability. Because this situation is variable in the soil due to the nonuniform distribution of organic material, the redox potential also shows a high spatial variability (Fiedler et al., 2007; Mansfeldt, 2004).

The main microbial processes controlling the redox status in soils are (i) redox processes in which inorganic substances are used as electron acceptors (O_2, NO_3^-, NO_2^-, NO, N_2O, oxidized Mn compounds, ferric oxides, sulfate, CO_2) and (ii) fermentative processes in which organic molecules are used as electron donors (Delaune and Reddy, 2005). Under O_2 rich conditions, the organic sources are the most important sources for redox reactions (Pezeshki and DeLaune, 2012). The abundance and activity of oxidized and reduced chemical substances cause specific electrochemical potentials that can be measured as a potential difference between an inert indicator electrode and a reference electrode using a voltmeter (Delaune and Reddy, 2005; Farrell et al., 1991; Fiedler et al., 2007; Flessa and Beese, 1995; Mansfeldt, 2004; Wang et al., 1993; Yu et al., 2001). The soil redox potential typically follows quickly the changes in O_2 availability in the soil (Fiedler et al., 2007). In addition, redox potential measurements are relatively inexpensive and easy to maintain and thus are suitable for laboratory as well as field applications for the long-term measurements of redox conditions in soil.

Figure 2.1 shows the interrelation between GHG emissions, N-cycle processes, saturation status, and redox potential. This study aimed for a better understanding of the relationship between soil water content, soil water potential, redox potentials, and the biogeochemical soil processes related to GHG emissions using a set of continuously monitored long-term laboratory column experiments with controlled water levels. The specific objectives of the study were (i) to identify soil Eh characteristics under different soil saturation conditions with in situ redox measurements in laboratory experiments with a lysimeter setup, (ii) to investigate the relationship between redox potential changes and N_2O and CO_2 emissions, and (iii) to discuss the potential of in situ redox measurements for the investigation of the controlling processes of GHG emission.

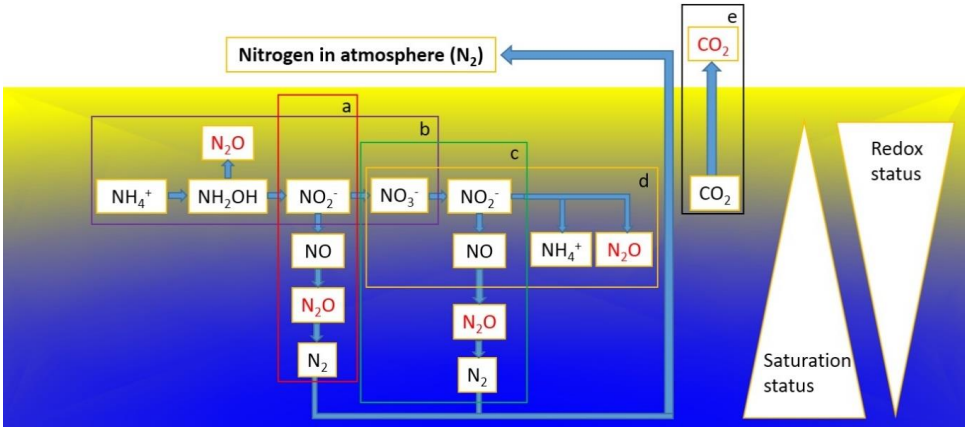

Figure 2.1 Interrelation between greenhouse gas emissions, N-cycle processes, saturation status, and redox status: nitrifier denitrification (a), nitrification (b), denitrification (c), nitrite ammonification (d), and respiration (e).

2.2 Materials and methods

2.2.1 Soil samples

The soil material used for the lysimeter experiments originated from the TERENO agricultural test site Selhausen, which is part of the TERENO observatory Eifel/Lower Rhine Valley (Bogena et al., 2012). The Selhausen site is a 9.6-ha agricultural field located in the lower Rhine valley in western Germany, a heterogeneous rural agricultural area that belongs to the temperate maritime climate zone (Korres et al., 2015). The mean annual temperature and precipitation from 1961 to 2014 were about 10°C and 714 mm, respectively. The main soil type is Haplic Luvisol with a silt loam texture. On 17 January 2016, 30 samples from the Ap horizon (0-30 cm depth) were taken at 15 different points evenly distributed across the field to capture the local soil variability. The soil material was mixed, air dried, sieved to particle sizes < 2 mm, and analyzed for important soil physical and chemical properties in the laboratory. The amount of soil particles > 2 mm was negligible. The main characteristics of the soil material are shown in Table 2.1.

Table 2.1 Main characteristics of the soil material used for the lysimeter experiment (SDW: soil dry weight).

Soil texture		**Main characteristics of soil**	
Clay	17.8%	C_{org} (%)	1.12 ± 0.01
Fine silt	7.5%	N_{total} (%)	0.14 ± 0.01
Middle silt	19.7%	pH	7.3 ± 0.1
Coarse silt	41.2%	NH_4^+ (mg·kg^{-1} SDW †)	46.42 ± 5
Sand	13.8%	NO_3^- (mg·kg^{-1} SDW †)	4.25 ± 0.4

† SDW, soil dry weight

2.2.2 Experimental design

For the experiments on the effect of varying water table depth and fertilization on soil GHG fluxes, a laboratory lysimeter (EcoTech; schematic setup shown in Figure 2.2) was used (height, 50 cm; diameter, 30 cm) as the container for the soil column. The soil column height was ~ 47 cm. The lower boundary of the lysimeter was a porous nylon membrane plate with an air-entry pressure of 0.2 MPa. The lysimeter was carefully filled with ~ 42.7 kg of dried Selhausen soil material. The soil was compacted every 8 cm to achieve a homogenous bulk density corresponding to the bulk density of the soil in the field (1.26 g cm^{-3}). During the experiment, the soil column was partially saturated with tap water, and the water table inside the lysimeter was controlled using a Mariotte bottle and monitored with a transparent tube connected to the line between the Mariotte bottle and the lysimeter (Figure 2.2). The depth of the capillary in the Mariotte bottle defined Weigand et al. (2010). To secure a proper contact between the soil and salt bridge, the hole was filled with slurry from the soil material. The soil water potential was measured at depths of 3, 11, 19, and 35 cm with eight laboratory tensiometers (T5, Meter Group AG).

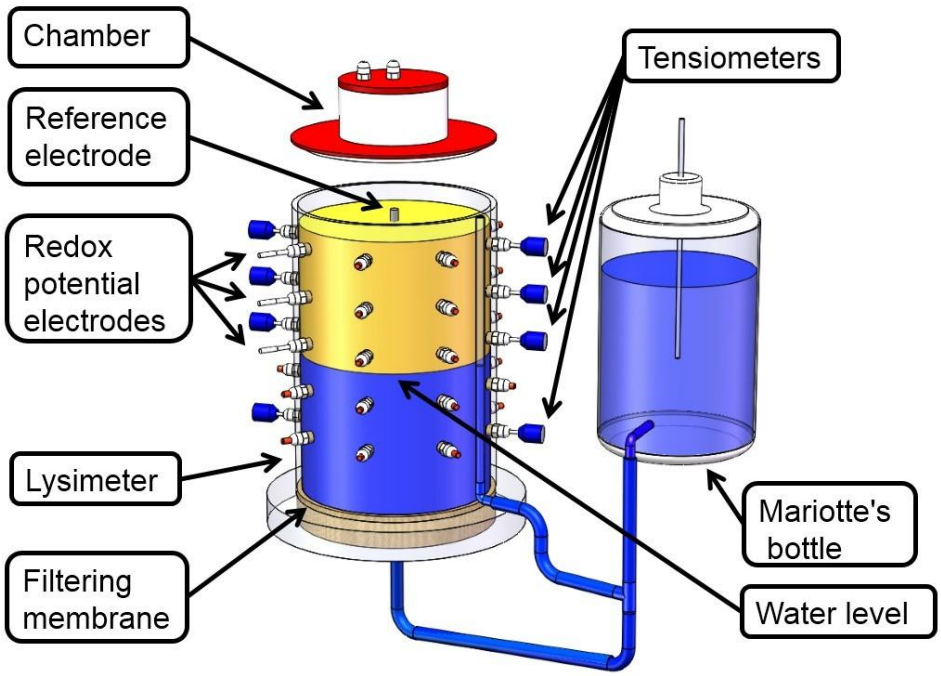

Figure 2.2 Schematic diagram of the lysimeter system used for the experiments. A Mariotte bottle was used to control the water table height in the lysimeter, and the closed chamber method was used to measure the fluxes of greenhouse gases (PT100 sensors are not show).

To check whether the tensiometers provided reliable data, we compared the tensiometer data with the measured water levels (i.e., the positive pressure values should correspond to the water column above the tensiometer). We corrected deviations between the water table and pressure heights by calculating the respective offset values for each tensiometer (Figure 2.3). Stronger deviations occurred after a longer

period of unsaturated soil conditions between Experiments 2 and 3, possibly due to air intrusion into the porous cups of the tensiometers.

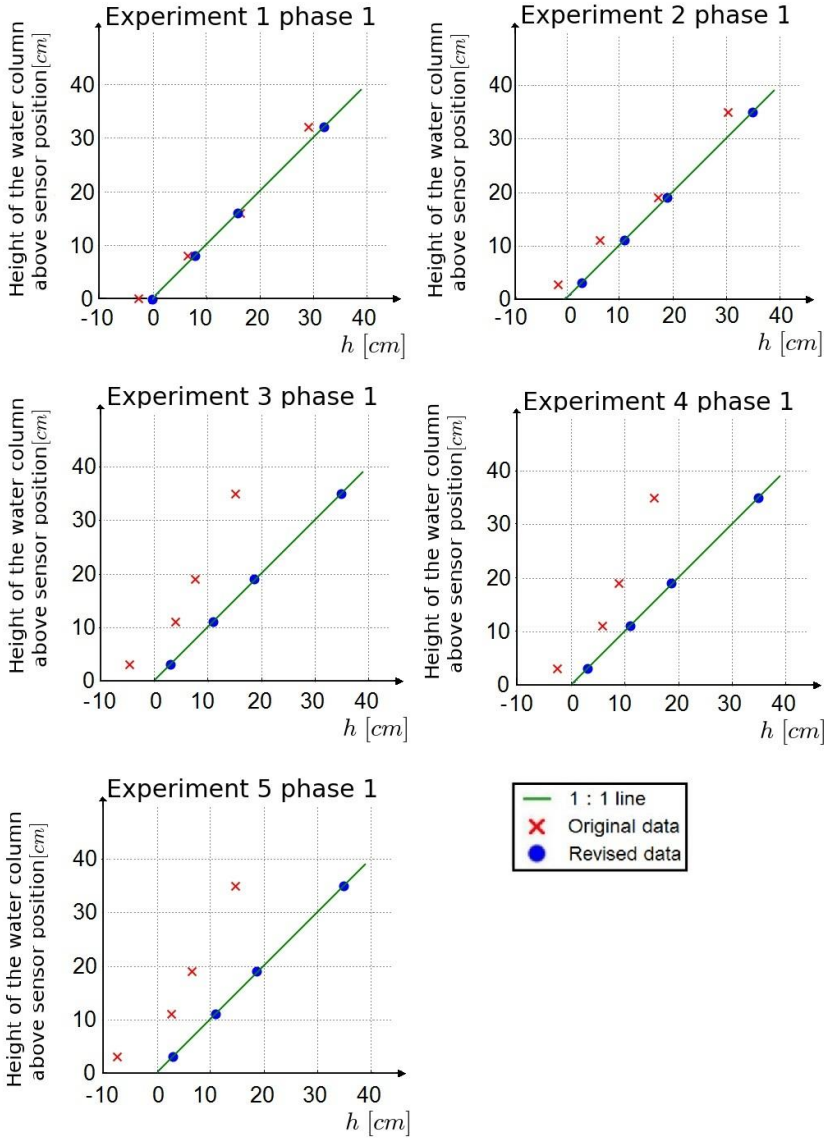

Figure 2.3 Measured water potential (h) vs. the corresponding water depth above the sensor (z) averaged under quasi-equilibrium conditions (after ~3 days) before and after offset correction by taking the mean value of tensiometers at four different depths. Phase 1 indicates the period with the highest water table level.

Two PT100 temperature sensors and two soil moisture sensors were installed at two different depths (SMT100, Truebner GmbH). All measured data were continuously logged every minute with a DataTaker DT 85 datalogger (Thermo Fisher Scientific).

2.2.3 Multistep groundwater level experiments

In our lysimeter experiments, different soil saturation and redox potential states were induced by controlling the groundwater table in the lysimeter by means of the Mariotte bottle as shown in Figure 2.2. In total, five multistep groundwater level experiments were performed at a constant temperature of ~18°C. Before the first experiment, the soil was well drained from 22 May to 3 June. At each step, the water table was kept stable for about 1 week, and gas samples were taken once or twice every day. The five experiments can be divided into two parts (i.e., two experiments before and three experiments after the onset of fertilization). Each experiment took about 1 month, during which time the water table level, soil water potential, and redox potentials were continuously monitored. At the beginning of each experiment, the soil was fully saturated by setting the water table to the level of the soil surface (Figures 2.4a and 2.5a). In the first experiment, the water table did not fully reach the soil surface because of a missing water table level control, which was installed before the second experiment to improve the leveling of the water table (Figure 2.2). Subsequently, the water table was lowered in a multistep fashion in which the water table was kept stable for about 7 days and then decreased by about 8 cm each time. About 2 days after changing the level of the tube in the Mariotte bottle, the water table inside the lysimeter had returned to equilibrium with the pressure level of the Mariotte bottle. The first and the second experiments were performed with original field soil without additional fertilization. After Experiment 2 was complete, the soil in the lysimeter was fertilized with 1.6 g calcium ammonium nitrate (13.5% NO_3^--N, 13.5% NH_4^+-N, corresponding to 60 kg N ha^{-1}) dissolved in 5.2 L of tap water in the Mariotte bottle. We introduced the fertilizer in dissolved form via the Mariotte bottle to achieve a virtually homogeneous distribution throughout the soil column.

At the end of the experiments, ~ 2 g of soil material was sampled from the soil column at depths of 3, 11, 19, 27, and 35 cm. Each soil sample was extracted using 50 mL of 0.1 M $CaCl_2$ solution. The concentrations of NH_4^+ and NO_3^- in the extracted soil solution were analyzed using a Dionex ICS-3000. The air temperature in the experiments ranged from 16.6 to 22.5°C (mean, 18.0°C; SD, 0.9°C) (data not shown). The mean temperature in the soil was 18.0°C at the 11-cm depth (SD, 0.8°C) and 19.0°C at the 35-cm depth (SD, 0.7°C), indicating increasing soil temperature with depth (data not shown). Given these low variations in temperature, we assumed that changes in soil temperature were not a critical factor for CO_2 and N_2O formation and emission in our experiments. We found that the soil CO_2 and N_2O fluxes could be better described with variations in soil water potential and water table depths than with soil temperature changes, which can be explained by the low temperature range of 5.9°C in our experiments (Schaufler et al., 2010).

2.2.4 Greenhouse gas flux measurements

A long (1.5 m) and thin (diameter, 0.2 cm) tube was used to connect the chamber (diameter, 20 cm; height, 18 cm; volume, 5.65 L) with the ambient air as a vent tube to keep the inner air pressure equal to the ambient atmospheric pressure. Gas samples were taken every day throughout most of the experimental periods. Before the air samples were taken, the chamber was connected gas-tight with the soil column to avoid contamination with ambient air.

The gas samples (40 mL each) were taken every 10 min during a 40-min period with a gas-tight syringe. The first sample was taken directly after closing the chamber to determine the GHG concentration of the ambient air (i.e., each flux measurement consisted of five samples). Each sample was transferred to a preevacuated glass vial (22 mL each), creating overpressure, and GHG concentrations were analyzed within 20 days after sampling with a gas chromatograph (Model 8610C, SRI). For flux calculations, a linear regression of the concentration-time correlation for each set of five samples of one gas flux measurement was performed. Parkin and Venterea (2010) provided a thorough discussion of uncertainties in the gas flux calculation. The slope of the respective regression equations was used to calculate CO_2 and N_2O fluxes:

$$F = \frac{b \times V_{Ch} \times MW \times 10^6}{A_{Ch} \times MV_{Corr} \times 10^9} \qquad (2.1)$$

where *F* represents the flux rates of CO_2 (mg C m^{-2} h^{-1}) or N_2O (µg N m^{-2} h^{-1}), respectively, b is the measured increase of CO_2-C or N_2O-N in the chamber (slope of the linear regression) (ppm h^{-1}) or (ppb h^{-1}), MW is the molecular weight of CO_2-C or N_2O-N, A_{Ch} (m^2) and V_{Ch} (m^3) are the base area and the volume of the chamber, respectively, and MV_{Corr} is the pressure and temperature-corrected molar volume of air (m^3 mol^{-1}). MV_{Corr} was calculated using:

$$MV_{Corr} = 0.02241 \times \left(\frac{273.15 + t}{273.15}\right) \times \left(\frac{p_0}{p_1}\right) \qquad (2.2)$$

where t is the air temperature during measurements (℃), p_0 is the standard atmospheric air pressure (Pa), and p_1 is the air pressure during measurements (Pa) (Brümmer et al., 2008; Collier et al., 2014). The mean R^2 values of the linear correlations for the CO_2 and N_2O flux calculations were 0.92 and 0.97, respectively. Flux values were accepted when the R^2 of the linear regression was greater than 0.8, or assumed to be zero when the deviation of the concentration values of the five different time points from the mean of the five samples was smaller than two standard deviations. Negative CO_2 fluxes, which occurred when the initial CO_2 background in the chamber headspace was higher than normal, leading to a CO_2 flux into the soil column, were omitted.

2.2.5 Identification of N_2O source processes

In order to identify the source processes of N_2O in Experiment 5, additional gas samples were taken for the isotopic signature analysis of N_2O ($\delta^{15}N$, $\delta^{18}O$ and ^{15}N site preference, SP). The SP is defined as the difference between $\delta^{15}N^{\alpha}$ (central N) and $\delta^{15}N^{\beta}$ (terminal N) in the asymmetric N_2O molecule. Decock and Six (2013) classified the average SP values (± standard deviation) for N_2O from denitrification and nitrifier denitrification as -1.6‰ ± 3.8 ‰ on the one hand, and as 32.8‰ ± 4.0‰ from ammonia or hydroxylamine oxidation by ammonia-oxidizing bacteria (AOB) and archaea (AOA), fungal denitrification and abiotic hydroxylamine oxidation on the other hand.

Immediately after the end of each GHG measurement in Experiment 5 (i.e. after 40 min closure time) a gas sample of 125 ml was taken from the chamber which was still placed on top of the soil column, and transferred to a 120-ml serum bottle, which had been crimped gas-tight with an aluminum cap and a butyl rubber septum and pre-evacuated before use. Subsequently, $\delta^{15}N_{bulk}$, $\delta^{18}O$ and SP of N_2O were analyzed using an IRMS (IsoPrime 100, Elementar Analysensysteme, Hanau, Germany). For details of the analysis, see Heil et al. (2015). The SP and $\delta^{18}O$ values of N_2O source were calculated according to the binary mixing model of Wei et al. (2017), correcting for the N_2O background of the ambient air:

$$SP_s = \frac{SP_m \times C_m - SP_a \times C_a}{C_m - C_a} \quad (2.3)$$

where SP_s, SP_m and SP_a are the SP values of N_2O from soil, the mixture of N_2O from soil and ambient air in the vial headspace and of N_2O in ambient air, respectively. C_m and C_a are the N_2O concentration in the vial headspace and ambient air, respectively.

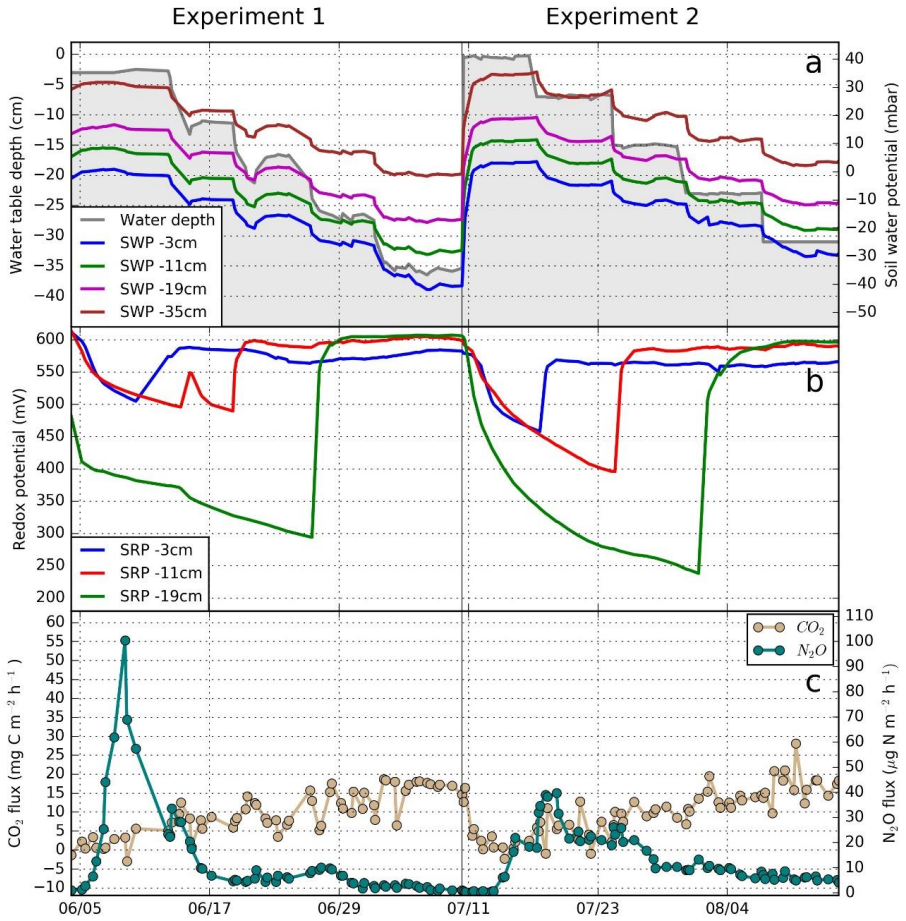

Figure 2.4 Changes in water table, soil water potential (SWP; 1 mbar = 0.1 kPa), soil redox potential (SRP), and CO_2 and N_2O emission rates during Experiments 1 and 2 (before fertilizer application).

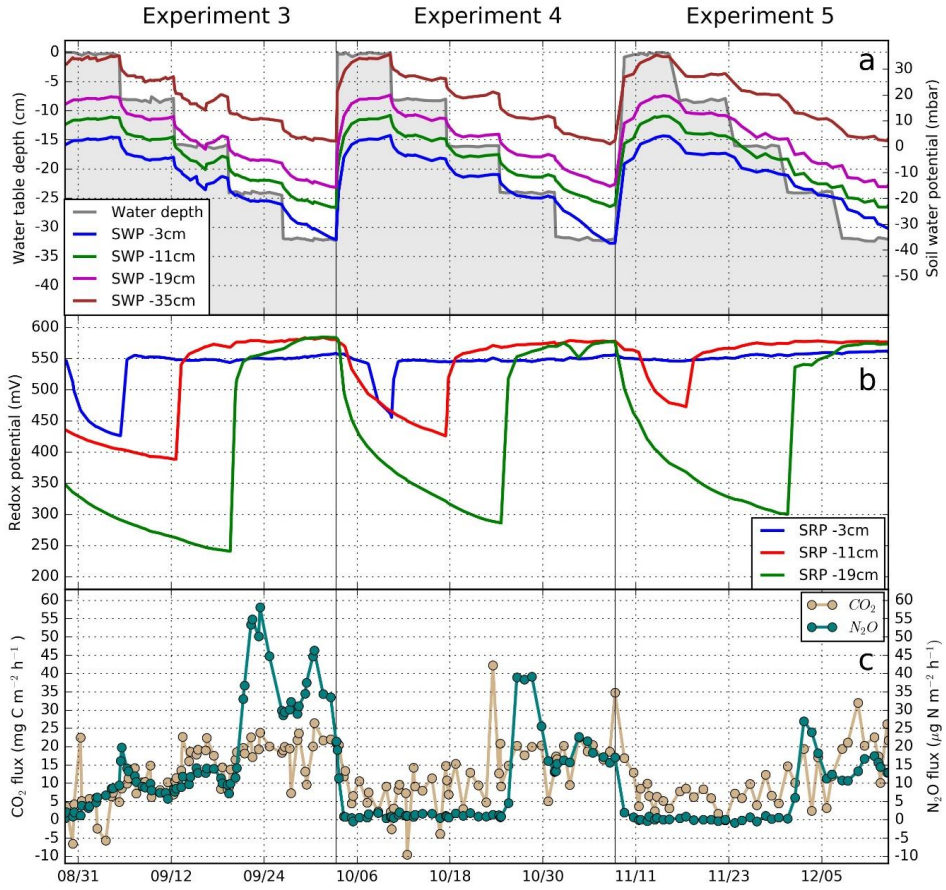

Figure 2.5 Changes in water table, soil water potential (SWP; 1 mbar = 0.1 kPa), soil redox potential (SRP), and CO_2 and N_2O emission rates during Experiments 3, 4, and 5 (after fertilizer application).

2.2.6 Redox potential measurements

The relative proportions of oxidized and reduced substances in the soil determine the redox status of the soil, which can be expressed as redox potential in V or mV by the Nernst equation (Mitsch and Gosselink, 2007):

$$\mathrm{Eh} = \mathrm{E_0} + 2.3\frac{\mathrm{RT}}{\mathrm{nF}}\log_{\mathrm{e}}\frac{\mathrm{A}}{\mathrm{B}} \qquad (2.4)$$

in which *A* and *B* are the concentrations of oxidized and reduced compounds, respectively, E_0 is the standard half-cell potential, *R* is the universal gas constant, *T* is the absolute temperature, *F* is the Faraday constant and n is the number of electrons exchanged. The higher the proportion of oxidized to reduced compounds the higher *Eh*, and vice versa. The redox potential can be measured using a reference electrode (e.g. Ag/AgCl) and a working electrode (e.g. Pt). The redox potential measurements are related to the normal hydrogen electrode using the following equation:

$$\mathrm{Eh} = \mathrm{E} + \mathrm{E_{ref}} \qquad (2.5)$$

in which E is the potential measured against the Ag/AgCl reference electrode, and E_{ref} is the voltage difference between the standard hydrogen reference electrode and the Ag/AgCl reference electrode (210.5 mV at 20°C) (Fiedler et al., 2007).

2.2.7 Statistical analysis

Statistical analyses were conducted with Python package, version 3.6 (Python Software Foundation, 2016), using Pandas and NumPy libraries. Regression analysis was carried out to identify the optimal regression function based on maximum R^2 value for the relationship between the water potential at the respective depth and CO_2 and N_2O emissions before and after fertilization (Table 2.2).

2.3 Results and discussion

2.3.1 Soil redox potential

During each phase of saturated conditions, the redox potential started to decrease in each of the three depths, indicating O_2 consumption by soil microbial activity (Figure 2.4b). However, the redox potential in the upper part of the soil column declined more slowly than the redox potential in the lower part of the lysimeter, where oxygen was more rapidly consumed as indicated by the fast decline in redox potential. The total range of the redox potential differed largely between the three depths (from 450 to 600 mV at -3 cm, and from 250 to 600 mV at -19 cm). During the following three experiments after adding fertilizer to the water reservoir of the Mariotte's bottle, the water table was controlled in the same fashion as in the first two experiments producing very similar responses in soil water potential (Figure 2.4a) and redox potential (Figure 2.4b).

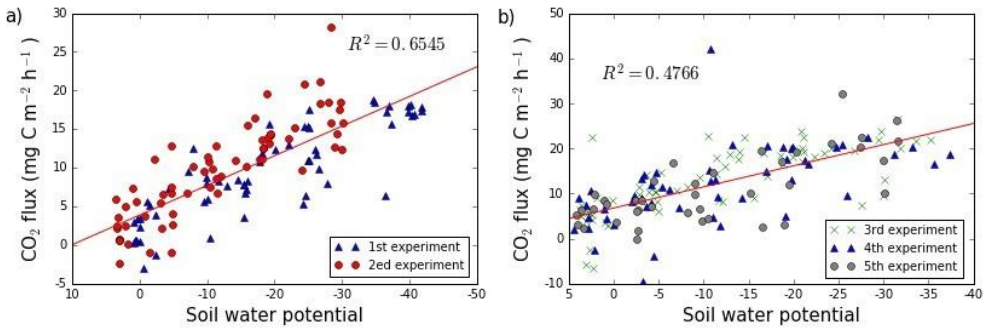

Figure 2.6 Carbon dioxide emissions vs. the soil water potential (in mbar; 1 mbar = 0.1 kPa) measured at 3 cm below the soil surface (a) without and (b) with fertilization application. The corresponding regression equations are given in Table 2.2.

2.3.2 Carbon dioxide emission

The soil water potential measurements (average of two sensors per depth) showed at each level close correlation with water table changes, indicating that soil water drainage was not hindered during the

experiments (Figure 2.4a). Because the water potential changes were virtually identical at the different depths, we compared CO_2 fluxes only with the water potential at 3 cm depth. We found a positive correlation between soil water potential and CO_2 fluxes in both unfertilized soil ($R^2 = 0.65$) and in fertilized soil ($R^2 = 0.47$) (Figure 2.6, Table 2.2). The slope of the linear regression equation of CO_2 emission vs. water potential ranged between -0.42 and -0.36 before the fertilization (Table 2.2). After onset of fertilization the slope increased to values between -0.44 and -0.42. It is also noteworthy that the R^2 was substantially lower for the experiments after onset of fertilization. Also the CO_2 emissions showed a similar response to changes in soil water potential as during the earlier experiments and thus seemed not to be strongly influenced by the fertilization event (Figure 2.5c).

Table 2.2 Functional relationships between soil water potential and CO_2 and N_2O emissions (ψ: soil water potential in mbar; F_{CO_2}: CO_2 emission rate in mg C m^{-2} h^{-1}; F_{N_2O}: N_2O emission rate in µg N m^{-2} h^{-1}).

Experimental phase	Depth	Linear regression			Linear or exponential regression		
		Equation	R^2	P-value	Equation	R^2	P-value
Before fertilization (Exp. 1-2)	3 cm	$F_{CO_2} = -0.3647\psi + 4.481$	0.654	<0.001	$F_{N_2O} = 61.84*e^{0.10*(\psi - 5.55)} + 2.54$	0.464	<0.001
	11 cm	$F_{CO_2} = -0.3878\psi + 7.28$	0.653	<0.001	$F_{N_2O} = 81.84*e^{0.10*(\psi - 16.19)} + 2.28$	0.455	<0.001
	19 cm	$F_{CO_2} = -0.4168\psi + 10.70$	0.666	<0.001	$F_{N_2O} = 87.27*e^{0.07*(\psi - 31.37)} - 0.11$	0.454	<0.001
	35 cm	$F_{CO_2} = -0.4195\psi + 16.99$	0.688	<0.001	$F_{N_2O} = 78.84*e^{0.14*(\psi - 36.45)} + 4.07$	0.500	0.332
After fertilization (Exp. 3-5)	3 cm	$F_{CO_2} = -0.4237\psi + 7.86$	0.468	<0.001	$F_{N_2O} = -0.7614\psi + 2.697$	0.451	<0.001
	11 cm	$F_{CO_2} = -0.4326\psi + 11.19$	0.446	<0.001	$F_{N_2O} = -0.7871\psi + 8.639$	0.442	<0.001
	19 cm	$F_{CO_2} = -0.4366\psi + 14.58$	0.445	<0.001	$F_{N_2O} = -0.7967\psi + 14.82$	0.443	<0.001
	35 cm	$F_{CO_2} = -0.4404\psi + 1.47$	0.438	<0.001	$F_{N_2O} = -0.8087\psi + 27.48$	0.442	<0.001

Under saturated conditions, the CO_2 fluxes were very low, ranging from 3 to 5 mg C m^{-2} h^{-1}. With decreasing water levels, the emission of CO_2 increased gradually, reaching maximum values of 20 to 25 mg C m^{-2} h^{-1} as the water table reached -32 cm (Figure 2.4c). The mean CO_2 emission rates in Experiments 1 to 5 were 223.0, 242.3, 323.9, 298.4 and 263.5 mg CO_2-C m^{-2} d^{-1}, respectively. The variation of water table and soil water potential were primarily responsible for the observed variations in CO_2 emission through their influence on O_2 availability and respiration by soil microorganisms (Hou et al., 2000; Oertel et al., 2016; Sainju et al., 2006; Weihermüller et al., 2009). In addition, as water content decreases, the water-gas interfacial area enlarges due to the increase in soil air content, leading to enhanced gaseous diffusion and exchange with the atmosphere (Oertel, et al., 2016). It is very likely that this effect also contributed to the enhanced CO_2 emission rates during lower saturation conditions in our experiments. Because there were no CO_2 and N_2O emissions determined during the onset of the fertilization event, this period is not shown in Figures 2.4 and 2.5.

2.3.3 Nitrous oxide emission

Before fertilization, an initial peak of N_2O emission of about 100 µg N_2O-N m^{-2} h^{-1} was observed in Experiment 1, a few days after saturation of the soil column. This was followed by a fast decrease (Figure 2.4c), which is consistent with an initial nitrate pool being quickly depleted via denitrification. With each step of lowering the water table in Experiment 1, the N_2O emission rate slightly increased, but then started to decrease again. The highest N_2O emission rate during Experiment 1 went along with the lowest redox potential at 3 cm depth, and was about 2.5 times as high as compared to the highest N_2O emission during Experiment 2 (~100 µg N m^{-2} h^{-1} compared to less than 40 µg N m^{-2} h^{-1}, Figure 2.4c), which might be the result of progressive consumption of nitrogen substrate (nitrate) in the soil (note that in the first two experiments no nitrogen was added). Also in the second experiment the highest N_2O emission rate occurred when the redox potential at 3 cm depth was minimal. Figure 2.4c also reveals a certain time lag of the emission peaks of N_2O after the redox potential changes. The N_2O emission was more strongly affected by the fertilizer treatment (Figure 2.5c). In contrast to the first two experiments before fertilization, where N_2O emissions peaked at decreasing redox potential, N_2O emissions after onset of fertilization occurred immediately after the redox potential at the lowest depth (19 cm) jumped up after the water table decreased below this depth (Figure 2.5a-c). In addition, peak N_2O emission rates decreased from Experiment 3 to Experiment 5 (from ~60 µg N m^{-2} h^{-1} to less than 30 µg N m^{-2} h^{-1}), but were much lower compared to the emission peak in Experiment 1 (~100 µg N m^{-2} h^{-1}). However, the N_2O emission peak in the third experiment (60 µg N m^{-2} h^{-1}) was higher than the peak in Experiment 2 (40 µg N m^{-2} h^{-1}). The mean N_2O emission rates in Experiments 1 to 5 were 341.9, 310.8, 459.8, 224.7 and 137.5 µg N_2O-N m^{-2} d^{-1}, respectively.

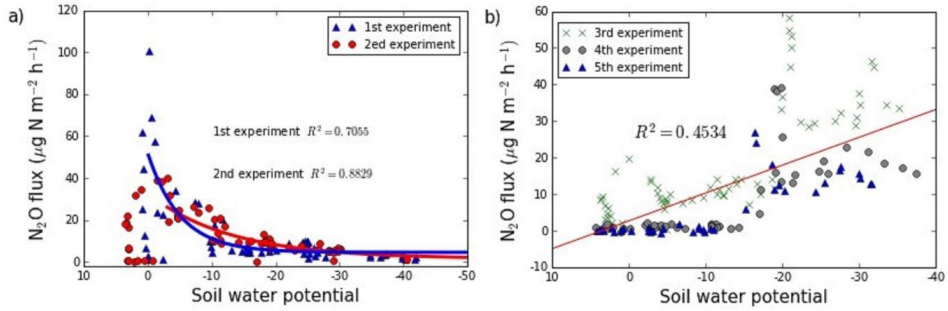

Figure 2.7 Nitrous oxide emissions vs. the soil water potential (in mbar; 1 mbar = 0.1 kPa) measured at 3 cm below the soil surface (a) without and (b) with fertilization application. The corresponding regression equations are given in Table 2.2.

Figure 2.7a shows an exponential relationship between N_2O emissions and water potential changes, where most of the large N_2O emissions occur at lower redox potential (wet conditions) before the onset of fertilization. This effect can be explained by the strong depletion of oxygen in the soil column, promoting anoxic microsites which foster N_2O emissions by denitrification (Flessa and Beese, 1995). In contrast, a positive linear correlation between soil water potential and N_2O production was found after fertilization (Figure 2.7b), which points to nitrification as main source of N_2O at lower water potential, which primarily occurs at higher redox potential. Thus, the determination of the relationship between N_2O emission and soil water potential in different depths could be useful for quantifying the relative contribution of the different source processes of N_2O in the soil, i.e. nitrification and denitrification.

The peak N_2O emissions in Experiments 1 and 2 occurred with a time lag of about 3 days after complete saturation of the soil. Even though this change in water regime restricted the oxygen availability in the soil, there might have been still some residual air stored in the air-filled pore space (Gardner et al., 1999), which might have retarded the onset of denitrification. However, when the soil is waterlogged for a longer time, the N_2O will be reduced to N_2, which also can explain the decrease of N_2O emissions after the N_2O peaks in Experiments 1 and 2. A further explanation for the decrease in N_2O emissions might be the depletion of available substrate, mainly NO_3^-.

Figure 2.8 shows the redox potential in three different depths and the CO_2 emissions before (Figure 2.8a) and after (Figure 2.8b) fertilization. Figure 2.9 shows the redox potential in three different depths and the N_2O emissions before (Figure 2.9a) and after (Figure 2.9b) fertilization. Compared to the fertilized soil, the release of N_2O in unfertilized soil mainly occurred when the soil redox potential was lower. The highest N_2O emission occurred when the redox potential at 19 cm depth ranged between 350 mV and 400 mV, and when the values below 19 cm depth should have been lower than 350 mV. In incubation experiments with paddy soils, Yu et al. (2007) observed a significant N_2O production between 200 and 500 mV and noted that nitrification could have contributed to N_2O production at Eh values above 500 mV at well-aerated conditions (Tokarz and Urban, 2015). Furthermore, Brettar et al. (2002) suggested that an even lower range of redox potentials (between 10 and 300 mV) indicated denitrification in forest soils. Therefore, in our experiments without fertilization (Figure 2.9a) denitrification was most likely the source of N_2O emissions. In contrast, Figure 2.9b indicates that nitrification was the dominant source of N_2O after the soil had been fertilized, although smaller N_2O emission peaks also occurred at lower redox potentials, possibly due to

denitrification.

Figure 2.10 shows the concentration of NO_3^- in the soil had decreased with soil depth at the end of Experiment 5. This may be a result of denitrification that utilized NO_3^- as substrate under anaerobic conditions, as with increasing soil depth saturated conditions lasted much longer. Accordingly, more NO_3^- was consumed in the lower part of soil column, but without detectable N_2O release at the surface, which was very likely due to full N_2O reduction to N_2O under the strictly anaerobic conditions in the lower part of the soil column during most of the experiments. Since the fertilizer solution was added to the soil from the bottom of the lysimeter, and as the mobility of NH_4^+ is relatively low, NH_4^+ accumulated in the lower part of the soil column. In addition, the consumption of NH_4^+ through nitrification under aerobic conditions reduced the NH_4^+ content in the upper part of soil column and led to nitrate concentrations above the level of the original soil.

Nitrous oxide emission from the soil is facilitated via different interrelated processes (Butterbach-Bahl et al., 2013; Lewicka-Szczebak et al., 2017). The interpretation of the relations from the particular isotopic signatures in N_2O can be facilitated by an end-member analysis. End-member maps of ^{15}N site preference (SP) and the $\delta^{18}O$ signatures of N_2O emitted are used to identify the sources of N_2O (Lewicka-Szczebak et al., 2017; Toyoda et al., 2017; Wei et al., 2017). The range of SP and $\delta^{18}O$ values was defined as 27 to 37 ‰ and 40 to 50 ‰, respectively, for nitrification (Sutka et al., 2006), as 34 to 40 ‰ and 30 to 40 ‰, respectively, for fungal denitrification (Sutka et al., 2008; Wu et al., 2017), and as -11 to 1.4 ‰ and 10 to 20 ‰, respectively, for bacterial denitrification (Toyoda et al., 2005; Wei et al., 2017; Zou et al., 2014). The specific SP/$\delta^{18}O$ relationship ranges for the different N_2O production processes are symbolized as square areas in Figure 2.11. From Figure 2.11 it can be concluded that nitrification was the main source of N_2O in Experiment 5, which is consistent with the NO_3^- and NH_4^+ distribution in the soil column shown in Figure 2.9. Different responses of N_2O emissions from the soil at different water table depths before and after fertilization imply that N_2O production was greatly influenced by redox potential and availability of different N substrates. Our results demonstrated that denitrification dominated N_2O emissions in the unfertilized soil, while nitrification was the main source of N_2O production in the fertilized soil. This assumption was supported by the SP values as well as by the redox potential and N substrate distribution in the soil column.

2.3.4 Implications for GHG emission modelling

Modelling GHG emission is essential in order to regionalize local flux measurements and to come up with large scale GHG budgets (Oertel et al., 2016). Several process-based models have been developed to predict the production, transport and spatial distribution of GHG in soil (Li et al., 1994; Šimůnek and Suarez, 1993; Pattey et al., 2007). These models have detailed descriptions of the transport processes, e.g. diffusion in liquid and gas phases, as well as for convection/dispersion in the liquid phase and convection in the gas phase. However, the production of GHG is mostly modelled in a rather simplistic and conceptual way, e.g. use of the Michaelis-Menten equation as a control of CO_2 production (Herbst et al., 2008).

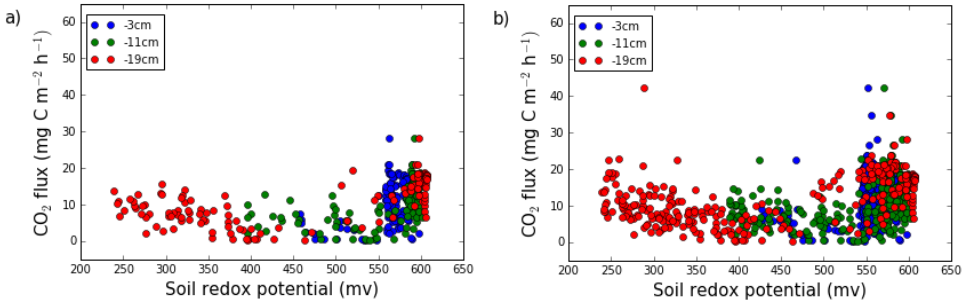

Figure 2.8 Carbon dioxide emissions vs. the soil redox potential measured at 3, 11, and 19 cm below the soil surface (a) before and (b) after fertilization.

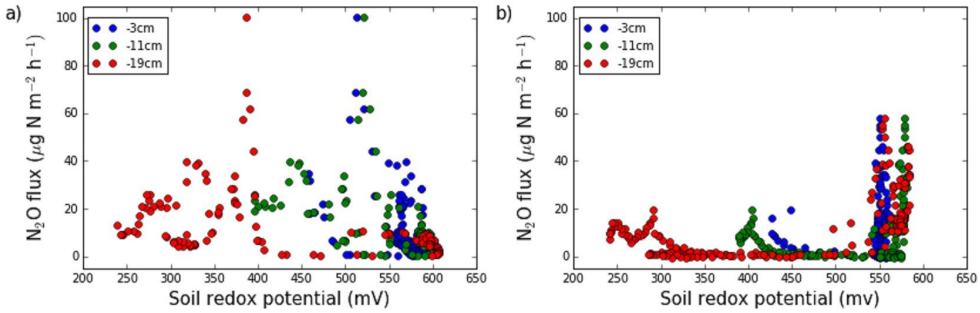

Figure 2.9 Nitrous oxide emissions vs. soil redox potential measured at 3, 11, and 19 cm below the soil surface (a) before and (b) after fertilization.

In fact, the kinetics of GHG production and consumption control to a large extent the spatiotemporal variation of GHG, and the lack of representation of important GHG production processes in emission models reduces the applicability of these models across different ecosystems (Li et al., 2000). For instance, the simulation of redox potential dynamics in the soil is important to accurately simulate N_2O and NO emission rates, as the redox potential actually determines the dominant production process (e.g. nitrification versus denitrification).

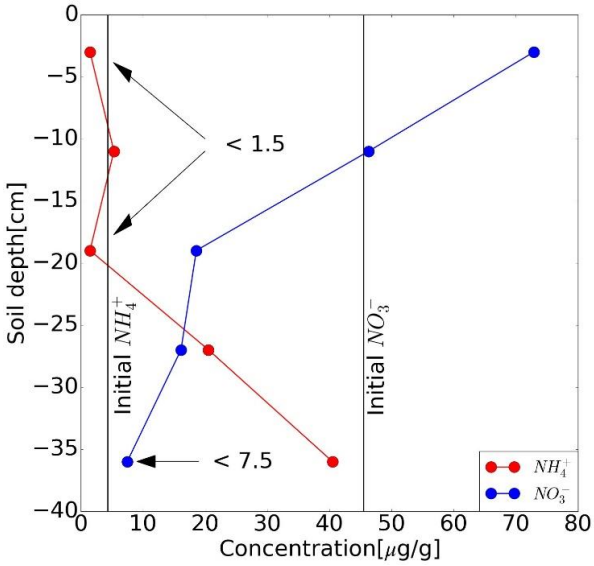

Figure 2.10 Concentrations of NH_4^+ and NO_3^- in the lysimeter at the end of Experiment 5 (<1.5 mg g^{-1} for NH_4^+ and < 7.5 mg g^{-1} for NO_3^- are the detection limits of the ion chromatography system).

However, most of the GHG models (SoilCO_2, CASA, DNDC etc.) use soil water content as an indicator of soil aeration status, whereas our results show that the redox potential is often not well correlated with the saturation status (Figures 2.4 and 2.5), which questions the reliability of this simplified approach. Thus, in our opinion, measurements of redox potential dynamics would be a better constraint for process-based GHG models, especially related to N_2O and NO. In addition, the redox potential enables the discrimination of the dominant GHG production processes and thus enables a more rigorous testing of new model concepts.

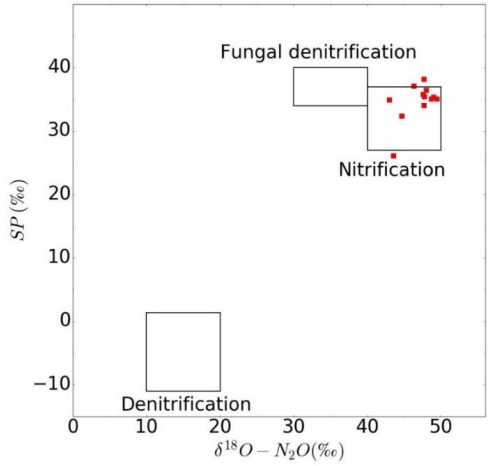

Figure 2.11 End-member maps of N_2O source partitioning for Experiment 5. The squares indicate typical ranges for the different processes of N_2O production (Wei et al., 2017); SP, site preference.

2.4 Conclusions

Overall, our study has tested the relationships between changes in soil water potential, soil redox potential and GHG emissions in laboratory experiments. We were able to show that shifts in soil moisture led to a change in soil redox potential, and those changes in soil redox potential triggered changes in GHG emission flux rates, especially in N_2O emissions. Soil redox potential proved to be an important parameter associated with changes in GHG flux rates, and the N_2O flux rate depended also on the availability of NO_3^- and NH_4^+ in the soil. Highest N_2O fluxes occurred at soil redox potentials between 300 and 550 mV before fertilization (indicating denitrification as main N_2O source process) and above 550 mV after fertilization (indicating nitrification as main N_2O source process). Using an end-member analysis of N_2O isotopic signatures we were able to confirm this interpretation for one of the experiments. However, our study also had its limitations, i.e. in the first place a lack of replication. Furthermore, in our experiment we applied the fertilizer from the bottom of soil column, which does not correspond to the common practice of surface application of fertilizers. As we did the experiments only with one soil so far, the applicability of the regression models might be limited to similar soils. Finally, the relationship between redox potential and N_2O emission was found to be discontinuous, preventing the application of simple statistical models. Finally, in our experiment we applied the fertilizer from the bottom of soil column, which does not correspond to the common practice of surface application of fertilizers. Nevertheless, we could show that redox potential measurements allow for the discrimination of the dominant N_2O production processes, enabling also a more rigorous testing of GHG models.

Chapter 3

Stable-isotope-aided investigation of the effect of redox potential on nitrous oxide emissions as affected by water status and N fertilization

Based on:

Wang, J., H.R. Bogena, H. Vereecken, and N. Brüggemann. (2020) Stable-Isotope-Aided Investigation of the Effect of Redox Potential on Nitrous Oxide Emissions as Affected by Water Status and N Fertilization. Water 12: 2918.

3.1 Introduction

The greenhouse gases (GHG) carbon dioxide (CO_2), nitrous oxide (N_2O), and methane (CH_4) are recognized as the most significant contributors to global warming (IPCC, 2014). Soils comprise the largest terrestrial carbon and nitrogen pools for the emission of CO_2, N_2O and CH_4 (Kutsch et al., 2009; Nieder and Benbi, 2008; Schaufler et al., 2010; Schlesinger and Andrews, 2000). According to Smith et al. (2014) and the IPCC (2007), agricultural activities (such as fertilizer application) contribute around 12% (10 - 14%) to the global anthropogenic GHG emissions, accounting for about 60% of total anthropogenic N_2O emissions (Reay et al., 2012; Smith et al., 2007). Due to its high global warming potential, even small fluxes of N_2O contribute considerably to the total GHG budget (IPCC, 2014). However, due to the relatively low N_2O concentrations and fluxes, as well as the complexity of processes governing N_2O emission from the soil, our ability to model N_2O emissions lags behind that of CO_2 emissions (Butterbach-Bahl et al., 2013).

N_2O emission from soils is influenced by a multitude of factors, such as variations in soil water content and associated redox potentials, as well as soil temperature, land management, and nutrient concentrations (Baggs et al., 2000; Fang and Moncrieff, 2001; Minick et al., 2016; Oertel et al., 2016; Ruser et al., 2006). As these controlling factors are interrelated in a complicated way, more information on the interplay of oxygen availability, redox potential, and N_2O emission is of paramount importance to improve the accuracy of N_2O emission models (Rubol et al., 2012).

The N_2O production is strongly linked to the soil microbial community, which is highly sensitive to soil aeration conditions (Porter et al., 2004). For instance, aerobic microorganism populations thrive under oxic conditions, whereas the activity of anaerobic microorganisms is suppressed (Fierer et al., 2003; Li et al., 2014). Therefore, the redox potential (Eh) is often used as an indicator for the activity of specific microbial populations that control N_2O emission (Flessa and Beese, 1995; Hunting and Kampfraath, 2013; Tokarz and Urban, 2015; Wang et al., 2018).

For instance, Yu and Patrick (2003) found that the highest emission of N_2O occurred during intermediate redox conditions in which Eh ranged between 200 and 400 mV. Other studies found that at high redox potentials (400 mV and higher) N_2O is typically produced by nitrification (e.g., Masscheleyn et al., 1993), while denitrification takes place in oxygen-deficient environments (200 mV and lower) (Fiedler et al., 2007; Marin et al., 2016; Ruser et al., 2006; Yu and Patrick, 2003).

Because of the influence on oxygen availability, soil water content is an essential control factor for N_2O emissions as it influences the ratio of nitrification and denitrification in soils (Cheng et al., 2015; Li and Lang, 2014; Linn and Doran, 1984; Minick et al., 2016; Smith and Tiedje, 1979). However, the interpretation of Eh towards a better understanding of the control factors of N_2O emission is still limited due to the low number of experiments with continuous Eh measurements (Brümmer et al., 2008; Wolf et al., 2010; Yu et al., 2003). Therefore, the suitability of continuous Eh measurements for a better understanding of the N-cycle and N_2O emissions still needs to be better exploited, which may provide valuable information for optimizing land management towards lower N_2O emission rates (Hunting and Geest et al., 2011).

Recent sensor developments open the possibility for combined long-term monitoring of field-scale soil water content and soil Eh changes to increase the understanding of the N_2O emission originated. In a recent

study, Wang et al. (2018) conducted laboratory lysimeter experiments to investigate how changes in Eh induced by the changes in the water level affect N_2O emissions from agricultural soil. They found that soil Eh proved to be an important indicator for N_2O flux rates, as well as the availability of NO_3^- and NH_4^+ in the soil. However, one drawback of this study was that the fertilizer had to be applied from the bottom of the soil column, which does not correspond to the common practice of the surface application of fertilizers. In order better mimic the actual field conditions, we conducted new lysimeter experiments with agricultural soils, in which water and fertilizer were applied to the soil column with a rainfall simulator. The source processes of N_2O and their modification by fertilization, irrigation, or drainage events were characterized by combined Eh measurements and stable isotope analysis. The objectives of this study were: (i) to induce variations in soil water content and Eh by a series of irrigation and drainage experiments (hydrological events) with a laboratory lysimeter; (ii) to investigate the effects of Eh and fertilizer application on N_2O emission rates; and (iii) to determine the dominant processes of N_2O production during the different hydrological events based on stable isotope analysis.

3.2 Materials and methods

3.2.1 Soil characters

For the lysimeter experiments, we used soil material from the agricultural test site Selhausen (50.865° N, 6.447° E, 203 m a.s.l.), which is a part of the TERENO observatory Eifel/Lower Rhine Valley and which represents the heterogeneous agricultural area of that region (Bogena et al., 2018). This site belongs to the temperate maritime climate zone with a mean annual temperature and precipitation of 10.2 °C and 714 mm, respectively (1961-2014). The main crops at our sampling site are winter wheat (*Triticum aestivum*), winter barley (*Hordeum vulgare*), sugar beet (*Betula vulgaris*), and potato (*Solanum tuberosum*). The main soil type is Haplic Luvisol with a silt loam texture (13.8% sand, 68.4% silt, and 17.8% clay), with good drainage and gas permeability (Korres et al., 2015). On February 23, 2018, 60 kg original soil samples from the AP horizon (0 - 30 cm depth) were collected from a wheat field. The air-dried soil was passed through a 2-mm sieve and mixed. The total soil nitrogen content was 0.14%, the organic carbon content was 0.98%, and the pH value was 6.98. Before the soil was filled into the column, the soil was air-dried until the gravimetric water content of the soil was about 7%. An overview of the main characteristics of the soil can be found in Wang et al. (2018).

3.2.2 Soil lysimeter experimental setup

The laboratory soil lysimeter experiments were performed at a constant room temperature of approx. 20 °C using a laboratory lysimeter (EcoTech, Bonn, Germany) with internal diameter of 30 cm and a depth of 50 cm. A schematic diagram of the lysimeter and irrigation setup is shown in Figure 3.1. The opaque lysimeter wall was made of polypropylene and PVC with 0.6 cm wall thickness. The lower boundary of the lysimeter was made of a porous nylon membrane plate with a pore size of 0.45 μm and an air-entry pressure of about

0.2 MPa for flow through. The lysimeter was carefully packed with the soil material to a homogenous bulk density of 1.26 g cm^{-3}.

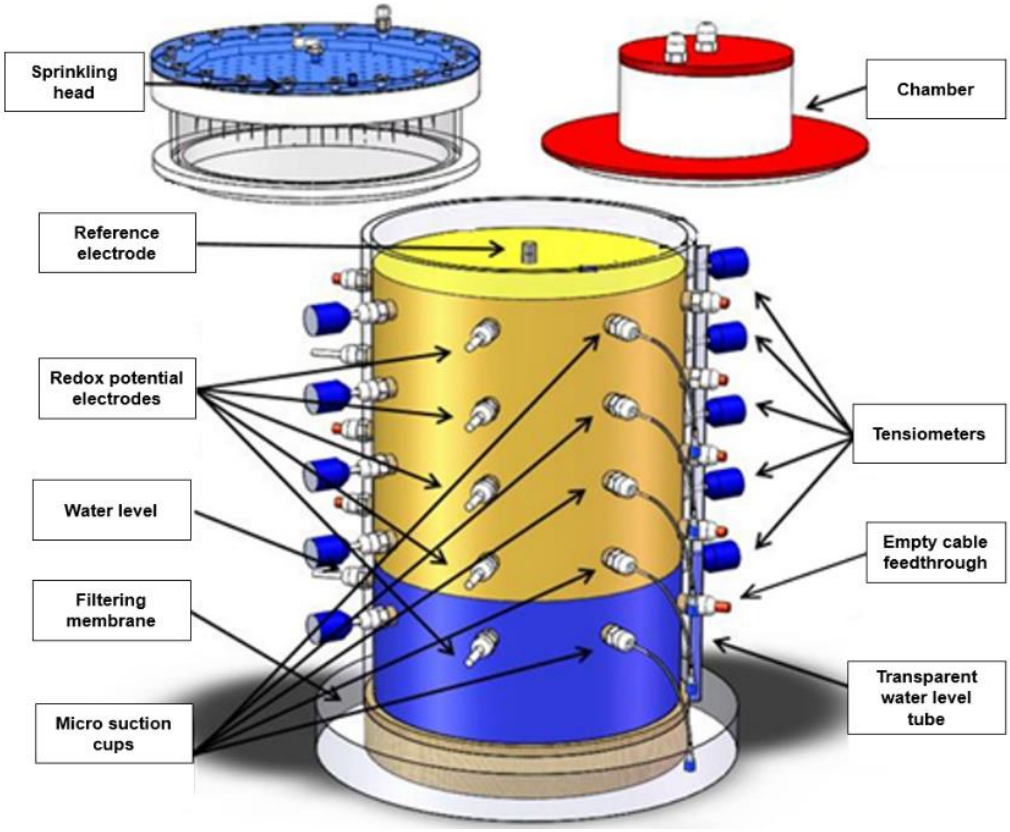

Figure 3.1 Schematic diagram of the lysimeter system (internal diameter: 30 cm, height: 50 cm). A sprinkling system was used to simulate precipitation or fertilization process in the lysimeter, and the closed chamber method was used to measure the fluxes of greenhouse gases (PT100 sensors are not shown).

Precipitation was simulated using a dedicated sprinkling head (EcoTech), which ensured uniform irrigation of the soil surface through 163 geometrically equally distributed capillaries. The static chamber method was used for N_2O emission flux measurements (see detailed description in Section 3.2.4). The redox potential was measured using a set of Pt electrodes and one Ag/AgCl reference electrode (EcoTech). The ten Pt electrodes were installed at five depths (3, 11, 19, 27 and 35 cm below soil surface), and two replicate Pt electrodes were inserted opposite to each other in each layer. The reference electrode was installed vertically from the soil surface and inserted into a 15 cm borehole in the center of the soil column and was then sluiced to optimize soil contact.

Soil water potential was measured with ten laboratory tensiometers (T5, Meter Group AG, Munich, Germany), which were installed at the same depths as the Pt electrodes. A data logger (DT 85, Thermo Fisher Scientific Inc., Melbourne, Australia) was used to collect the sensor data at 15 min resolution. In addition, we installed nylon suction cups (Rhizon samplers, MOM 19.21.21, Rhizosphere Research

Products, Wageningen, The Netherlands) at depths of 3, 11, 19, 27, and 35 cm, respectively, to collect soil pore water for regular analysis of ammonium, nitrate, and dissolved greenhouse gases. The suction cups had a diameter of 2.5 mm and a mean pore size of 0.15 µm. Soil temperature was measured at depths of 11 and 35 cm using PT100 sensors.

The initial soil NO_3^- and NH_4^+ concentrations were determined from soil samples taken at the same five depths at which the soil redox electrodes, the tensiometers, and the microsuction cups had been installed. The determinations took place by extracting 2 g of soil with 50 mL 0.1 M $CaCl_2$ solution and analysis of the extract with Dionex ICS-3000 ion chromatography (Dionex Corp., Sunnyvale, USA).

3.2.3 Experimental procedures

The lysimeter experiment was run continuously for more than 165 days in 2018, in which the lower boundary was controlled either with a constant positive pressure head using a Mariotte's bottle to induce a water table, or by applying a negative pressure using a hose pump to induce drainage flow (see Wang et al., 2018, for more details of the setup). During periods of water saturation, soil pore water was sampled using the suction cups installed at the five different depths and analyzed for NO_3^-, NH_4^+ and N_2O concentration on June 5, June 15, July 7, and August 8.

The entire study consisted of four different experimental phases (see also Table 3.1): First a period without fertilization (called Experiment 1, from March 21 to June 1). Experiment 1 aimed to investigate the relationship between N_2O emissions and Eh in soil during long periods of saturation and the resulting consumption of dissolved N. Then two periods followed, each of which started with a fertilization event (Experiment 2, from June 2 to 29; and Experiment 3, from June 30 to August 3) to investigate the effects of irrigation after fertilization on N_2O emissions. Finally, a post-fertilization period with saturated conditions (Experiment 4, from August 4 to 26) was carried out. The experimental procedures during these four phases are described in detail below. Saturation means the whole soil column was saturated as indicated by the soil water potential (Figures 3.2a, 3.3a, 3.4a, and 3.5a).

Table 3.1 Mean, maximum, and minimum daily soil redox potential values and N_2O fluxes. In addition, the range, standard deviation (SD) and the coefficient of variation (CV) are provided.

	Redox Potential						N_2O
	−3 cm	−11 cm	−19 cm	−27 cm	−35 cm	All	Fluxes (μg N m^{-2} h^{-1})
	Experiment 1: Before fertilization (n = 72)						
Mean	516.2	175.3	376.5	374.7	229.5	334.4	12.1
Max	558.5	597.9	621.1	601.6	598.9	583.0	91.7
Min	291.7	−195.4	85.4	98.6	−141.1	83.6	0.0
Range	266.8	793.3	535.7	503.0	740.0	499.4	91.7
SD	61.2	228.2	196.8	165.0	247.4	164.9	23.3
CV (%)	11.9	130.1	52.3	44.0	107.8	49.3	192.4
	Experiment 2: 1st fertilization (n = 28)						
Mean	570.3	510.5	513.3	531.6	352.2	495.6	137.8
Max	608.1	627.4	634.1	624.4	579.3	608.6	539.4
Min	451.0	214.5	295.8	367.9	99.3	340.2	4.1
Range	157.1	412.9	338.3	256.5	480.0	268.4	535.3
SD	42.6	121.4	99.3	73.4	161.0	87.1	158.5
CV (%)	7.5	23.8	19.3	13.8	45.7	17.6	115.1
	Experiment 3: 2nd fertilization (n = 35)						
Mean	537.7	629.3	611.2	603.6	480.1	572.4	38.4
Max	582.2	634.2	647.6	634.4	585.4	609.8	187.4
Min	475.3	607.2	495.9	514.7	241.9	476.7	0.6
Range	106.9	27.0	151.7	119.7	343.4	133.0	186.8
SD	32.9	5.8	43.9	33.8	109.5	37.5	51.0
CV (%)	6.1	0.9	7.2	5.6	22.8	6.5	131.9
	Experiment 4: Post-fertilization saturation phase (n = 29)						
Mean	574.1	632.0	639.3	622.8	531.3	599.9	50.2
Max	616.5	640.3	658.2	637.8	603.2	631.2	360.2
Min	503.6	565.0	545.6	542.1	260.3	496.3	0.2
Range	112.9	75.3	112.6	95.7	342.9	134.9	360.0
SD	32.6	14.7	27.2	23.7	87.7	33.6	95.2
CV (%)	5.7	2.3	4.3	3.8	16.5	5.6	189.8

n, number of days of the experiment. The period before fertilization lasted from 21 March to 1 June, the 1st fertilization experiment from 2 June to 29 June, the 2nd fertilization experiment from 30 June to 3 August, and the post-fertilization saturation phase from 4 August to 1st September.

On March 21 and 23, the soil was irrigated with 4.2 L of tap water (corresponding to a rainfall event of 60 mm). In the following, the irrigation intensity was reduced to match the decreasing infiltration capacity. From March 29 to April 3, the soil column was irrigated with 2.1 L (30 mm) of water every day, and on April 8, 9, 12, and 21 with 1.05 L (15 mm) of water. Throughout the irrigation activities, we tried to avoid infiltration excess; nevertheless, there was 4-6 h of water ponding on the soil surface following each irrigation event. During three periods (from April 23 to May 11, June 2 to 8, and June 12 to 15) a low amount of water was continuously applied (~2 mm/day) to compensate for the evaporation loss of the soil and thus maintaining an anoxic state in the soil column. Subsequently, drainage was initiated on May 24 and maintained until June 1 by inducing a negative pressure of -1 atm at the lower boundary with the vacuum pump for 2 h per day (Figure 3.2a). On May 30, 2 g of soil material was collected from each of the five depths (3, 11, 19, 27, and 35 cm) to determine the soil NH_4^+ and NO_3^- concentrations.

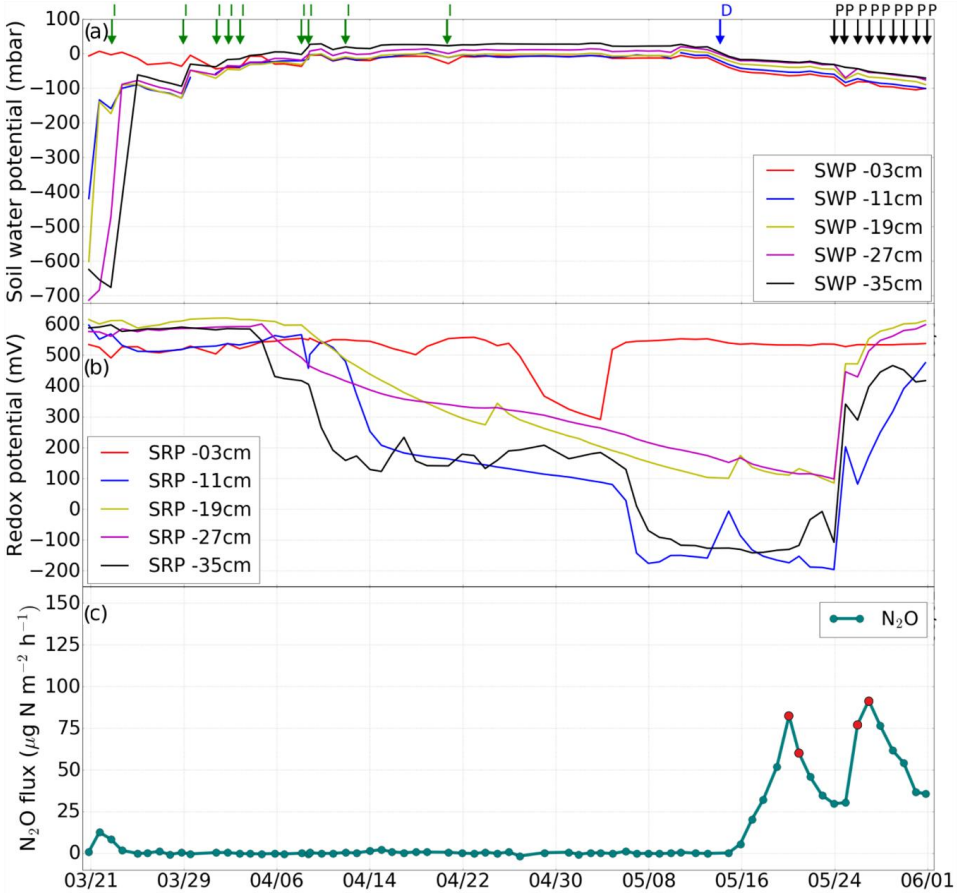

Figure 3.2 Experiment 1 (before fertilization). Changes in (a) soil water potential (SWP), (b) soil redox potential (SRP), and (c) N_2O emission rate induced by irrigation (I), drainage (D), irrigation with fertilizer (F), desaturation of the soil with pump (P). The red dots in panel c indicate the N_2O isotope sampling days.

In a second experiment (Figure 3.3), the soil in the lysimeter was fertilized on June 2 with 1.98 g ^{15}N-labeled ammonium sulfate (1.9 atom% ^{15}N, corresponding to 60 kg N ha^{-1}) dissolved in 2.1 L of tap water, to apply fertilization and irrigation simultaneously (also known as fertigation). Subsequently, two further irrigation events without fertilizer application (2.1 L and 4.2 L) were carried out on June 5 and 12 (Figure 3.3a). The drainage events were performed on June 8 and 15.

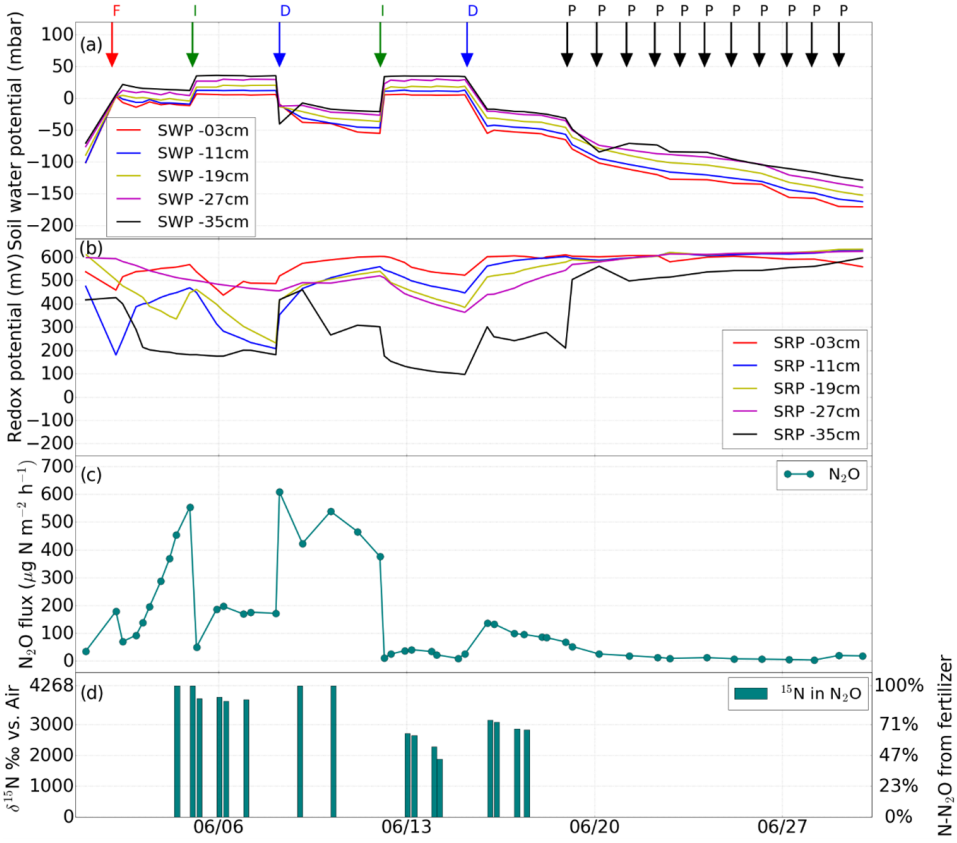

Figure 3.3 Experiment 2 (1st fertilization). Changes in (a) soil water potential (SWP), (b) soil redox potential (SRP), (c) flux of N_2O and CO_2 induced by irrigation (I), drainage (D), irrigation with fertilizer (F), desaturation of the soil with pump (P) , (d) percentage of N_2O from the added fertilizer.

A second application of the ^{15}N-labeled fertilizer (again 1.98 g of g ^{15}N-labeled ammonium sulfate with 1.9 atom% ^{15}N) took place on June 30, after which the soil was subjected to free drainage for four days. With the help of the Mariotte bottle, the water level in the soil column was then adjusted first to 23 cm and on July 6 to 15 cm for another eight days. On July 16, drainage was initiated using the pump.

The final irrigations with 2.1 L of tap water each took place on August 4 and 8, and soil drainage was again activated on August 12, until the soil was desaturated to a water potential lower than -150 mbar at 35 cm.

At the end of the experiment, soil samples were taken using stainless-steel cylinders (8 cm diameter) in the center of the lysimeter at six depth sections (0-7, 7-15, 15-23, 23-31, 31-39, and 39-47 cm, respectively). The soil of each depth section was mixed, and NH_4^+ and NO_3^- concentrations were determined as described

above. The results of mineral N concentrations in the different depth sections were considered as representative for the five depths of the soil redox sensors.

3.2.4 N_2O flux measurements

Nitrous oxide fluxes were determined daily throughout most of the experimental periods with the static chamber method by placing a PVC chamber (volume 5.65 L) gastight on the soil column and collecting gas samples manually with a syringe 0, 10, 20, 30, and 40 min after chamber closure. A 1.5 m long polyethylene tube with 2 mm inner diameter was connected to the chamber to keep the air pressure in the chamber headspace equal to the ambient air. The first sample was collected directly after the chamber was closed, and the samples were transferred to pre-evacuated (-1 atm) 22-mL GC glass vials. The gas samples were then analyzed with a gas chromatograph (8610C, SRI Instruments, Torrance, USA). The gas flux rates were determined using a simple linear regression for the five concentration points as described by Parkin and Venterea (2010). Flux values were accepted if the coefficient of determination (R^2) was larger than 0.8, or assumed to be zero when the deviation of the concentration values of the five different time points from the mean of the five samples was below two standard deviations (Wang et al., 2018). In all other cases, calculated flux rates were discarded. The N_2O fluxes were calculated using Equations (1) and (2) in Wang et al. (2018).

For the analysis of gas concentrations in soil solution, soil pore water was collected with the Rhizon samplers at the different depths in 22-mL GC vials. For the GC analysis, a headspace of 7 mL was created in the 22-mL GC vials using ambient air, and after 24 h equilibration the N_2O concentrations in the vial headspace were measured with the GC as described above. The dissolved gas concentrations were calculated with Henry's law, based on the air pressure and the concentration of the gases in the vial headspace according to Xu et al. (2009).

3.2.5 Isotope-ratio measurements

For tracing the source process (nitrification or denitrification) of the N_2O, additional gas samples were collected after the routine gas flux measurement. Eighty minutes after the chamber was closed, 120 mL of gas in the static chamber headspace was transferred to a 120-mL pre-evacuated serum bottle for further analysis of the isotopic signature. Before fertilization (i.e., ^{15}N application), the analysis of the natural N_2O isotopocule abundances, i.e., the $\delta^{15}N$, $\delta^{18}O$, and ^{15}N site preference (^{15}N SP), was used to identify the source process of N_2O (Ibraim et al., 2019). The $\delta^{15}N^{bulk}$, $\delta^{18}O$, and ^{15}N SP of N_2O in the gas samples and laboratory background air samples were analyzed using an isotope ratio mass spectrometer (IRMS, IsoPrime 100, Elementar Analysensysteme, Hanau, Germany). For more details of the IRMS analysis we refer to Heil et al. (2015) and Wei et al. (2017). Decock and Six (2013) summarized the average SP values for N_2O produced via the different pathways, with 32.8 ‰ (± 4.0 ‰ SD) for all known processes involving NH_2OH oxidation (i.e., nitrification and fungal denitrification), and -1.6 ± 3.8 ‰ for all known processes involving nitrate or nitrite reduction (i.e., bacterial denitrification). An intermediate SP value would indicate mixed source processes of N_2O (Toyoda et al., 2017).

After ^{15}N fertilizer application, only $\delta^{15}N^{bulk}$ of N_2O was used as isotopic information to calculate the contribution of fertilizer N to the total N_2O emission by application of a two-end member mixing model approach (Nason and Myrold, 1991), as the natural abundance signal was no longer usable. The $\delta^{15}N$ of the applied N fertilizer (4268 ‰) was used as one end member and the $\delta^{15}N^{bulk}$ of N_2O in background air (6.6 ‰) as the second end member in the mixing model. Due to the relatively low ^{15}N content of the fertilizer (1.9 atom% ^{15}N), the contribution of doubly ^{15}N-labeled N_2O to the total N_2O emission was negligible.

The ^{15}N signature of soil NH_4^+ was determined with the micro-diffusion method (Mulvaney et al., 1997), followed by elemental analyzer (EA)-IRMS analysis (Flash EA 2000 with Delta V Plus; Thermo Fisher Scientific, Bremen, Germany). The ^{15}N isotope analysis of soil NO_3^- was performed in a first step with a liquid-liquid extraction method (Huber et al., 2012), followed by EA-IRMS analysis. Soil total organic N was analyzed also using EA-IRMS. For a detailed description of soil ^{15}N measurement procedures see (Wei et al., 2020).

3.2.6 Eh measurements

The reduction-oxidation (redox, Eh) potential is a quantitative measure of the electrochemical potential in a solution containing oxidizing and reducing chemical species (Mitsch and Gosselink, 2015). The standard Eh is defined as the potential of a red/ox pair measured against the standard hydrogen reference electrode (E_0). The in-situ redox potential measured in the soil against the Ag/AgCl reference electrode can be converted to the standard Eh by adding the temperature-dependent offset between the normal hydrogen electrode and the Ag/AgCl electrode (E_{ref}) (Fiedler et al., 2007). As the soil temperature was close to 20 °C throughout the experiment, the measured redox potential values were converted to Eh by adding an E_{ref} of 210.5 mV.

3.2.7 Statistical approach

The statistical analyses were conducted using the Python statistics package, version 3.6 (Python Software Foundation, 2016), using Pandas and NumPy libraries.

3.3 Results

3.3.1 Impact of hydrological events on on soil water potential and Eh

The soil Eh and soil water potential at the different depths changed in response to irrigation events during the experiments. After several irrigation events at the beginning of the experiment, the soil was water-saturated and the soil Eh rapidly decreased (Figure 3.2b). During the first two weeks of the experiment, the soil Eh was above 500 mV in the entire soil profile. From April 4 to May 13, the soil Eh at 11 cm and 35 cm dropped from 550 mV to the lowest value (around -150 mV) and became stable afterwards, suggesting that also the microbial activity had stabilized. Reducing conditions can

be separated into weakly reducing (400 > Eh > 200 mV), moderately reducing (200 > Eh > -100 mV), and strongly reducing (Eh < -100 mV) conditions.

The following fertilization experiment showed a similar pattern, but the influence on Eh was more pronounced. After onset of irrigation on June 2, the Eh values showed a stronger decrease near the surface (3 and 11 cm) than at greater depth. The Eh values down to 27 cm depth remained above 500 mV, regardless of whether fertilization, drainage or waterlogging occurred. In contrast, Eh at 35 cm decreased to values below 200 mV, indicating reducing conditions in the lower part of soil column. A short-term decrease of Eh at shallow depth (from 500 to 200 mV at 11 cm) was observed on June 3 after fertilizer irrigation (Figure 3.3b), and similarly on June 30 (Figure 3.4b). During the final period from August 9 to 12, only Eh at 35 cm indicated intermediate redox conditions (300 mV) (Figure 3.5b).

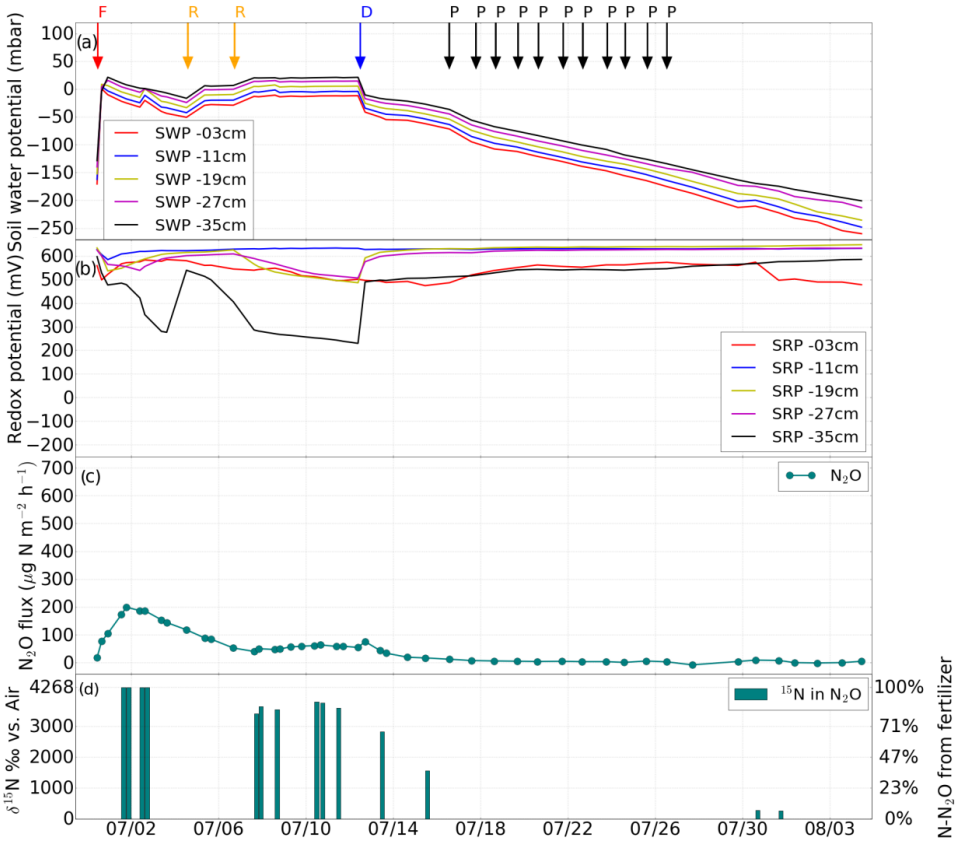

Figure 3.4 Experiment 3 (second fertilization). Changes in (a) soil water potential (SWP), (b) soil redox potential (SRP), (c) N_2O flux induced by drainage (D), irrigation with fertilizer (F), desaturation of the soil with pump (P), water table rise (R), (d) percentage of N_2O derived from the added fertilizer.

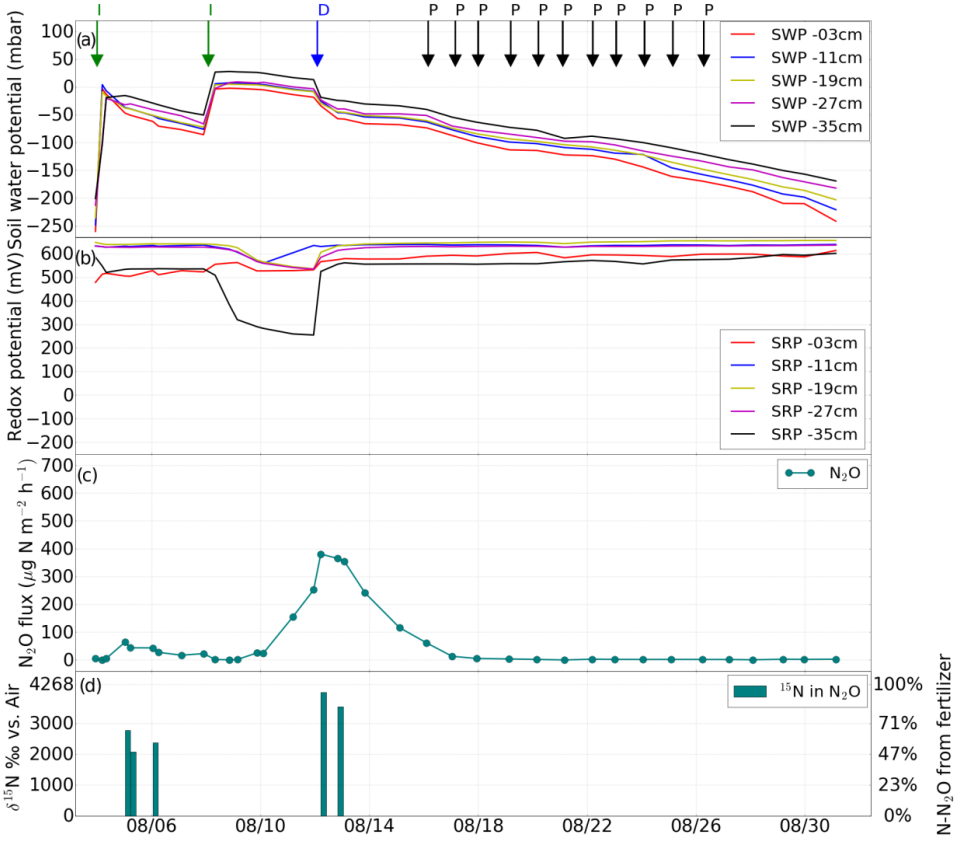

Figure 3.5 Experiment 4 (post-fertilization saturation phase). Changes in (a) soil water potential (SWP), (b) soil redox potential (SRP), (c) flux of N_2O and CO_2 induced by irrigation (I), drainage (D), desaturation of the soil with pump (P), (d) percentage of N_2O from the added fertilizer.

The Eh variations during different phases are shown in Table 3.1. From pre- to post-fertilization phase, a strong decline of the coefficient variation of mean Eh values (from 49% to 5%) was observed, whereas the mean Eh values increased after N addition to the soil at all depths (from 334 mV to 599 mV). Before fertilization, negative redox values were also observed after a long saturation period (Figures 3.2b and 3.6a), which was not the case after fertilization (Figures 3.3b, 3.4b, 3.5b and 3.6b). Furthermore, after fertilization redox potential values were rarely below 400 mV at shallower soil depth (Figure 3.6b), whereas before fertilization also at shallower depths redox potential was frequently below 400 mv (Figure 3.6a).

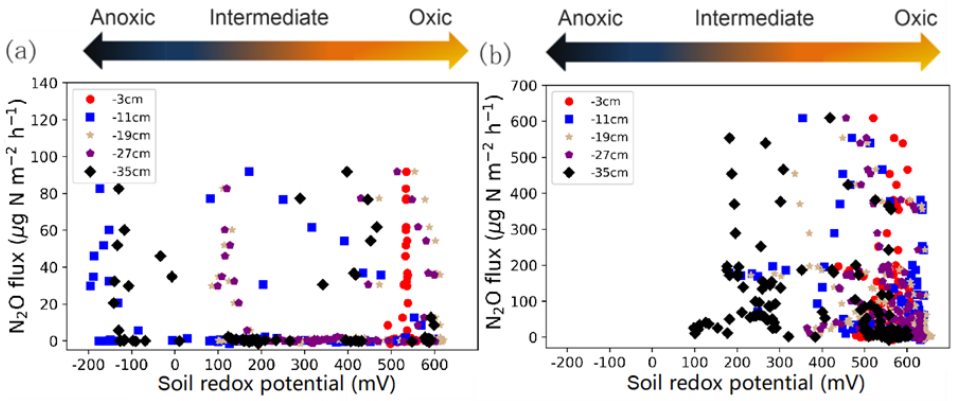

Figure 3.6 Nitrous oxide emissions versus soil redox potential measured at 3, 11, 19, 27 and 35 cm below the soil surface (a) before and (b) after fertilization.

3.3.2 Impact of hydrological events on N_2O emissions

The average soil temperature during the experiments was 19.4 °C (SD 0.7 °C) at 11 cm and 18.9 °C (SD 0.7 °C) at 35 cm. Given these low variations in temperature, we assumed that changes in soil temperature were not a critical control factor of N_2O formation and emission in our experiments.

The first experiment without fertilization (from March 24 to May 14) was characterized by relatively low N_2O emission (on average 2.3 µg N m^{-2} h^{-1}), indicating that N consumption was dominant (Figure 3.2c). However, after initiating free drainage on May 14, the N_2O flux gradually increased in the following days, peaking at 82.6 µg N m^{-2} h^{-1} after six days. On May 24, drainage was initiated by pumping, which led to a strong increase in Eh at all measurement depths, except for 3 cm, where Eh had been high before. Three days later, a further N_2O emission peak with 91.7 µg N m^{-2} h^{-1} occurred (Figure 3.2c).

During the second experiment that featured the first fertilization via irrigation on June 5, N_2O emission become generally more dynamic, with larger N_2O fluxes especially after forced drainage by pumping (Figure 3.3c). Directly after the fertilizer application, an increase in N_2O emissions was observed, and N_2O flux further increased gradually until the next irrigation event (from 0 to above 550 µg N_2O-N m^{-2} h^{-1}). After the irrigation, a sharp decrease in N_2O emission occurred, indicating transport limitation due to water-filled pores, from above 500 to around 200 µg N_2O-N m^{-2} h^{-1} after saturation on June 5. This effect was even more pronounced after the irrigation event on June 12, when N_2O emissions decreased from about 400 µg N_2O-N m^{-2} h^{-1} down to almost 0 µg N_2O-N m^{-2} h^{-1}. The N_2O emissions increased rapidly during the first five days after drainage on June 8 to values between 400 and 550 µg N_2O-N m^{-2} h^{-1}. The peak of N_2O emission was more than five times higher than during the first experiment without fertilization.

After the second fertilization event on June 30, N_2O emission started to increase (Figure 3.4c), and peaked at about 200 µg N_2O-N m^{-2} h^{-1} on July 2 and deceased to around 50 µg N_2O-N m^{-2} h^{-1} in the following five days. The emission rate stayed between 40 and 65 µg N_2O-N m^{-2} h^{-1} despite the rising water table. After drainage on July 12, the N_2O emission rate progressively decreased to 0 (Figure 3.4c).

The final irrigation experiment started on August 8, during which the N_2O emission constantly increased from 0 to 400 µg N_2O-N m^{-2} h^{-1} within four days, and then gradually decreased to zero emission within five days after drainage. After August 18, the soil N_2O flux returned to pre-irrigation level (Figure 3.5c).

Table 3.1 shows the mean, minimum and maximum N_2O fluxes during the four different experiments. With 137.8 µg N_2O-N m^{-2} h^{-1} the highest mean N_2O emission rate occurred during Experiment 2, i.e., after the first fertilization. This value was about 3.6 times higher than the mean N_2O emission rate of Experiment 3 (38.4 µg N_2O-N m^{-2} h^{-1}). Figure 3.6 shows the mean Eh of the five different depths of the soil column and the N_2O fluxes before (Figure 3.6a, Experiment 1) and after (Figure 3.6b) fertilization (Experiments 2, 3 and 4). Before fertilization, Eh showed considerable variability at the different depths, with Eh values at some depths even indicating reducing conditions (Figure 3.6a), while after fertilization, most of the Eh values were in the oxic range (above 400 mV) (Figure 3.6b).

3.3.3 Variations of $\delta^{15}N^{bulk}$, ^{15}N SP and $\delta^{18}O$ of N_2O emissions

The contribution of the different microbial source processes to the emission of N_2O before fertilization (Figure 3.2c) was analyzed at the level of natural isotope abundance. The isotopic signature ($\delta^{15}N^{bulk}$, $\delta^{18}O$, ^{15}N SP) of N_2O emission after drainage on June 19, 20, 26, and 27 indicated that the N_2O originated exclusively from bacterial or archaeal nitrification, and not from bacterial denitrification or nitrifier denitrification (Figure 3.7).

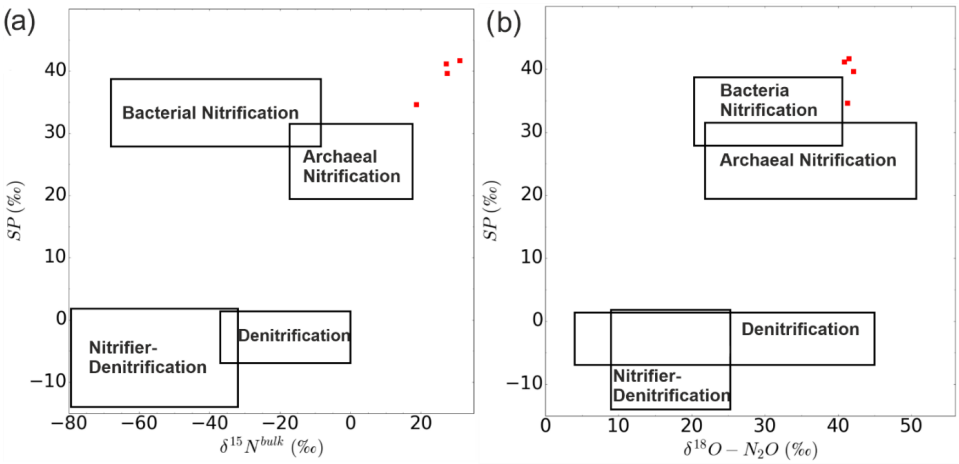

Figure 3.7 Dual isotope end-member map for N_2O source partitioning before fertilization. The squares indicate typical ranges for the microbial processes of N_2O production. The red squares represent the isotope signatures of N_2O emission on May 20, 21, 27, and 28 (shown in Figure 3.2c as red dots) before fertilization in this study. The rectangles are taken from Toyoda et al., (2019).

Two to three days after the onset of fertilization, the $\delta^{15}N$ value of N_2O indicated that almost 100% of $\delta^{15}N$-N_2O originated from the applied fertilizer (Figures 3.3d and 3.4d). Another peak of $\delta^{15}N$-N_2O occurred after drainage on June 9 and 10, indicating that again all of the $\delta^{15}N$-N_2O originated from the applied fertilizer. As can be seen in Figure 3.3d, the high $\delta^{15}N$-N_2O during the first fertilization phase occurred when the soil was at low water potential. About 90% of the N_2O originated from the added fertilizer on June 6 and 7, while 44 - 55 % of N_2O was fertilizer-derived on June 13 and 14. After the onset of the second fertilization, $\delta^{15}N$-N_2O increased again with values between 3056 and 4268 ‰ before drainage. After drainage on July 13, the $\delta^{15}N$-N_2O decreased from 2467 to 1204 ‰ on July 15 (Figure 3.4d).

After irrigation on August 5, the mean $\delta^{15}N\text{-}N_2O$ was 2451‰ during a period with low water potential (Figure 3.5c). However, as soon as saturation was initiated on August 8, $\delta^{15}N\text{-}N_2O$ gradually increased again to values around 3418 to 4014 ‰, accompanied by high N_2O emissions, meaning that around 80 - 95% $N\text{-}N_2O$ originated from the added fertilizer (Figure 3.5d).

3.3.4 Impact of different hydrological events on mineral N and dissolved N_2O concentrations along the soil profile

The concentration distribution of gaseous N_2O in the soil solution extracted with the suction cups showed that the highest N_2O concentrations in soil solution occurred after irrigation and nitrogen fertilization events (Figure 3.8). On June 5, the gaseous N_2O concentration profile was V-shaped with the lowest concentration at intermediate depth, and with a similar depth distribution as the NO_3^- concentration in the soil solution (Figure 3.9c).

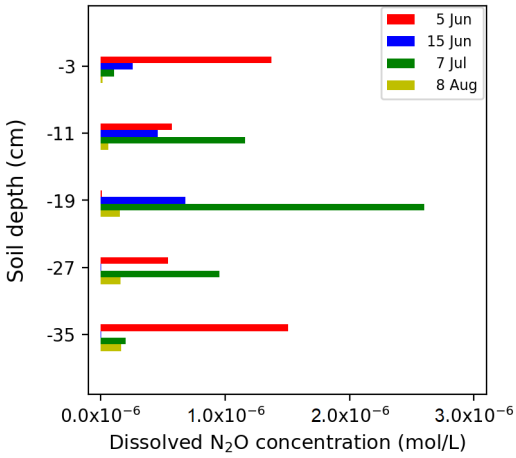

Figure 3.8 Concentration of dissolved N_2O.

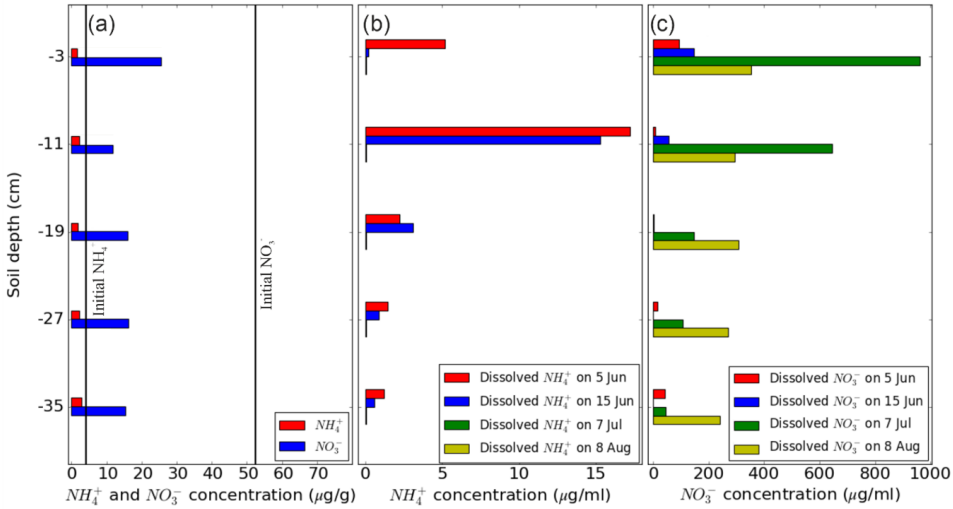

Figure 3.9 Concentration of mineral N at different depths of the soil column, (a) of ammonium (NH_4^+) and nitrate (NO_3^-) extracted from soil samples taken after drainage on May 30, (b) and (c) of NH_4^+ and NO_3^-, respectively, in soil solution sampled at the four different time points indicated.

The fertilization and hydrological events (i.e., irrigation and drainage) significantly altered soil mineral nitrogen and gas concentrations both in space and time. Figure 3.9 illustrates the dissolved NH_4^+ and NO_3^- concentration in soil solution on May 30, June 5 and 15, July 7, and August 8. While NH_4^+ was close to the detection limit before fertilization, NO_3^- ranged between 10-25 µg g^{-1} soil dry weight (Figure 3.9a). After fertilization, NH_4^+ concentration was highest at 11 cm on June 5 and 15, but was basically at the detection limit on July 7 and August 8 (Figure 3.9b). In contrast, NO_3^- showed a different pattern, with low values across the soil profile on June 5 and 15, highest values on July 7 at 3 cm and 11 cm, and intermediate concentrations without clear depth dependence on August 8 (Figure 3.9c).

At the end of Experiment 4, concentrations of total N and NH_4^+ were uniformly distributed along the soil profile (Figure 3.10a,b), but the soil NO_3^- concentration was highest at -3 cm, and much lower from 11 cm to greater depth (Figure 3.10c). There was a pronounced decrease in ^{15}N enrichment of all three parameters with increasing soil depth (Figure 3.10d-f). However, compared to $\delta^{15}N$ of NO_3^-, the $\delta^{15}N$ of NH_4^+ value was very low, indicating that only 3.4% of the N in NH_4^+ was from the added fertilizer at 0-7 cm soil depth, and in the rest of the soil the contribution of fertilizer N to the residual NH_4^+ was below 1%. In contrast, the fraction of fertilizer-derived N was high in NO_3^-, amounting to 80%, 49%, 37%, 27%, 17%, and 11% in the different depth sections from the topsoil to the bottom of the lysimeter, respectively.

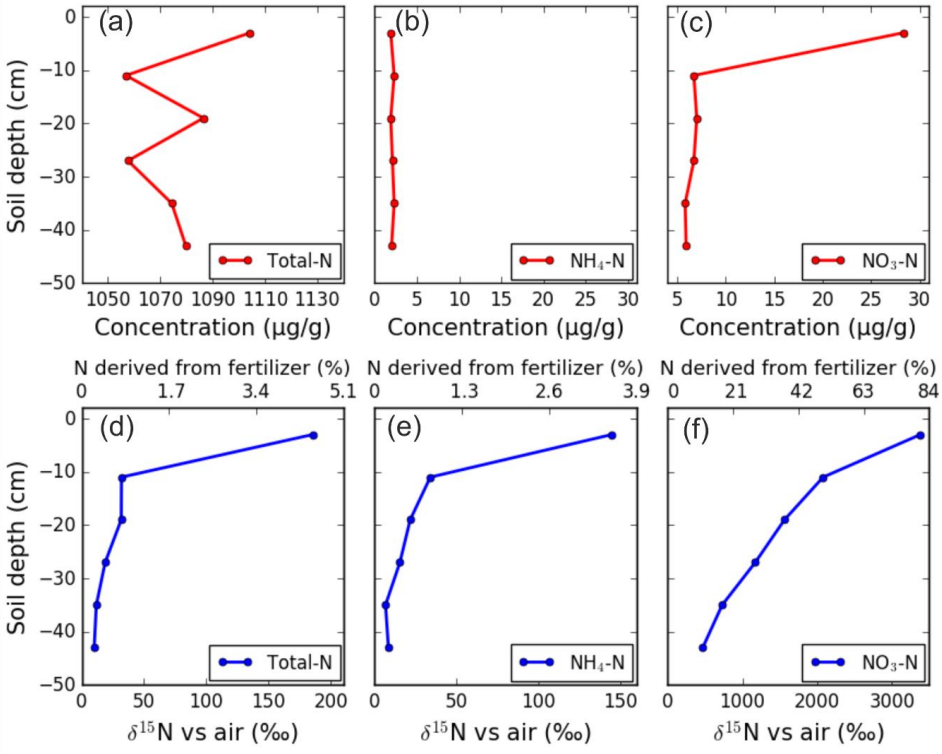

Figure 3.10 Concentration of (a) total N, (b) ammonium (NH_4^+), and (c) nitrate (NO_3^-) in soil, and $\delta^{15}N$ of (d) total N, (e) NH_4^+ and (f) NO_3^- at the end of the series of experiments.

3.4 Discussion

In farmland systems, management activities (e.g., fertilization, irrigation) exert a strong control the occurrence and intensity of nitrification and denitrification processes in soils and related N fluxes (e.g. transport of dissolved N and emission of N_2O) (Butterbach-Bahl et al., 2013; de Klein et al., 2011; Luo et al., 2008; Skiba et al., 1998). Variations in N_2O flux rates from soils are induced by complex interactions between fertilizer application, microbial processes and soil physical conditions (Oertel et al., 2016). For example, the infiltration of rainwater or irrigation water will induce changes in Eh that affect microbial processes as well as the transport of electron acceptors and nutrients. The application of stable isotopes can help to elucidate these processes. In this study, the natural abundance of ^{15}N and its intramolecular distribution in N_2O as well as ^{15}N-labelled mineral fertilizer were used to better understand the effects of variations in soil water content and soil Eh on N_2O production and emission.

3.4.1 Effects of Soil Hydrological Conditions on Eh and Dissolved N

The distribution of dissolved NH_4^+ and NO_3^- along the soil profile varied in response to irrigation and fertilization (Figure 3.9b,c), similar to the study of Rubol et al. (2012). Before fertilization, the soil Eh was

low in the lower parts of the soil column (Figure 3.2b), since during the prolonged soil saturation the active soil microorganisms use alternative electron acceptors instead of oxygen (Dorau et al., 2018; Morales-Olmedo et al., 2015; Pezeshki, 2001). Therefore, consistent with the high consumption rate of nitrate at -11 cm (Figure 9a), the Eh decreased even further and faster at -11 cm (Figure 3.2b). The low NO_3^- concentration at that same depth might have led to the use of other substrates like Mn^{4+} as electron acceptor (Tokarz and Urban, 2015).

Kralova et al. (1992) found that an increase of Eh from 550 to 600 mV led to the transition from mineralization to nitrification, associated with an increase in nitrate content. Accordingly, in our experiments soil Eh above -27 cm was around 600 mV after the second fertilization event, and allowed a large part of the added NH_4^+ to be converted to NO_3^- from June 30 to July 7 (Figure 3.9b,c). The higher redox potential values after fertilization compared to those before fertilization may be explained by the lack of prolonged periods of saturation. The higher Eh values after fertilization compared to those before fertilization may be explained by the lack of prolonged periods of saturation. The microorganisms did not have enough time to consume the different alternative electron acceptors pools sequentially, and it may be the reason for the soil Eh remaining at a higher level compared to the per-fertilization period (Burgin et al., 2011). Another reason for the higher Eh observed after fertilization may be the larger availability of nitrate after the addition of ammonium due to its conversion to nitrate via nitrification, which prevents a further decrease in Eh as long as sufficient nitrate is available in the soil column. The addition of NO_3^- can significantly increase Eh when the soil is in reduced conditions, as a strong electron acceptor is added to the soil (Buresh and Patrick, 1981). This result is similar to that of Buresh and Patrick (1978), who found that after addition of NO_3^- the soil Eh increased significantly from -300 to 160 mV. The increase of Eh was maintained until the NO_3^- was consumed, i.e., reduced. In accord with the results of Hasen et al. (2014), the Eh can help to interpret the possible N transformation processes in the soil.

3.4.2 Changes in N_2O emissions in response to changes in soil water potential, Eh, and available N

Yu et al. (2016) found that in paddy soil, N_2O emission occurred after the water level dropped after long-term flooding, similar to our results in the experiment before fertilization. The simultaneous irrigation with ^{15}N-labeled NH_4^+ fertilizer triggered nitrification, associated with the consumption of added NH_4^+ and the accumulation of NO_3^- in the upper part of the soil column (Figures 3.9b,c and 3.10b,c,e,f). This is consistent with the relatively high mean Eh near the soil surface that was not favorable for denitrification. In contrast, at the bottom of the column, we found low N_2O concentrations in the soil water, suggesting reduction of N_2O to N_2 (Martikainen et al., 1993; Regina et al., 1996; Rubol et al., 2012).

In our study, N_2O emission rates were affected by hydrologic conditions and events, but with different dynamics. As Figures 3.2c and 3.3c illustrate, N_2O emission gradually increased after the initiation of drainage and after the first fertilization, respectively, possibly because of the activation of nitrification induced by the drainage (Experiment 1, Figure 3.2c) and fertilization (Experiment 2, Figure 3.3c). A similar delay in N_2O emission after fertilization or irrigation was also observed in other studies (Akiyama et al., 2000; Baggs et al., 2000; Comfort et al., 1990; Wang et al., 2018). In all cases, the apparent delay in N_2O emission corresponded to water content changes after the soil was saturated or fertigated. Once nitrification

was activated, any fast changes in the hydrologic conditions led also to immediate changes in N_2O emissions, which was decreased by further irrigation and increased immediately again after subsequent drainage (Figure 3.3c). A possible explanation is that it takes several days to activate the microbial nitrifier community, which then oxidizes ammonium to nitrite (ammonia-oxidizing bacteria and archaea) and then further to nitrate (nitrite-oxidizing bacteria). Any short-term changes in aeration status which are imposed then on the soil by changes in the water content and water table height will immediately affect the activity of this microbial community by the decrease or increase in oxygen availability, because ammonia and nitrite oxidizers are obligate aerobic. As oxygen is expelled from the soil pores during irrigation, and as oxygen quickly re-enters the soil profile after drainage, the activity of obligate aerobes can be basically switched on and off very quickly, if the anoxic periods do not last too long. This assumption is supported by the changes in redox potential in our experiments, which quickly recovered after drainage to values in excess of 400 mV, indicating optimal conditions for the nitrification process (Tokarz and Urban, 2015). Another possible explanation of the lag of N_2O emission in the soil after the saturation may be the decrease in N_2O diffusivity in the soil due to the increased water content, leading to initially low N_2O emission from the soil surface.

Before fertilization, most of the N_2O fluxes from the surface of the soil column originated from nitrification, as indicated by the end-member map in the dual isotope plot (Figure 3.7). Our results indicated that there was no or very weak ammonification of organic (i.e., unlabeled) N involved. Although the organic N can be nitrified and denitrified after the ammonification, the N mainly involved in the soil N-cycle was from the added ^{15}N-labeled N. Thus, the most important N-conversion processes in our experiments were nitrification and denitrification, which convert NH_4^+ to NO_3^-, and NO_3^- via N_2O to N_2, respectively. The change in the fraction of N_2O derived from nitrification or denitrification could be deduced from the simultaneously determined ^{15}N-signatures of N_2O and mineral N.

Moreover, after fertilization, nitrification dominated N_2O production in soil with high Eh in the upper part of the soil column, when NH_4^+ was still available in sufficient quantities (Figure 3.9b), indicated by the high $\delta^{15}N$ of N_2O. However, after August 8 (i.e., after the two fertilization experiments), when the concentration of NO_3^- dissolved in soil water reached values above 200 µg ml^{-1} at all five depths, the decrease in Eh below 300 mV at -35 cm suggested that denitrification could have become the primary source of N_2O after the last irrigation event at -35 cm or below (Hansen et al., 2014). This assumption is supported by the observation that the subsequent drainage event led to an increase in Eh, but a decrease in N_2O emission. This is consistent with previous studies, in which the maximal denitrification rate occurred in an Eh range of 150 to 300 mV (Husson 2013; Włodarczyk et al., 2002).

3.5 Conclusions

We established a lysimeter system for the determination of soil water and Eh as well as N_2O gas emissions in the laboratory to study the effects of irrigation and drainage events on soil N dynamics and N_2O emissions from agricultural soils. Our lysimeter experiments mimicked agricultural irrigation and fertilization management. Overall, our results revealed a close relationship between soil hydrologic

conditions, soil Eh, and soil N dynamics in a controlled environment. At an intermediate soil moisture level, nitrification was the dominant source of N_2O, and fertilization with NH_4^+ stimulated nitrification and further increased its N_2O source strength. Near soil saturation, the dominating N_2O source process shifted from nitrification towards denitrification. Our results suggest that the soil Eh is a suitable indicator for the two dominant N_2O source processes, i.e., hydroxylamine oxidation and nitrite reduction. Furthermore, the results of this study identify soil Eh variations as an additional control variable of soil N turnover, beside soil water and mineral N content. However, we also found that the change in Eh is not only related to soil water potential, but also to the type and abundance of ions and to the activity of microorganisms in the soil. There is still a need for a transfer of our experimental approach to field conditions across different soil textures to extend the implications of our findings. In particular, stable isotope measurements should be conducted simultaneously to the Eh and N_2O emission measurements in the field experiments to trace the N_2O pathways along the soil profile. This will allow the identification of the hotspots of N_2O reduction, as the formation and consumption of N_2O can occur in close vicinity to each other in the soil and cannot be disentangled by Eh measurements alone. Finally, more research is required to unravel the link between Eh variations and soil microbial activities and to disentangle the relative effects of the variations of soil Eh, water content, and water table height on soil N dynamics and N_2O emissions.

Chapter 4

Investigating the controls on greenhouse gas emission in the riparian zone of a small headwater catchment using an automated monitoring system

Based on:

Wang, J., H.R., Bogena, T., Suess, A., Graf, A, Weuthen and N. Brüggemann. *Vadose Zone J. 21:e20149.*

4.1 Introduction

Soils act as sink and source of carbon (C) and nitrogen (N) via large greenhouse gas (GHG) fluxes (Smith et al., 2007). Forest soils play an important role in controlling global warming because forests cover 31% of the global land area and are important sources of atmospheric CO_2 and N_2O (Adams et al., 2012; Oertel et al., 2016). Soils are also an important source and sink of N_2O and CH_4, thus strongly influence the N_2O and CH_4 budget of the atmosphere (Chapuis-Lardy et al., 2007; Dutaur and Verchot, 2007). Oxic and anoxic zones in soils control redox reactions, including nitrification, denitrification, and the oxidation or reduction of iron, manganese, and sulfate (Smith and DeLaune, 1984; Reddy et al., 1989; Patrick and Jugsujinda, 1992; DeLaune and Reddy, 2005; Tokarz and Urban, 2015). In riparian areas, groundwater table level fluctuations cause variations of oxygen and other alternative electron acceptors (e.g. NO_3^-, Mn^{4+}, Fe^{3+}, SO_4^{2-}, and CO_2), and the soil redox potential (Eh) provides a quantitative measure of oxidizing or reducing conditions in soil (Mansfeldt, 2003; Delaune and Reddy et al., 2005; Husson et al., 2016). The soil redox potential range can be differentiated into oxic (> 400 mV), weakly reducing (400 mV to 200 mV), moderately reducing (200 mV to -100 mV) and strongly reducing (< -100 mV) conditions (Delaune and Reddy, 2005). The different oxidizing or reducing conditions govern the dynamics of CO_2, N_2O, and CH_4, and significant CH_4 production (methanogenesis) is generally active when soils are under strictly reducing conditions (Yu et al., 2008). Numerous studies investigated relationships between soil water saturation and soil redox potential due to the influence of groundwater (Vepraskas and Wilding, 1983; Cogger et al., 1992; Comerford et al., 1996; Seybold et al., 2002; Thomas et al., 2009; Wanzek et al., 2018), water table changes (McDaniel et al., 2001), flooding (Brettar et al., 2002; Rinklebe et al., 2016) and irrigation (Wang et al., 2020). Redox conditions in wetland soils are strongly influenced by groundwater level fluctuations, leading to relatively fast (hourly) spatial and temporal changes of oxic and anoxic conditions and correspondingly to changes in the predominance of processes of the N cycle (i.e. ammonification and nitrification versus denitrification) (Reddy et al., 1989; Clément et al., 2002). Furthermore, the intensity of soil redox reactions is controlled by the metabolism and biochemical transformations of microorganisms in the soil (Husson, 2013). Besides soil temperature and water content, pH and nutrient contents (e.g. C/N ratio, NH_4^+, and NO_3^-) will influence soil biological process and cause variations of soil GHG emissions (Oertel et al., 2016). However, despite the importance of soil redox potential effects, only a few studies have focused on the relationship between the soil redox potential and GHG emissions in the riparian zone and found a close relationship (Yu et al., 2004; Phillips and Beeri, 2008; Marín-Muñiz et al., 2015). Soil profile analysis of soil CO_2, N_2O, and CH_4 emissions across a hydrological gradient indicated a close relationship between soil redox conditions, soil temperature, groundwater level, and potential CO_2, N_2O and CH_4 emissions (Yu et al., 2006). Some studies reported relationships between greenhouse gas concentrations and redox potential in riparian zones from water extraction or by measuring only the surface layer (0-5 cm) (Marín-Muñiz et al., 2015; Poblador et al., 2017). However, these studies failed to obtain a full picture of the controlling factors of biogeochemical processes in riparian zones, and important influencing factors on GHG emissions were not analyzed in detail at the different depths with high time resolution, such as soil redox potential or matrix potential, which are essential for estimating soil GHG emissions more accurately and for improving the current estimates or models.

In this paper, we present a newly developed automated soil redox potential measurement system, in which the variations in GHG (CO_2, CH_4 and N_2O) emissions along with other important soil variables (soil water content, soil temperature, soil matrix potential, and groundwater table level) can be simultaneously observed. We deployed this monitoring system in the riparian zone of the Wüstebach catchment, Germany and conducted continuous measurements over one year. The obtained dataset was used to investigate the aforementioned control parameters and their effect on GHG emissions in the riparian zone.

The main objectives of this study were (1) to establish continuous sub-daily soil redox potential and soil CO_2, N_2O and CH_4 flux measurements in a riparian zone; (2) to identify if the variations of soil redox potential influenced by slope and water table fluctuations in different distances from the stream, and (3) to study the relationships between GHG fluxes and environmental factors.

4.2 Methods

4.2.1 Site description and instrumentation

The study was carried out in the TERENO test site Wüstebach (50°34' N, 6°25' E), a headwater catchment covering an area of 38.5 ha (Figure 4.1, Bogena et al., 2018). The catchment is located in the German low mountain range near the German-Belgian border and belongs to the Eifel National Park. Elevation ranges from 595 to 628 m above sea level with an average slope of 3.6% (Bogena et al., 2018). The catchment is located in the humid temperate climatic zone with a mean annual precipitation of 1200 mm and a mean annual temperature of 7°C (Wiekenkamp et al., 2016). The bedrock consists of Devonian shales with sporadic sandstone inclusions, and is covered by a 1 to 2 m thick periglacial solifluction layer in which mainly Cambisols in the western part and stagnic Cambisols in the eastern part have developed in the groundwater distant hillslopes. In the valleys, groundwater has a considerable influence, and here Planosols are associated with Gleysols and semi bogs (Histosols) (Bogena et al., 2018). The soil texture is silty clay loam with medium to very high fraction of coarse material. Prior to the forest redevelopment, the catchment area was almost completely covered by Norwegian spruce (*Picea abies* L.) and Sitka spruce (*Picea sitchensis* [Bong.] Carr.), which were planted in the late 1940s with an average density of 370 trees/ha. In August 2013, a partial deforestation took place in the catchment area of the Wüstebach, whereby all spruce trees in the riparian zone and its immediate surroundings were removed using a cut-to-length method (Figure 4.1).

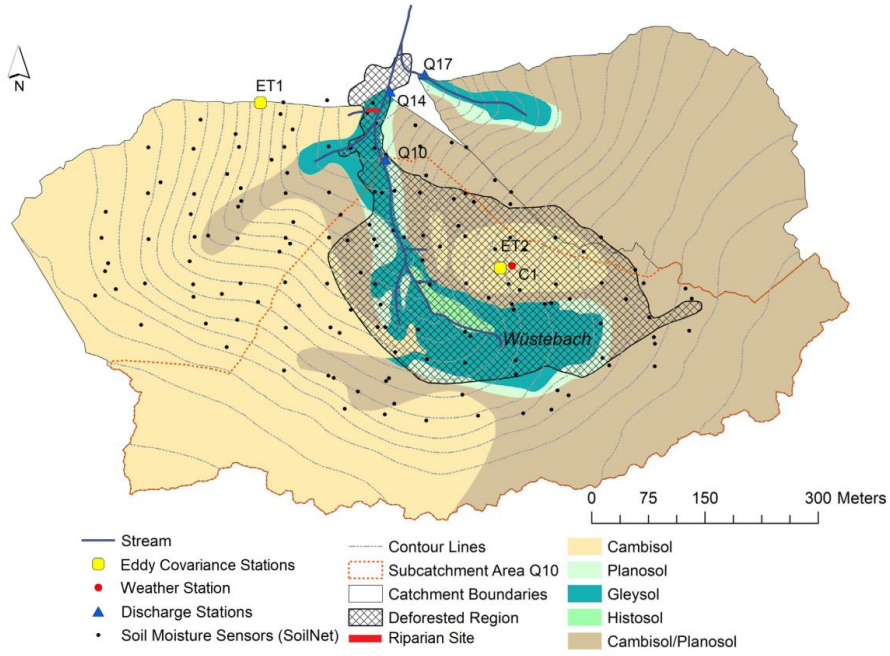

Figure 4.1 Map of the Wüstebach catchment including the riparian site and the weather station (Wiekenkamp et al. 2016, modified).

4.2.2 Experimental setup

The experimental setup was installed in the deforested riparian zone (Figure 4.1) and consisted of five soil stations combined with automated soil chambers for GHG flux measurements, which were set up along a transect perpendicular to the stream (Figure 4.2).

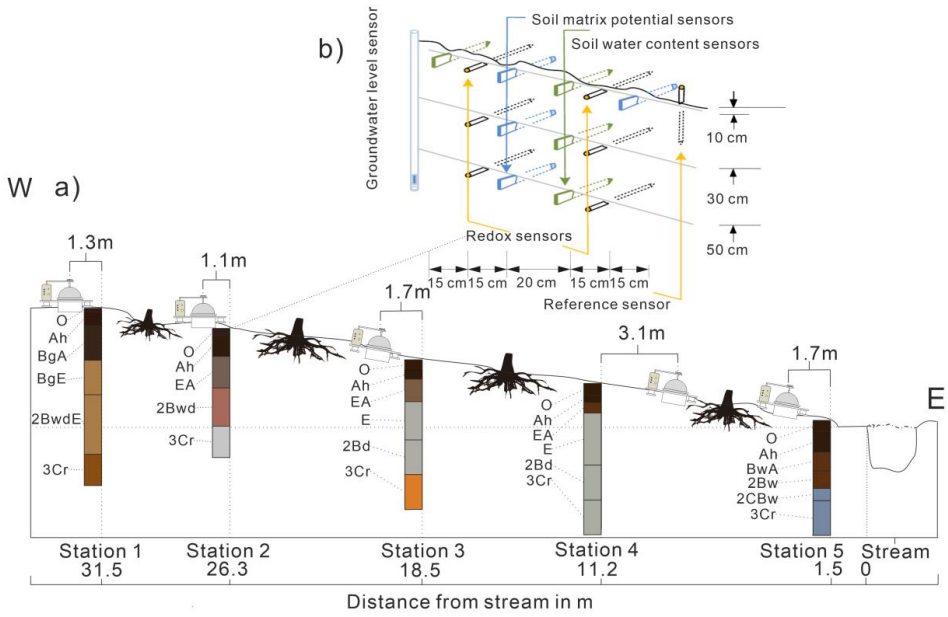

Figure 4.2 (a) Locations of the soil profiles and chambers along the experimental transect in the riparian zone of the Wüstebach catchment. Individual soil layers are indicated by different colors, and letters indicate horizon names based on USDA classification (see Table 4.1). (b) Schematic depicting the soil monitoring system consisting of four soil moisture sensors, four matrix potential sensors, six redox potential sensors and one groundwater level sensor.

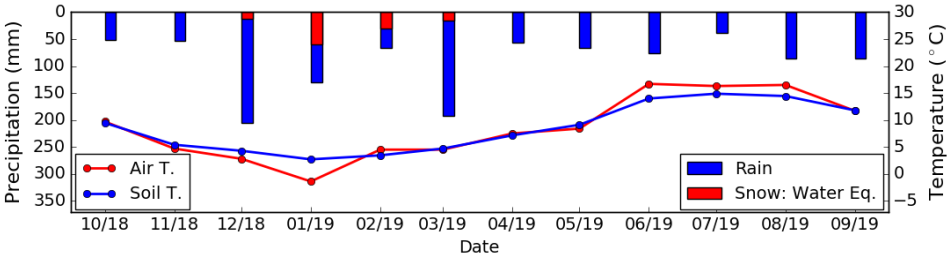

Figure 4.3 Monthly precipitation and temperature data during the observation period.

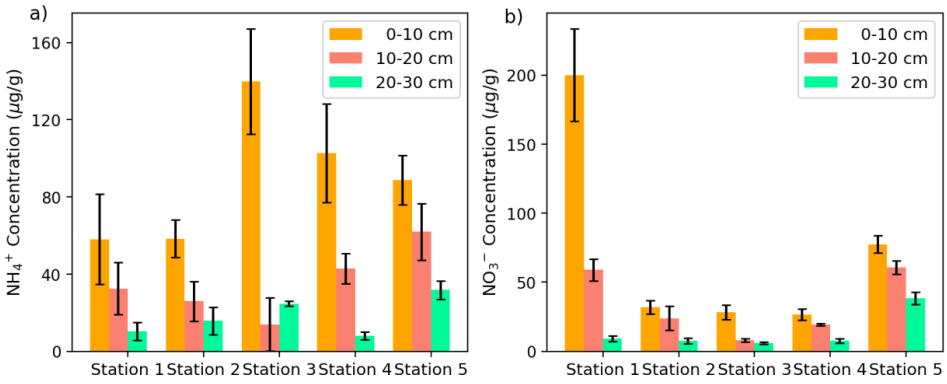

Figure 4.4 Soil NH_4^+ (a) and NO_3^- (b) concentration in the three different soil layers (from 0-10 cm, 10-20 cm, and 20-30 cm) from the soil sampling on 20 December 2018 and the error bars represent the standard deviations.

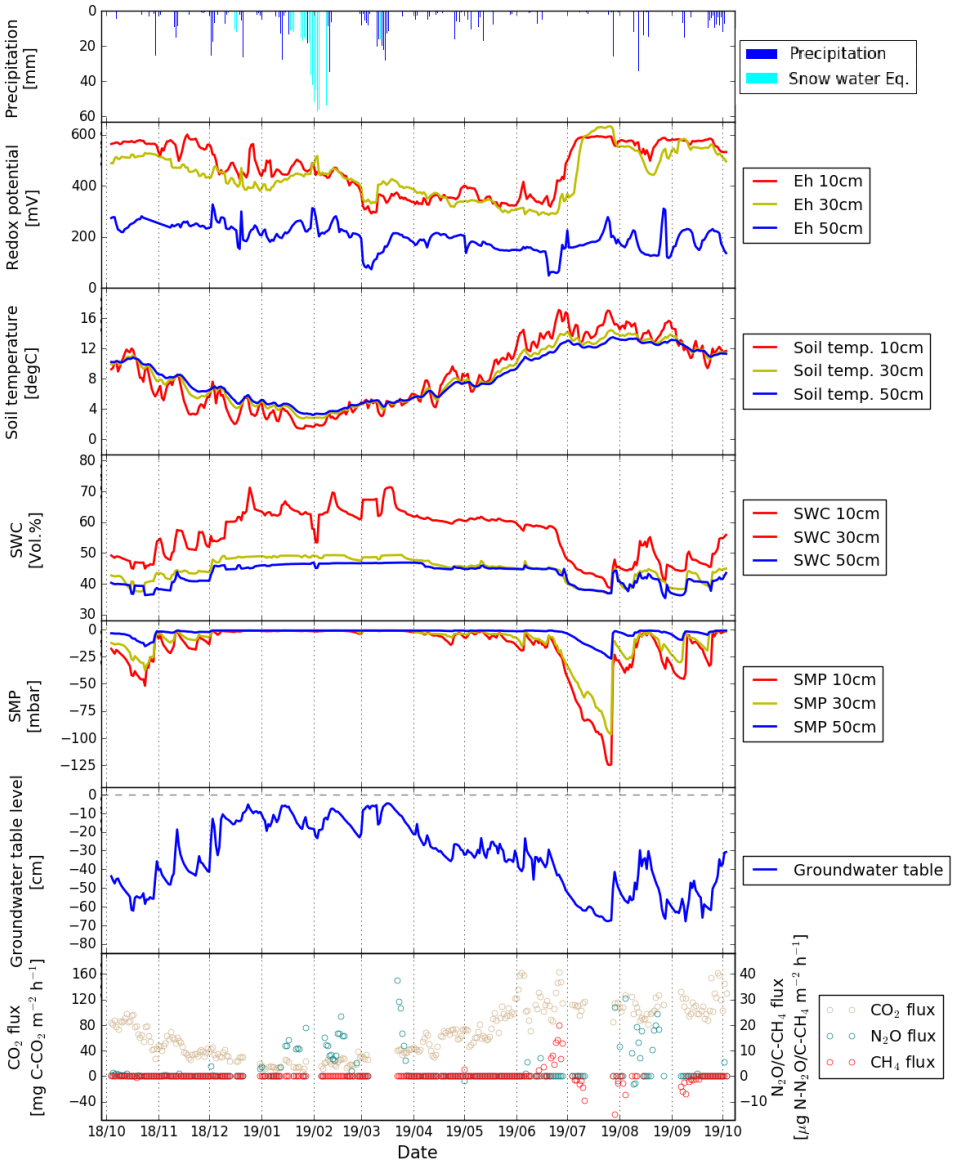

Figure 4.5 Time series of daily sums of precipitation, snow cover, and daily means of Eh, soil temperature, SWC (volumetric soil water content), SMP (soil matrix potential), groundwater table depth and GHG fluxes at all five stations.

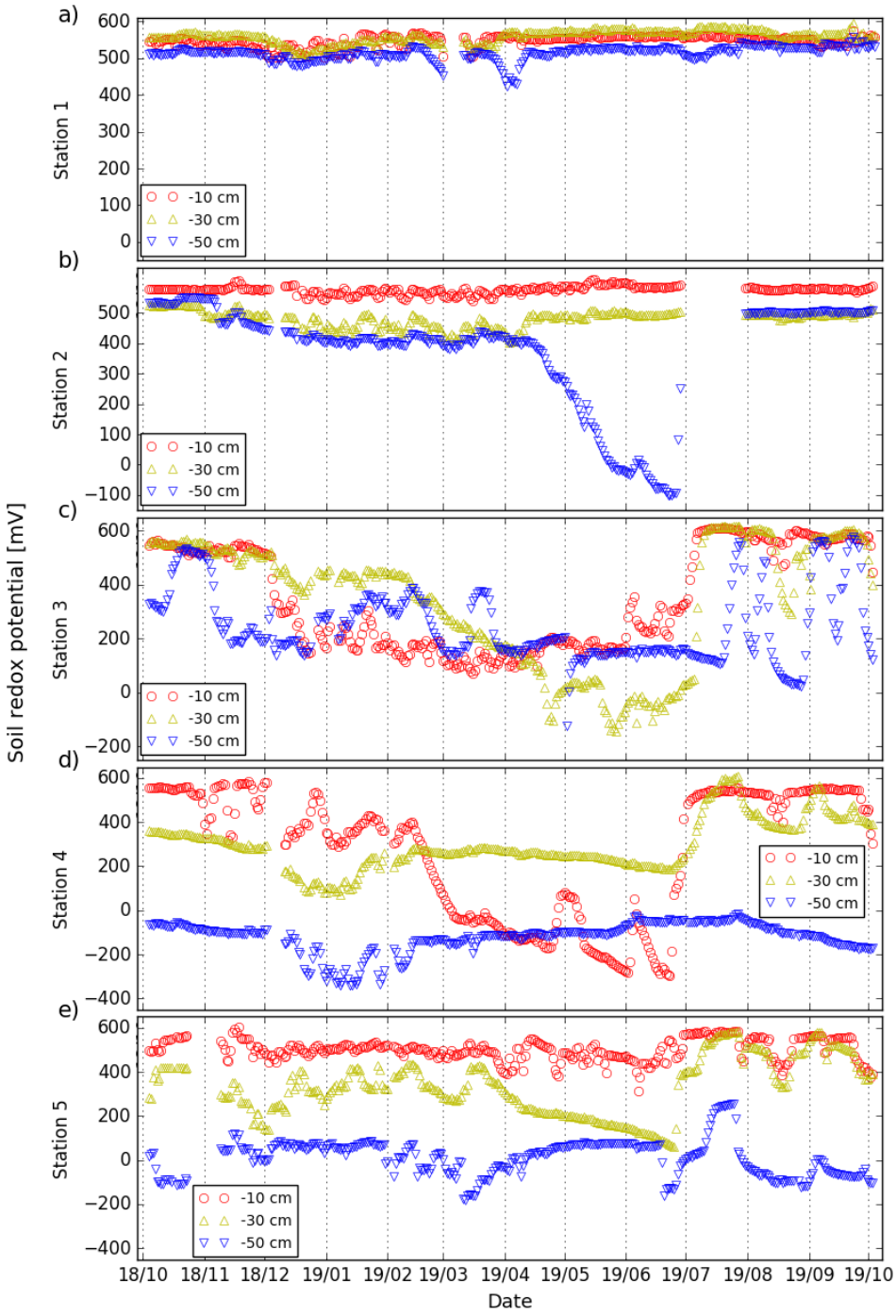

Figure 4.6 Daily redox potential at different depths at the five stations.

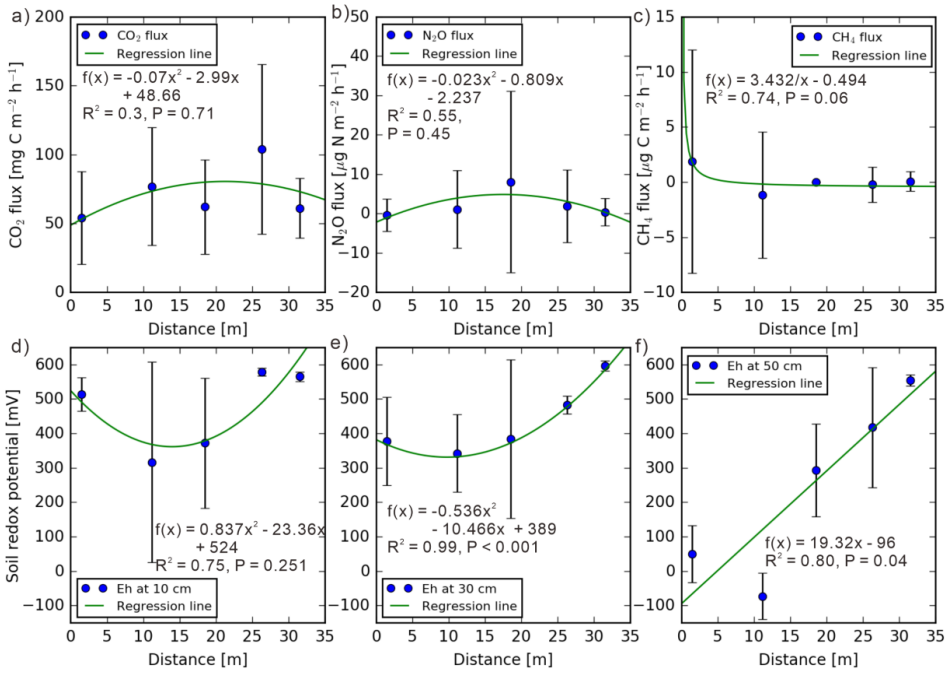

Figure 4.7 GHG fluxes, soil redox potential and the different distances from the stream.

The soil stations were installed on 19 and 20 July 2018 and were equipped with multiple soil sensors in three depths (Figure 4.2b). The measurement period lasted from October 2018 to September 2019. The soil greenhouse gas collection system was installed in October 2018. All soil sensors had been installed previously and had been allowed to equilibrate in situ two months prior to the start of data collection. Due to the varying depth and high stone content of the subsoil, it was not possible to select exactly the same depths for the medium and deep sensor levels. In order to be able to capture short-term changes in GHG emission rates during hydrological events (for example, soil redox conditions can change within hours after rainfall due to soil saturation or groundwater rise and promoting the emission of CH_4 or N_2O), soil redox potential measurements were performed with high time resolution, which is a prerequisite for the detailed analysis of the controls of redox potential on GHG emissions. All measurement data (except GHG flux data) were recorded continuously every 15 minutes and transmitted using the recently developed wireless sensor network SoilNetLoRa (Forschungszentrum Jülich GmbH, Jülich, Germany), which is based on the sub-gigahertz LoRa technology (Bogena, 2019). Data was transmitted and uploaded in near-real-time to a network server where it was retrieved by an application software. Meteorological data were taken from the TERENO climate station WU_EC_002 (50°50' N, 6°33' E) also located in the deforested area of the Wüstebach catchment (Figure 4.1). In the following, the automated soil and GHG emission monitoring system is described in detail:

Redox potential was measured using a system of several platinum electrodes and one reference electrodes (Type 4621, Ecotech, Bonn) with a resolution of 0.1 ± 3 mV. This soil redox potential measurement system was first developed by Mansfeldt (2004). Six platinum electrodes were installed ~10, ~30 and ~50 cm below the soil surface, and a reference electrode with Ag/AgCl salt bridge (Ecotech GmbH, Bonn, Germany)

was inserted next (within 45 cm) to the soil profile (Mansfeldt, 2003). The KCl gel of the reference electrodes were refilled every 2 to 4 weeks (depending on soil dryness) to ensure good contact between soil and redox electrode. The Eh measurements were related to the normal hydrogen electrode using the following equation:

$$Eh = E + E_{ref} \quad (4.1)$$

in which E is the potential measured against the Ag/AgCl reference electrode, and E_{ref} is the voltage difference between the standard hydrogen reference electrode and the Ag/AgCl reference electrode (+210.5 mV at 20°C). The E values were corrected by adding a correction value, relating them to the standard hydrogen electrodes according to the temperature and pH value in different layer. The pH values of the different soil layers were between 3.3 and 3.9 (Table 4.1). A predicted change in Eh of -59 mV occurs if the pH changes by one unit. Therefore, Eh is commonly referenced to pH 7 to make Eh values in different soils comparable (Bohn, 1971; Fiedler et al., 2007).

Soil water content and matrix potential were measured using SMT100 sensors (Truebner GmbH, Neustadt, Germany) and TensioMark sensors (Ecotech GmbH, Bonn, Germany), respectively. While two redox sensors were installed in parallel at each depth, SMT100 and TensioMark sensors were only doubled in the first layer (Figure 4.2) because the surface soil and its stronger variations of soil microbial activity has a higher impact on the surface gas emissions. The SMT100 soil water content sensor uses a ring oscillator with a steep pulse and oscillation frequencies between 150 and 300 MHz (Bogena et al., 2017) and also measures soil temperature using a digital temperature sensor (ADT7410, Analog Devices Inc., Norwood, United States) with an accuracy of ± 0.4 °C. The TensioMark sensor determines the matric potential from 1 to 10^7 hPa by measuring the water content of a porous ceramic with known water retention characteristics using heat dissipation (Durner and Or, 2006). Soil water-filled pore space (WFPS) values were derived from the soil water content measurements according to the following equation:

$$WFPS = \frac{SWC}{1-\frac{BD}{2.65}} \quad (4.2)$$

where WFPS is the water-filled pore space value (%), SWC is the soil water content (Vol.%), BD is the soil bulk density (g cm^{-3}) and 2.65 is the typical density of soil minerals (g cm^{-3}).

Groundwater level was monitored at each of the five locations using CTD-10 sensors (METER Group Inc., USA) installed in groundwater wells. The CTD-10 sensor uses a vented differential pressure transducer to measure the pressure from the water column to determine water depth with a resolution of 2 mm. The depths of groundwater wells ranged between 57.8 and 73.5 cm depending on soil thickness. The trends in the redox potential data at the beginning of the measurement period indicate that an equilibration period of 2-3 weeks is needed after installation before the sensors provide reliable measurements (e.g. due to contact issues). At Station 3, a longer data gap occurred from August 10 to August 28 in 2018 because the agar gel of the reference electrode shrank, and the electrode lost contact with the soil due to the dry soil conditions. Thus, it is important to check the agar gel condition on a weekly basis during the summer months and the reference electrode needs to be refilled with new agar gel if needed. However, because the redox potential sensors were not yet in equilibrium and the failure of sensors and power supply often occurred during the period, we did not use the data from this period.

GHG emissions were determined at each of the five stations with automated opaque long-term chambers (8100-104, LI-COR Biosciences, Lincoln, NE, USA) as depicted in Figure 4.2. The height of the chamber was 33 cm, and the chamber covered a soil area of 317.8 cm² and has a volume of 4076 cm³. The atmosphere of the chambers was circulated via the LI-8150 multiplexer (LI-COR Biosciences, Lincoln, NE, USA) to the central infrared CO_2 gas analyzer (LI-8100A, LI-COR Biosciences, Lincoln, NE, USA). A Fourier transform infrared spectrometer (DX4015 FTIR analyzer, Gasmet Technologies, Helsinki, Finland) was used to measure CO_2, CH_4 and N_2O concentrations. The FTIR analyzer was passively integrated in the flow system, using the pump of the LI-8100A and the multiplexer. After FTIR analysis, the gas flowed back to the multiplexer and from there to the corresponding chamber, resulting in a closed-loop system. The maximal flow rate of the loop system was 1.7l min^{-1}. Due to the flow-through setup, the effective chamber volume used for the GHG flux calculation consisted of the total volume of the measurement loop (5868.7 cm³ for Stations 1 and 2, and 5631.7 cm³ for the remaining stations).

The closure time of the chambers was set to 5 minutes at the beginning of the experiment, resulting in 24 measurements per day. On 15 January 2019, the closure time was set to 15 min to allow more stable GHG flow measurements, resulting in eight measurements per day (3-hour frequency). In contrast, the FTIR analyzer continuously measured with an interval of 20 sec. Therefore, the data had to be merged during the data post-processing. The automatic GHG flux measurement system and data post-processing compared the CO_2 fluxes measurements from the FTIR and Li-Cor system; when the results are similar and the start CO_2 concentration was below 1000 ppm, the fluxes results of N_2O are accepted (Figure S1 in the Supplementary Material). Subsequently, the processed chamber headspace GHG concentrations were used to calculate CO_2 CH_4 and N_2O fluxes from linear regression functions (Brümmer et al., 2008; Parkin et al., 2010; Collier et al., 2014; Wang et al., 2018; Wagner, 2019):

$$F = \frac{\Delta c}{\Delta t} \cdot \frac{10^6}{10^9} \cdot \frac{60 \cdot V_{Ch} MW}{A_{Ch} MV_{Corr}} \qquad (4.3)$$

F is the flux in mg m^{-2} h^{-1} or µg m^{-2} h^{-1}, and $\Delta c/\Delta t$ the slope of the linear regression in ppm·min^{-1} or ppb·min^{-1}. A_{Ch} (m^{-2}) and V_{Ch} (m^{-3}) are the base area and volume of the Li-COR chamber, respectively. MV_{Corr} is the pressure- and temperature-corrected molar volume of air (m^{-3} mol^{-1}), with $MV_{Corr} = 0.02241 \cdot [(273.15 + t)/273.15)] / (p_0/p_1)$, where t is the chamber headspace air temperature during the measurement (°C), p_0 is the standard atmospheric air pressure (Pa), and p_1 is the air pressure during the measurements (Pa). MW is the molecular weight of CO_2-C, CH_4-C or N_2O-N. Snow on the soil surface was removed during periods of snowfall. Due to occasional instrument failure of the GHG collecting system, in situ soil gas emission measurements were not continuously available at our sites. Therefore, GHG data with at least one valid CH_4 and CO_2 flux measurement per day are only available for 283 days, and for N_2O only for 269 days.

4.2.3 Sample collection and laboratory analysis

The soil horizons of the five soil profiles were sampled on 18 and 19 June 2018. The soil properties of the five soil stations are summarized in Table 4.1.

Table 4.1 Soil properties of the five soil profiles.

Profile	Horizon	Depth	pH($CaCl_2$)	TOC	N_{tot}	Bulk density	Total pore volume
	USDA	cm		%	%	g cm^{-3}	%
1	O	2-0	3.3	-	-	-	-

	Ah	0-8	3.5	10.5	0.61	0.5	-
	BgA	8-28	3.8	5.2	0.35	0.8	84
	BgE	28-48	4	0.94	0.12	1.4	73.2
	2BwdE	48-82	4	0.38	0.09	1.6	52.9
	3Cr	82+	4	0.38	0.07	n.d.	46.4
	O	4-0	3.3	-	-	-	-
	Ah	0-12	3.3	12.2	0.62	0.6	77.9
2	EA	12-30	3.9	9.3	0.53	0.7	75.8
	2Bwd	30-52	4	0.45	0.08	1.4	49.2
	3Cr	52-75+	-	-	-	n.d.	-
	O	6-0	3.7	-	-	-	-
	Ah	0-5	3.6	15.4	-	0.4	88.3
3	EA	5-18	3.7	-	-	0.8	86
	E	18-40	4	-	-	1.2	59.3
	2Bd	40-60	4.1	-	-	n.d.	-
	3Cr	60-80+	4.2	-	-	n.d.	-
	O	7-0	-	-	-	-	-
	Ah	0-4	3.6	15.4	-	0.4	-
4	EA	4-10	3.7	-	-	0.8	88.3
	E	10-40	4	-	-	1.2	86
	2Bd	40-60	4.1	-	-	n.d.	59.3
	3Cr	60-80+	4.2	-	-	n.d.	-
	O	6-0	-	-	-	-	-
	Ah	0-12	3.5	15.4	>1.2	0.4	81.3
5	BwA	12-23	3.5	16.9	1.2	1.3	82.1
	2Bw	23-33	3.9	12.5	0.96	-	-
	2CBw	33-40	3.9	-	-	-	-
	3Cr	40-70+	4	-	-	-	-

Additionally, soil samples were collected on 20 December 2018 for soil NH_4^+ and NO_3^- concentration analysis. Theses samples (three replicates) were taken from 0-30 cm using a HUMAX SH 300 soil sampler (Humax Soil Sampling Technologies, Switzerland) at five points near the automated soil chambers. After collection, the samples were divided into three different depths (0-10 cm, 10-20 cm and 20-30 cm), sieved to 2 mm and then extracted with 50 ml 0.1 M $CaCl_2$ solution. The extract was then analyzed for inorganic N concentrations (NH_4^+ and NO_3^-) using a Dionex ICS-3000 Ion Chromatography System.

4.2.4 Statistical analysis

We performed regression analyses and explored the relationships between WFPS, soil temperature, and GHG fluxes linear mixed-model analysis of variance (ANOVA) to test for significant differences. Multiple linear and nonlinear regression analyses were performed with the corresponding R packages (R Core Team 2019) to evaluate the influence of soil temperature and soil water content and to obtain a simple model of GHG emission rates. The calculation of the annual CO_2 emission rate was based on daily average values, and a linear interpolation between adjacent values was applied to fill the periods when data were missing.

4.3 Results

4.3.1 Meteorology and soil data

The highest and lowest monthly rainfall during the observation period (October 2018 to October 2019) occurred in December (205 mm) and July (38 mm), respectively (Figure 4.3). Total precipitation was 1079 mm, below the average annual precipitation of 1220 mm (Bogena et al., 2018). Monthly air temperature ranged between -1.4 and 16.7 °C, and soil temperature ranged between 2.7 and 14.9 °C. Figure 4.4 presents the concentrations of soil NO_3^- and NH_4^+ at the five measurements stations for three different soil layers (0-10 cm, 10-20 cm and 20-30 cm). At almost all stations, NH_4^+ and NO_3^- concentrations in the soil decreased with depth (Figures 4.4a and 4.4b). The mean NH_4^+ concentrations of the first layer down to the third layer were 89.5, 35.4, and 18.1 µg g^{-1}, respectively, while the corresponding mean NO_3^- concentrations were 72.8, 34.2, and 13.7 µg g^{-1}, respectively.

Table 4.2 Statistics of redox potential measurement in five stations in various depths.

	Depth (cm)	Mean Eh (mV)	Min Eh (mV)	Max Eh (mV)	Range	CV[a] (%)	Redox status[b]
Station 1	10	565 ± 14[c]	520	591	71	2.5	I
	30	596 ± 15	545	628	83	2.6	I
	50	554 ± 17	466	597	130	3.1	I
Station 2	10	578 ± 11	544	611	67	1.9	I
	30	483 ± 26	405	528	122	5.4	I
	50	417 ± 174	-60	592	652	41.8	I
Station 3	10	372 ± 189	96	630	533	50.8	II
	30	384 ± 230	-104	656	760	59.9	II
	50	293 ± 135	-75	624	700	46.1	II
Station 4	10	316 ± 291	-257	631	888	92	II
	30	342 ± 113	117	645	527	32.9	II
	50	-73 ± 68	-292	28	321	-93.1	III
Station 5	10	513 ± 49	321	621	300	9.5	I
	30	377 ± 128	99	621	521	34	II
	50	50±83	-136	293	429	165	III

[a]CV, coefficient of variation; [b]Redox status, I, Oxidating(> 400mV); II, weekly reducing(400 to 200mV); III, moderately reducing(200 to -100 mV); IV, strongly reducing (< -100 mV) (Mansfeldt et al., 2003); [c]SD, Standard deviation.

4.3.2 Variations in soil hydrological state variables and redox potential

Compared to summer, the relatively high amounts of precipitation and low evapotranspiration rates during the winter and spring months resulted in a generally shallow groundwater table with correspondingly high soil water contents and soil matrix potentials close to 0 mbar (Figure 4.5). The high soil wetness reduced the exchange of air between atmosphere and soil which led to a decline in the average soil redox potential at all depths until a rainless period in June 2019 occurred and the soil started to dry out, as indicated by a significant decrease in matrix potential (Figure 4.5). The groundwater level and the matrix potential were generally higher at the two stations closest to the stream (Stations 4 and 5, Figures S5 and S6), indicating a hydrological gradient within the riparian zone. During June 2019, redox potential at both -10 and -30 cm depth increased from below 400 mV to values above 600 mV within 15 days indicating oxic conditions due to better air exchange with the atmosphere (Figure 4.6). After June 2019, the soil redox potential values at 50 cm depth remained largely at a low level (< 200 mV) at Station 3, 4, and 5. The WFPS (46% to 100%) and soil redox potential (-292 mV to 656 mV) in the five stations exhibited large variability across the riparian zone (Table 4.2 and Figures S2-S6 in Supplementary material). From Table S1, the correlation values (Pearson's r) between redox potential and groundwater table level were between 0.70 and 0.74, and between SWC and groundwater table they ranged from -0.93 to -0.91. The soil redox potential was below 400 mV during winter and spring, and most of soil under oxic conditions after June 2019, with the soil

redox potential at -30 cm increased to values above 400 mV. Surprisingly, the lowest redox potential values were recorded at -10 cm (-257 mV) at Station 4 after a long period of water saturation, which was even more than 100 mV lower than the minimum redox value at the other stations (1, 2, 3 and 5). When the groundwater table level was above the electrode at -10 cm after strong rainfall events during the rainy period, redox potential at -10 cm at Station 2 and 3 dropped by 200 mV or more. At stations 4 and 5, both redox sensors installed at -50 cm were fully immersed in the groundwater during most of the monitoring period (Figures S5 and S6 in Supplementary material). Accordingly, the redox potentials deviated only slightly from the mean value of this depth (-73 ± 68 and 50 ± 83 mV respectively), and indicated reducing conditions in this layer (Table 4.2). On the other hand, the redox sensors installed at -10 and -30 cm depths as Stations 3, 4 and 5 showed considerably higher redox potential and larger SD values (Table 2). Figure 4.7 shows daily average redox potentials at the different depths and the relations with the distance to the stream. The distance to the stream had a quadric relation with redox potential at -30 cm ($R^2 = 0.99$, $p < 0.001$), whereas it had a linear relationship with the redox potential at -50 cm ($R^2 = 0.80$, $p = 0.04$). Except at Station 5, the soil redox potential values at -30 and -50 cm were positively correlated with the distance to the stream. Moreover, Figure S7 shows a negative linear relationship between redox potential at -10 cm and groundwater table level on a daily scale. This relation showed hysteretic behavior: the green and red dots indicate the soil re-wetting phase, while the blue dots indicate the soil drying phase.

4.3.3 Variations in GHG emissions

Table 4.3 Mean annual and maximum and minimum mean daily fluxes of CO_2, N_2O and CH_4 with the coefficient of variation at wüstebach.

	Station 1	Station 2	Station 3	Station 4	Station 5	Mean Stations 1-5
			CO_2 Fluxes (mg C m^{-2} h^{-1})			
Annual mean (± SD[a])	61.09 ± 21.74	103.96 ± 61.73	62.05 ± 34.32	76.78 ± 42.75	54.00 ± 33.50	71.58 ± 44.73
Maximum	113.35	270.03	156.29	227.29	134.28	270.03
Minimum	23.04	9.17	7.10	7.09	7.14	7.09
N	231	244	257	267	251	1250
CV[b] (%)	35.67	59.39	55.31	55.68	62.04	62.49
			N_2O Fluxes (μg N m^{-2} h^{-1})			
Annual mean (± SD)	0.37 ± 3.51	1.93 ± 9.27	8.03 ± 23.05	1.09 ± 9.89	-0.34 ± 4.12	2.26 ± 12.72
Maximum	43.36	89.28	152.97	122.60	9.18	152.97
Minimum	-8.97	-15.70	-9.97	0	-46.93	-46.93
N	231	244	257	267	251	1250
CV (%)	962.44	482.00	287.29	911.52	-1193.47	563.99
			CH_4 Fluxes (μg C m^{-2} h^{-1})			
Annual mean (± SD)	0.06 ± 0.90	-0.22 ± 1.60	0 ± 0	-1.16 ± 5.73	1.88 ± 10.12	0.10 ± 5.40
Maximum	13.30	0	0	0	79.89	79.89
Minimum	0	-15.18	0	-59.12	0	-59.12
N	215	230	241	253	236	1175
CV (%)	1466.29	-711.83	0	-494.78	538.66	5660.81

[a]SD, Standard deviation; [b]CV, coefficient of variation; N, number of valid CO_2, N_2O and CH_4 fluxes.

All daily mean CO_2 fluxes were greater than zero and valid (non-zero), while N_2O and CH_4 fluxes were significantly different from zero on only 73 days and 32 days, respectively. The soil CO_2 emissions ranged

from 54.00 ± 33.50 to 103.96 ± 61.73 mg C m^{-2} h^{-1} between Station1 and Station 5. They tended to be lowest during the winter season, while the highest CO_2 emission rates were observed in June simultaneously with the lowest soil water content and the highest soil temperature (Figure 4.5). The CO_2 flux varied significantly between the stations ($p < 0.01$). The highest and lowest mean daily CO_2 flux rates were measured at Stations 2 and 4 with 270.03 and 7.09 mg C m^{-2} h^{-1}, respectively. The annual average soil CO_2 emission rate across all stations was 71.58 ± 44.73 mg C m^{-2} h^{-1} (Table 4.3). The coefficient of variation for CO_2 fluxes at Station 1 was 35.5% (Table 4.3), while it was between 55% and 63% at the other stations. The seasonal variations of N_2O emissions were less pronounced than for CO_2, and on most of the measurements (1177/1250, 94%) we found no N_2O emissions significantly different from zero (absolute flux value < 5 µg N m^{-2} h^{-1}). The lowest mean annual N_2O emission (0.37 ± 3.51 µg N m^{-2} h^{-1}) was found at Station 1 (Table 4.3), which was 16% of the mean annual N_2O emission rate of all the stations (2.26 ± 12.72 µg N m^{-2} h^{-1}), and the uptake of N_2O were observed at Station 5 (-0.34 ± 4.12 µg N m^{-2} h^{-1}) (Table 4.3). A significant short-term increase of the N_2O emission in winter was observed for Stations 2 and 3. The annual daily mean CH_4 fluxes fluctuated between the stations from -59.12 to 79.89 µg C m^{-2} h^{-1}. Substantial CH_4 emission was found at the near-stream Station 5, while at Station 4 negative CH_4 fluxes were observed indicating net CH_4 uptake (Table 4.3). However, for most of the measurements (1142/1175, 97%), CH_4 fluxes were zero or close to zero (absolute flux value < 5 µg C m^{-2} h^{-1}).

4.3.4 Correlation of CO_2 fluxes with environmental variables

Both soil temperature and WFPS played a vital role in governing CO_2 fluxes in our study. The CO_2 flux correlated significantly with soil temperature at -10 cm and water table depth (with a Pearson's correlation coefficient of 0.93 and 0.61, respectively) (Table S1). A simple exponential model was used to describe the temperature dependency of the soil CO_2 fluxes, using soil temperature measurements at 10 cm depth ($R^2 = 0.71$, $p < 0.001$) (Figure 4.8a). In contrast, a quadratic relationship of CO_2 fluxes with WFPS was found, but with much lower R^2 ($R^2 = 0.13$, $p < 0.001$) (Figure 4.8b). The lowest CO_2 emission was found at Station 5 (54 ± 33.5 mg C m^{-2} h^{-1}), while CO_2 emission rates where significantly higher for the other stations (61.09 ± 21.74 - 103.96 ± 61.73 mg C m^{-2} h^{-1}). Also a significant, albeit weaker, relationship between daily CO_2 flux and daily soil redox potential was found (Pearson's r = 0.20~0.22) (Table S1). Figure 4.9a shows the linear regression between the monthly mean CO_2 fluxes and the groundwater table depths (R^2 of 0.68, $p = 0.001$). Furthermore, Figures 4.9b and 4.9c show the quadratic relationship between monthly average CO_2 flux and redox potential at -10 cm and -30 cm. The minimum CO_2 flux values of the functions occurred when soil redox potential values were 389 and 433 mV, respectively, i.e. close to 400 mV, which is the value that separates the redox potential into oxic and weakly reducing conditions.

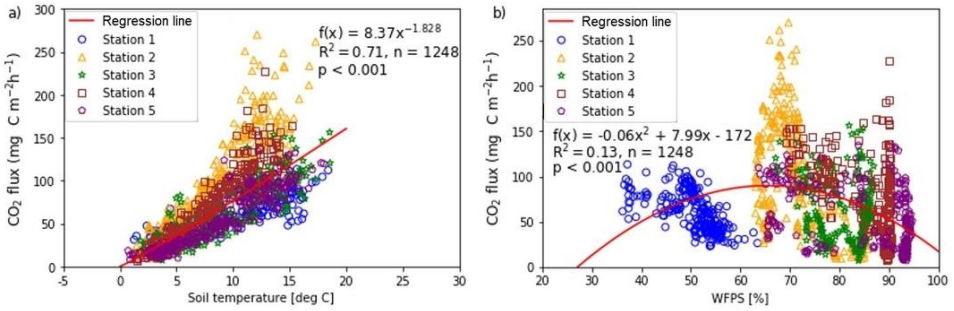

Figure 4.8 Relationship between daily CO_2 fluxes and soil temperature (a) and WFPS (soil water-filled pore space) (b).

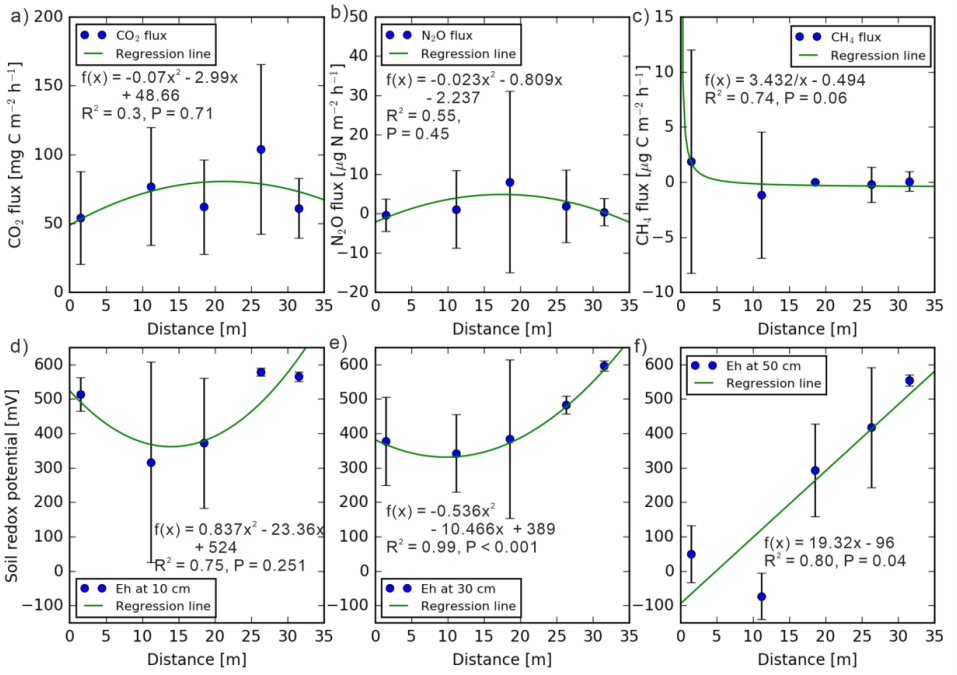

Figure 4.9 Correlations between monthly means of CO_2 fluxes and groundwater table level, and with soil redox potential Eh at different depths (mean of all stations).

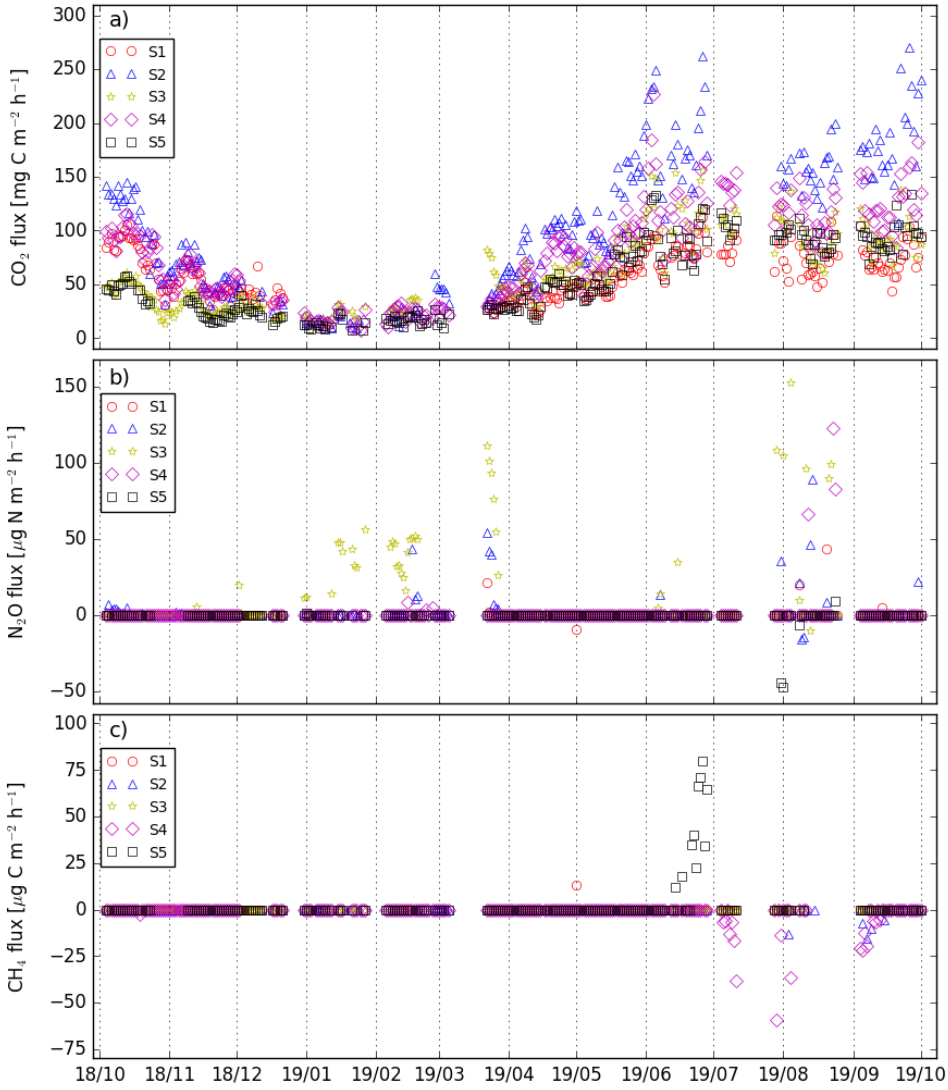

Figure 4.10 Variations in (a) CO_2 fluxes, (b) N_2O and (c) CH_4 fluxes at S1 (station 1), S2 (station 2), S3 (Station 3), S4 (station 4) and S5 (station 5).

4.3.5 Correlation of N_2O fluxes and CH_4 fluxes with environmental variables

During the periods of high groundwater table in winter, N_2O emission events occurred at all five stations, with the main emission events occurring at Stations 2 and 3 (Figure 4.10b). Most of the N_2O emissions events at Stations 3 occurred when the soil redox potential value at -10 cm was below 400 mV and between 100 and 200 mV. The correlations between the N_2O flux and the other soil variables were mostly weak (Table S1). The CH_4 emission rates during our experiment were rare. From Figure 4.10c it becomes apparent that only Station 5 showed notable CH_4 emissions between 18 and 28 June 2019, with a total CH_4 emission of 11.6 mg C m^{-2} (calculated from the daily average emission rates). The CH_4 emission events started after soil redox potential at -50 cm decreased to values below -100 mV as the result of stronger

rainfall events during summer 2019 (Figures 4.6e and 4.9c). The CH_4 emission coincided with low soil redox potential values (200 mV) at -30 cm that are suitable for CH_4 to pass through this soil layer without being oxidized (Figure S6). However, Station 3 showed no significant CH_4 emissions, even though the redox potential at -30 cm had a similarly low soil redox potential (-89 ± 13 mV) from May 24 to 28, 2019. In contrast, several CH_4 uptake events occurred at Station 4 in July and August at soil redox potential values above 400 mV at -10 cm and -30 cm and around 0 mV at -50 cm. The significant CH_4 uptake events at Station 4 occurred when the daily average soil redox potential was above 350 mV, and large quantities of CH_4 were produced after the redox potential fell below a critical threshold of 200 mV at Station 5 (Figure S8).

4.3.6 Multivariate regression analysis

In the following, a linear stepwise regression analysis was used to find environmental variables (soil temperature, water-filled pore space, soil matrix potential and soil redox potential) that can predict the measured soil GHG fluxes. It has to be noted that analyzed environmental variables were not completely independent and could change with depth (Table S2). In the model, the soil GHG fluxes are considered as dependent variable and the environmental factors as independent variables. The R^2 of the linear regression of CO_2 at the five stations ranged from 0.83 to 0.89, with soil temperature being the most important predictive variable (Table S2). However, the stepwise approach leads to many similar regression coefficients, e.g. the WFPS having opposite signs at different levels. The stepwise regression results for N_2O and CH_4 were poor ($R^2 < 0.45$), indicating that CH_4 and N_2O is difficult to predict with simple linear regression models.

4.4 Discussion

4.4.1 Redox potential monitoring

We found significant spatiotemporal differences in soil redox potential indicated that the biogeochemical processes and their controls differed between the stations and even within the same soil horizons (Vereecken et al., 2016; Wanzek et al., 2018). These soil redox potential variations in our studies are consistent with previous studies, i.e. the mean redox potential was lower for the soils that were stronger influenced by groundwater, and redox potential decreased with depth (Table 4.2 and Figure 4.5, Mansfeldt, 2003; Dwire et al., 2006; Yu et al., 2006), indicating limited oxygen diffusion during saturated conditions, which in turn triggered anoxic conditions (Ponnamperuma, 1972; Yang et al., 2006; Wang et al., 2018). Moreover, we found a distinct hysteresis in redox potential changes after the groundwater table level changed during drying or rewetting phases. As in other studies, we found that the fluctuation of the groundwater level rapidly changed redox potential, resulting in a more dynamic pattern (Seybold et al., 2002; Thomas et al., 2009). The large-scale pattern in the relationship between groundwater table and redox potential is consistent: Little variation in groundwater table depth resulted in relatively constant redox potential (e.g. Station 1, Figure S2), whereas increased variability in groundwater table resulted in stronger

redox potential variations. With the exception of Station 4, most redox sensors installed at 10 cm depth showed considerable higher redox potential values (around 600 mV) and only small variations after rainfall events occurred.

Even though the electrodes were below the water table level, the soil at -30 cm depths at Station 4 and 5 can exhibit higher redox potential values after precipitation or water level increase, potentially due to the ability of wetland plants to transport O_2 from the atmosphere to the root zone (Grosse et al., 1992). Flessa and Fischer (1992) found that when soil is at reducing condition, the root zone of vegetation can even raise the redox potential from the surface of the root from 120 mV to 420 mV.

The differences in soil wetness also affected re-vegetation of the deforested riparian zone: the further away from the stream, the more ryegrass (Lolium perenne L.) was growing, and the closer to the stream, the more bulrushes (Juncus effusus L.) were present. According to Shoemaker and Kröger (2017), the type of vegetation can also control the soil redox potential dynamics. It should also be noted that the small-scale spatial variability may not have been adequately captured since we could only use two redox potential sensors at each depth in our experiment. Other studies recommend the installation of 6 and up to 10 sensors per depth for soils with fluctuating groundwater levels (Fiedler et al. 2007; Wanzek et al., 2018).

4.4.2 Soil respiration

In our study, we found that the average CO_2 emission in the riparian zone of the Wüstebach catchment was 71.58 ± 44.73 mg C m^{-2} h^{-1}, which is slightly below the mean values of other studies in temperate forests in Europe (75-79 mg C m^{-2} h^{-1}) (Rosenkranz et al., 2006; Wu et al., 2010). Ney et al. (2019) compared the CO_2 fluxes at the deforested and forested part at our research site, and the annual emission rate ranged from 91 to 96 mg C m^{-2} h^{-1}, which was slightly higher than in our riparian zone. Poblado et al. (2017) found higher CO_2 emission rates in a riparian zone in Northeastern Spain (458 ± 308 mg C m^{-2} h^{-1} compared to 318 ± 195 mg C m^{-2} h^{-1}) in a sub-humid Mediterranean climate. On the other hand, our CO_2 emission rates were significantly higher compared to a rehabilitated forest riparian zone in Ontario, Canada (27 ± 3 mg C m^{-2} h^{-1}) in a temperate climate with hot, humid summers and cold winters (De Carlo et al., 2019). The distances of their measurement chambers to the streams were within 32 m. Their experiments were performed in 2013 and from May 2015 to May 2016, respectively. Phillips and Nickerson (2015) and other studies (e.g. Fang and Moncrieff, 2001; Ludwig et al., 2001; Tang et al., 2003) assumed an exponential relationship between soil respiration and soil temperature. In accord with this assumption, the CO_2 flux has an exponential relationship with soil temperature in our study. Previous studies showed a distinct seasonal pattern of CO_2 fluxes, indicating the close relationship between CO_2 emissions and soil temperature (Papen and Butterbach-Bahl, 1999; Schindlbacher et al., 2004; Teiter and Mander, 2005; Kitzler et al., 2006; Pilegaard et al., 2006; Wu et al., 2010; Suseela et al., 2012). A correlation analysis revealed that soil respiration in the riparian zone was mainly dominated by soil temperature and WFPS due to lower microbial activity and limited O_2 availability (Monson et al., 2006). In the summer, the low soil moisture and high temperature were favorable for enhancing microbial activity and CO_2 emissions. However, in the colder and wetter seasons (winter and spring) were unfavorable for the microbial activity (Mander et al., 2008). We found that CO_2 emission rates decreased with decreasing groundwater table depths (Figure S7), suggesting that soil water is also an important controlling factor for CO_2 emission in the riparian zone as

in other studies (e.g. Chang et al., 2014; Poblador et al., 2017). Station 1 showed the lowest CO_2 emissions during summer (July, August and September) in 2019 due to dry soil conditions, as indicated by the low WFPS (28.1 ± 4.7%) values at -10 cm (Figure 4.10 and Figure S2). Shi et al. (2014) found a positive correlation of CO_2 emissions with the C/N-ratio. Therefore, the C/N-ratio variations across the profiles at -10 cm soil layer may explain the higher annual CO_2 emission rate at Station 2 (C/N-ratio: 19.7) than at Station 1 (C/N-ratio: 12.8).

Marín-Muñiz et al. (2015) concluded that the redox potential plays a vital role in GHG emissions in coastal wetlands. However, we found that the daily mean soil redox potential had only a weak positive correlation with daily CO_2 emissions ($r = 0.21$) and similar to the results was conducted by Gebremichael et al. (2017). Overall, regarding the relationship between the monthly average soil redox potential at -30 cm and CO_2 fluxes, the soil redox potential may help to interpret the dominant CO_2 flux from aerobic and anaerobic respiration, but this still needs to be investigated in further studies.

4.4.3 Soil nitrous oxide emissions and N variations

Because the Wüstebach catchment is an oligotrophic natural ecosystem, the soil N mainly originates from atmospheric dry and wet deposition, with some potential biological nitrogen fixation. Unlike fertilized agricultural soils, such soils are therefore unlikely to be a significant source of N_2O (Galloway et al., 2008; Amundson and Davidson, 1990). We found daily average N_2O emissions of 2.26 ± 12.72 µg N m^{-2} h^{-1}, which similar to other studies in spruce forests (Krause et al., 2013; Wu et al., 2010) or riparian zones (Batson et al., 2015). Our results showed that the main N_2O emission occurred after heavy rainfall in winter followed by soil saturation, whereby denitrification can be assumed to be the main pathway due to the low soil redox potential and high WFPS values at station 3 (Pilegaard et al., 2006; Wolf and Russow, 2000; Yu et al., 2006). However, the N_2O emission occurred at Station 2 when the soil was in oxic condition at all depths (> 450 mV) during winter (Figure S3), indicating that nitrification may have been the dominant N_2O main pathway (Masscheleyn et al., 1993).

4.4.4 Methane emissions

Compared to other studies in typical riparian zone wetlands, the CH_4 emission rates we found in the riparian zone of the Wüstebach catchment were very low. However, the study of Vidon et al. (2016) also showed uptake of CH_4 from only -20.41 ± 55.80 to -48.30 ± 6.25 µg C m^{-2} h^{-1} in a riparian zone that compares well to our results (Table 2). The main CH_4 production occurred at Station 5, and as Figure 4.6e shows, the CH_4 emission events started when soil redox potential at -50 cm dropped below -150 mV, which has been described as a critical value for CH_4 production in soils (Wang et al., 1996; Yu and Patrick, 2003). However, also higher threshold values have been described in the literature, such as -110 mV for reed soils (Huang et al., 2001), or even as high as 300 mV, as found for a coastal forest at the Gulf of Mexico (Yu et al., 2006). In our study, conditions suitable for methanogenesis (high moisture and low soil redox potential) mainly occurred in winter and spring, but the low temperatures during this period may be the reason for the low methane production rate (Nazaries et al., 2013). Another explanation for the low observed CH_4 emission rates in our study could be that O_2 rich water of the lateral subsurface flow may have suppressed CH_4

production and emission in the riparian zone (Itoh et al., 2007). Although the soil redox potential measured during CH_4 production at Station 5 was critical for CH_4 emissions at this station, we found that this particular redox potential value was not suited to predict CH_4 emission at Station 3. Therefore, individual soil redox potential measurements may be required in different soil types in order to obtain the specific critical soil redox potential value for CH_4 production, especially in areas where soil properties, like in riparian zones, vary greatly at short distance. Stations 1, 2 and 3 showed hardly any CH_4 emission or uptake events, which is most likely due to the generally higher soil redox potential values especially in the topsoil, which could intercept potential CH_4 production from deeper areas and thus preventing further emission to the atmosphere. Furthermore, the CH_4 emissions from station 5 may have been enhanced by *Juncus effusus*, allowing CH_4 to enter the roots in the highly reduced soil and bypass the methanotrophic layer at -10 cm (Henneberg et al, 2016). The low CH_4 emission and uptake rate indicated that our site was neither an important CH_4 sink nor source. Therefore, the CH_4 oxidation or emission represented only a small fraction of C cycling in this riparian zone.

4.5 Conclusions

Here, we presented a newly developed automated measurement system for soil hydrological parameters and redox potential in combination with GHG flux measurements, featuring real-time data transmission for better data management and maintenance. The observation system was deployed in a riparian zone of a deforested Norway spruce forest for one year to trace the different microbial N_2O production pathways (nitrification or denitrification) and to characterize the dominant GHG. We found that mostly soil temperature as well as hydrologic events in the riparian zone controlled the GHG emissions. Most of the GHG emissions occurred in the form of CO_2 at our research site, even in the wet soils close to the stream. The daily mean soil-atmosphere exchange of CO_2 and N_2O at our site was 1717.92 ± 1073.52 mg CO_2-C m^{-2} d^{-1} and 54.24 ± 305.28 µg N m^{-2} d^{-1}. Soil temperature was identified as the most critical factor in controlling CO_2 emissions in our sites. We found that soil redox potential in the surface soil layer showed hysteretic behavior in wetting and drying phases, and that soil redox potential affected soil CO_2 emissions. In addition, by means of soil redox potential measurements we were able to determine if the soil entered highly reduced conditions, which is the prerequisite for CH_4 production. Soil N_2O emissions varied across temporal and spatial scales, while both soil moisture and soil redox potential helped to interpret soil N_2O sources and pathways. In summary, we could show that soil redox potential measurements in riparian zones help to better understand the controls of GHG production. Therefore, we recommend implementing soil redox potential measurements as routine components of long-term monitoring projects in critical zone observatories for better understanding the soil GHG production processes and their controlling factors.

Chapter 5

Synopsis

5.1 Summary

This research sought to describe and characterize the relationship between Eh and GHG production in soils at different scales and complexities, from controlled laboratory lysimeter experiments to long-term field measurements in a natural riparian zone. The Eh has been studied for decades and is frequently applied in a broad range of environmental disciplines, e.g., microbial ecology, geochemistry, biogeochemistry, limnology, and soil science. However, variations in soil Eh are still not well understood due to their high degree of heterogeneity and high number of influencing factors. Moreover, unlike soil moisture or temperature, the Eh has been neglected in most soil studies in GHG emissions. In the first part of this thesis, the state-of-the-art of Eh and GHG emissions and the experimental approaches used in this thesis are presented. The experiments focus on the characterization of the effect of Eh on soil GHG emission as triggered by water level changes, irrigation, and N fertilization. Furthermore, this thesis explores whether the soil Eh can be used as an indicator for the formation pathways of N_2O in the soil, in addition to other influencing factors like soil water potential, temperature, and fertilization. The second chapter of this thesis aimed to explore the possibility of utilizing Eh measurement as a predictor for GHG emissions in the lab lysimeter experiment under varying water table levels. It was found that the N_2O emission was highly correlated with water level changes and fertilizer application. Before fertilizer application, there was a negative relationship between N_2O emission and Eh. As Eh increased, N_2O emission rate decreased. Higher CO_2 emissions were detected after fertilization at high Eh, and in these periods the N_2O fluxes and Eh were positively correlated. The end-member analysis of the ^{15}N site preference and the $\delta^{18}O$ signatures of N_2O indicated that the main N_2O emissions resulted from the nitrification process after fertilization. Before fertilization, the soil water potential and N_2O showed an exponential decay relationship, but after fertilization, a positive linear correlation between soil water potential and N_2O production was found. Before fertilization, N_2O emission rates were higher after saturation, and the N_2O peaks occurred when the water table was lowered in the post-fertilization period. These could be attributed to the different availability of inorganic N substrates (NH_4^+ and NO_3^-).

Chapter 3 introduces a more complex laboratory experiment, which also considered the effects of precipitation, irrigation, and fertilization on GHG emission. In addition, a ^{15}N fertilizer tracing method was introduced for the investigation of the N_2O production and N conversion processes. A series of irrigation experiments revealed the Eh dynamics and ranges in the agricultural soil before and after the irrigation and fertilization events. The Eh at two depths (11 and 35 cm from soil surface) showed the strongest reducing conditions before fertilization. Significant variations of N_2O emissions due to hydrologic events like irrigation or fertilization were found. The N_2O fluxes reached up to 600 µg N m^{-2} h^{-1} at high dissolved NH_4^+ concentration in soil pore water (above 15 µg/ml at -11 cm).

Before fertilization, the results showed high variations and lower mean values of Eh. After the addition of NH_4^+ to the soil, the CV of Eh (from 49% to 5%) became lower with increasing NO_3^- concentration. A possible reason may be the effects of the prolonged saturated period before fertilization. The irrigation events caused limited oxygen supply in the soil, which led to a decreased Eh level. The fertilization events increased the dissolved NO_3^- concentration at the bottom of the soil column due to infiltration. Here, the NO_3^- acted as a redox buffer and slowed down the Eh decrease rate.

Interesting information was gained from the isotope measurements. As could be evaluated from the isotopic signature ($\delta^{15}N^{bulk}$, $\delta^{18}O$, ^{15}N SP), the N_2O before fertilization originated exclusively from bacterial or archaeal nitrification (i.e., hydroxylamine oxidation). The $\delta^{15}N$ value of N_2O after fertilization indicated that almost 100% of the emitted N_2O originated from the applied fertilizer, while most of the NH_4^+ was converted to NO_3^-. Furthermore, a decrease in ^{15}N enrichment occurred with increasing soil depth.

The experiments described in the fourth chapter studied the spatial variability of Eh and GHG emission rates in a deforested riparian zone. Precipitation events and fluctuating groundwater levels along the slope caused spatial and temporal Eh variations. Soil with reducing conditions was mainly found close to the stream. At the five stations in the riparian zone, a wide range of daily average Eh values was found, ranging from -292 mV to 656 mV within a year of observation. In addition, soil water content showed an increasing trend from the slope area to the near-stream area. The CO_2 emissions showed a distinct seasonal pattern with the highest emission rates in summer. The CO_2 fluxes were closely (positively) related to soil temperature and (negatively) to water content, but there was no significant correlation with Eh. In this experiment, only the near-stream soil showed a significant CH_4 emission (around 3 m from the stream), where the low Eh (<-150 mV) at -50 cm was suitable for methanogenesis, because this Eh value is the threshold for soil CH_4 production. In contrast, we observed CH_4 uptake events at the other stations which had shown low flux rates. We conclude that this site was neither an important sink nor source of CH_4, and that our study site was an oligotrophic near-natural ecosystem with low daily N_2O emissions of around 2.25 µg N_2O-N m^{-2} h^{-1}. N_2O emission events mainly occurred at mid-slope stations (26.3 and 18.5 m from the stream, respectively). N_2O source partitioning was performed on the bases of the Eh values at -10 cm. The long-term measurements of greenhouse gas emissions in the riparian zone indicated that CO_2 emissions were substantial, while N_2O and CH_4 fluxes were minor. This experiment revealed also that soil Eh measurements can be utilized for evaluating the contribution of oxidation and reduction processes to biogeochemical cycling in the soil and help to interpret the production of GHGs (CO_2, N_2O and CH_4) in the riparian zone.

5.2 Synthesis

This thesis aimed to evaluate the role of soil Eh in soil GHG emissions. Although experiments on soil GHG emissions have been conducted for many years, a detailed analysis of the involved processes is still challenging, and a full consideration of all soil variables in the biogeochemical process models has not been successfully implemented yet. This research aimed to extend our understanding of the suitability of soil Eh measurements for the characterization of biogeochemical processes and as indicator of the main sources of N_2O in the soil (nitrification and denitrification). Soil variables, like soil moisture and soil N substrates, affect N_2O production by switching between different pathways. Therefore, we designed a series of laboratory experiments with changing soil moisture conditions to modify the redox state of the soil and related GHG emissions.

The results presented in Chapter 2 show that through the deployment of soil Pt redox electrodes at different depths in the soil column, we can analyze the soil Eh changes at various depths which are affected by anoxic and aerobic conditions as well as variations in water levels. Soil saturation causes the soil Eh to decrease because soil microbial activities may deplete oxygen, and water table fluctuations cause spatial and temporal variations of Eh. However, through repeated experiments, we further discovered that the N content in the soil can also affect the change of soil Eh. Obviously, under the same level of soil saturation, the Eh increased after adding N fertilizer.

Unlike other experiments which added water from top of soil column (e.g. Flessa and Beese, 1995; Rubol et al, 2012), our experiments featured stable water tables which were set to ensure a more controlled water distribution in the soil and thus simplify the complexity of the interactions between soil moisture and redox potential. In this way it was possible to verify that under the condition of a certain water level and thus soil saturation, the change of Eh in the soil also depends on many other factors, such as the change in the soil ion composition. This also showed that N substrate monitoring is of great importance for subsequent experiments. Nevertheless, soil water potential could be used as a predictor for a preliminary model of CO_2 and N_2O production, which helps in interpreting the relationship between water level and GHG emissions under less complex conditions. Just as similar experiments have concluded (Yu et al., 2004; Yu et al., 2006), soil N_2O emission events occurred within certain Eh ranges, either in oxic or moderately anoxic conditions suitable for nitrification or denitrification, respectively. Based on these results one can conclude that soil moisture changes lead to variations in soil Eh and greenhouse gas emissions, and that a major contribution of nitrification or denitrification to N_2O fluxes can be distinguished on the basis of soil Eh ranges.

These experiments conducted confirmed the tight relationship between soil Eh and GHG emission changes. In particular, it was found that Eh can help distinguish the sources of soil-borne N_2O fluxes. However, the shortcomings of our experiments in the first results chapter were that Eh monitoring was only restricted to the first 19 cm of soil, and that the soil fertilizer was added from the bottom, which is not consistent with common agricultural practices. Therefore, in the experiments of the next results chapter these issues were addressed, and the focus was laid on studying soil Eh and the N cycle in the soil to explore this relationship further under more realistic conditions.

The research in Chapter 3 was brought to the next level, in which the Eh monitoring in the soil column consisted of monitoring the soil Eh variation after precipitation or fertigation, and with the help of

^{15}N-labeled ammonium sulfate, we were able to obtain useful information on the soil N cycle from the collected isotope data. In this experiment, precipitation and fertigation were simulated more similar to field conditions and more closely mimicking agricultural practices such that the results could better reflect agricultural N_2O production, while previous experiments did not fully take these factors into consideration. Because of the longer duration of the period of soil saturation, the results demonstrated that Eh ranges were larger in deep soil compared to surface soil, which is consistent with the finding of other studies (Mansfeldt, 2003; Wanzek et al., 2018). This phenomenon was due to oxygen diffusion impairment which occurs under high saturation levels, as remaining O_2 was consumed and alternative electron acceptors were utilized in deeper sections of the soil column. Compared with other studies that also studied soil Eh and N_2O emission in a soil column (Flessa and Beese, 1995; Rubol et al., 2012), our experiments also comprised N isotope tracing measurements and performed a high-resolution measurement of Eh to obtain more accurate results. We found that N fertilization affected the distribution of dissolved N_2O in the soil, the emission of N_2O in the soil, and the change in soil Eh. The added N became part of the soil electron acceptor pool (in the form of nitrate) and was the reason for the Eh remaining at an intermediate level despite the water saturation, which was consistent with the first experiment, because the converted NO_3^- served as alternative electron acceptor after oxygen had been consumed and Eh had decreased.

The soil ^{15}N signature and intramolecular distribution of ^{15}N in N_2O clearly revealed the main source of N_2O in the soil before fertilization. Combined with Eh change, this enables one to distinguish the source of N_2O fluxes from a specific part of the soil. These results indicated that the added fertilizer had the most significant impact on N_2O and was used as the main N_2O control factor in the agricultural soil. However, since it is difficult to quantify the conversion rate of dissolved N in the soil non-destructively, the level of and change in Eh could be used to evaluate and quantify the nitrification and/or denitrificationi rate after N fertilization. The change in Eh also controls the conversion efficiency of dissolved NH_4^+ to NO_3^-, where a high Eh level reflected a conversion of the added NH_4^+ to NO_3^-, which suggests that N may be consistently lost to groundwater as a result of permanently high Eh, combined with high drainage volume.

Eh variations and the natural abundance of ^{15}N and its intramolecular distribution in N_2O as well as ^{15}N-labelled mineral fertilizer allow for distinct N_2O formation partitioning. On the basis of this ^{15}N tracer approach, we proved that the Eh value might be a good indicator of the prevalence of nitrification or denitrification in the soil N cycle.

Similar to the experiments in Chapter 2, the same soil column was used for the experiments in Chapter 3, but these experiments were more comprehensive and deployed more Pt redox sensors in deeper soil layers to analyze the spatial and temporal variability of soil Eh. More accurate soil isotope tracing and analysis in these experiments made N_2O emission source analysis results more accurate. Moreover, the soil dissolved N illustrated the relationship between Eh, and fertigation and irrigation processes, making our experimental results more similar to the actual N_2O emission rates of agricultural soils. This chapter has increased our understanding of the relationship between Eh changes and N_2O emissions in farmland soils. However, the experiments of Chapter 2 and Chapter 3 are still limited because they were conducted under laboratory-controlled conditions. Further research would benefit

from carrying out *in-situ* experiments to determine whether the results of the laboratory experiments can be applied to field conditions.

In Chapter 4, the experiments were extended to the field scale, where the potential of Eh measurements for characterization of GHG emissions in a riparian zone was to test under natural conditions. In the riparian area of the forest catchment, the groundwater level changes were more dynamic, and Eh showed more variability than in a typical agricultural soil, because of the differences in the biogeochemical conditions in the wetland environment. These differences are mainly caused by the oxygen dynamics associated with the water-table fluctuations, but also by the presence of metal ions or differenes in soil gas permeability or other soil heterogeneities, resulting in the larger redox changes in this riparian area. Water table fluctuations caused spatial gradients and temporal variations in local redox conditions and soil water potentials. Moreover, our experiments also found Eh may be controlled by the type of vegetation and plant distribution. Unlike other studies in the temperate riparian zone (e.g. Batson et al., 2015; Poblador et al., 2017), our experiments showed that the riparian zone in our study was not an important source of N_2O. The most likely explanation is because our research site is an oligotrophic (N-limited) natural ecosystem, and the greenhouse gas emissions are therefore dominated by CO_2. Although CH_4 emission events were rare during the observation period, it proved that the Eh may be a useful indicator for the threshold of CH_4 emission and may be implemented as a measurement method in other soil CH_4 hot spots like paddy soils. As discussed above, our measurement results in the riparian zone revealed CO_2 as the main GHG emissions in this area, and hydrology also played a fundamental role in GHG production because it controls the substrate availability and the redox conditions in the soil.

The main N_2O emission events occurred at the mid-slope position and during rainy periods in winter, which was related to the water level dynamics. The scarcity of larger N_2O emission events called into question whether Eh and N_2O emissions are closely related in our riparian zone. However, based on the findings from our laboratory experiments, we can state the Eh can be utilized to distinguish the sources of soil N_2O emissions.

Compared with the laboratory experiments, in the field study there were more factors affecting soil Eh changes and GHG. Nevertheless, the field observations verified that the soil Eh variability increased during the transition period from dry to wet conditions. CO_2, N_2O, and CH_4 emission events occurred during the observation period and proved that Eh correlated with GHG emissions. Therefore, the field observations were of great significance for studying Eh and GHG emissions in temperate riparian zones.

In summary, the whole series of experiments were designed from the laboratory-controlled conditions to the field experiment in a riparian zone. A change in soil water content induced changes in Eh in all the experiments, in which different water statuses (e.g., changing water table or irrigation) were simulated or monitored. A close relationship between changes in Eh and GHG emissions was found, reflecting the important role of soil Eh in GHG production and consumption processes.

5.3 Perspective

In this thesis, three progressive experiments were undertaken in order to extend our knowledge regarding soil Eh and GHG emissions under various environmental conditions from the laboratory scale to natural soil environments. However, there are still some questions left, which need to be answered in the future. These questions are touched upon in the following.

5.3.1 Soil Eh measurements

Although this research demonstrates the possibility of soil Eh measurements with Pt and reference electrodes, our experiments still had limitations. The first is that different soil types with different physical and/or chemical characteristics influence the variations in Eh, and might result in different variations of GHG emissions (e.g., due to differences in soil pore volume or pH). Further studies should consider different soil types during longer periods to analyze the different soil Eh influences and to draw more definitive conclusions. Our field observations may not be representative for a wide range of conditions because the range of soil types at our study site was limited, and thus different wetlands should be investigated to test the transferability of the results of this study.

Because soils are heterogeneous, the Eh can also vary within a very small distance. For example, within wet soil aggregates, the Eh can be up to 200 mV lower than on their surface (Kaurichev and Tararina, 1972). Further experiments should consider implementing more Eh electrodes in soil to ensure the results can represent the variability of soil redox conditions. Therefore, we recommend deploying an electrode array to capture the heterogeneous soil variations in the critical zone and link the measured results to the areal extent of a certain soil type. The other factors like soil organic matter pool and soil pH metal ions will also influence the redox reactions, which should be considered in the future research field for interpretation of the soil Eh variations, especially in highly reduced conditions (Popenda, 2014; Dorau et al., 2016; Schlesinger and Emily, 2013). In addition, soil microbial activity and soil physical parameters change with soil depth, and these factors also influence soil Eh distribution (Brzezinska, 2004; Kralova et al., 1992; Theng and Orchard, 1995; Fenchel et al., 1998). Therefore, measurements of microbial activity measurements and/or pH should be included in further studies to provide more insight into soil biogeochemical processes.

In the laboratory experiments, the soil temperature and pH were kept at relatively constant levels, and thus further laboratory studies should utilize different environmental and soil conditions to cover more Eh variations. For the field measurements, observations over a longer period would be advantageous for capturing diurnal cycles as well as season and interannual variations within the soil. Given the importance of soil biogeochemical processes in soils, and the relative ease of implementation, we recommend deploying redox Pt-electrodes in long-term environmental monitoring programs in critical zone observatories.

5.3.2 N_2O source partitioning using stable isotopes

In our experiments, the partitioning of nitrification or denitrification as source processes of soil N_2O was estimated by stable isotope measurements and soil Eh values. The site-specific ^{15}N isotope data

(^{15}N SP) of N_2O emitted from the soil were essential for the validation of the Eh-based differentiation between the oxidative and reductive pathways of N_2O formation (Wei et al., 2017; Toyoda et al., 2019). In the future, ^{15}N SP measurements of N_2O with infrared laser spectroscopy equipment could enable high-resolution N_2O source partitioning and thereby enlarge our knowledge on soil N_2O production in addition to soil redox measurements. Furthermore, quantification of soil N_2O emissions from various soils and different pathways by ^{15}N SP measurement may help to constrain the ranges of Eh values for the different N_2O production pathways. This will finally allow to trace the origin of N_2O from the isotope signature of the N_2O emitted from soil surface and the Eh measured in the different soil layers.

5.3.3 Developing effective measures to mitigate soil GHG emissions

Although in our experiments, the Eh had no significant relationship with CO_2 emissions, the variety of microbiological processes in soil is still tightly linked with the oxygen availability in soil. The Eh reflects the O_2 supply as well as N_2O and CH_4 production. Modeling GHG emission is essential for upscaling of GHG fluxes and for calculating large-scale GHG budgets (Oertel et al., 2016). Most of the GHG models (e.g. SoilCO_2, CASA, DNDC, etc.) mainly use the soil water content as the indicator for soil aeration status, whereas our results show that the Eh could be another suitable indicator. The release of N_2O from arable land is mainly controlled by fertilization, precipitation or groundwater level influence. Besides the common control variable like temperature, soil moisture, and soil N content, the Eh may additionally aid in constructing a new model to mitigate excessive soil N_2O emissions. In such a new biogeochemical model, the Nernst equation for the redox-active elements, like O_2, NH_4^+, NO_2^-, NO_3^-, NO, and N_2O, would play an important role. At the same time, the model should also consider redox active metal ion pairs, such as Mn^{4+}/Mn^{2+} and Fe^{3+}/Fe^{2+}, which should be considered because they strongly influence N trace gas formation. For example, in highly reduced condition the N_2O will be reduced to N_2. Furthermore, utilizing Eh in such new models could affect agricultural management techniques and the potential mitigation of N_2O emissions and control the N losses from fertilizer. In order to refine the model for simulation of GHG emissions while taking into consideration various soil conditions and qualities, Eh can serve as an excellent indicator and would be a better constraint for process-based GHG models, and a more effective way to mitigate agricultural N_2O and NO production. For example, monitoring Eh increased our knowledge on CH_4 emissions from wetlands, and further CH_4 models should consider Eh variations because it is an important indicator of the methanogenesis thresholds. In summary, monitoring Eh enables the discrimination of the various GHG production and consumption pathways, and has the potential to create new model concepts that are more rigorous than previous models.

References

Adams, E.A. (2012) World forest area still on the decline. *Europe* **989**, 1-5.

Akiyama, H., Tsuruta, H. and Watanabe, T. (2000) N_2O and NO emissions from soils after the application of different chemical fertilizers. *Chemosphere* **2**, 313-320.

Amundson, R.G. and Davidson, E.A. (1990) Carbon dioxide and nitrogenous gases in the soil atmosphere. *Journal of Geochemical Exploration* **38**, 13-41.

Baggs, E.M. (2011) Soil microbial sources of nitrous oxide: recent advances in knowledge, emerging challenges and future direction. *Current Opinion in Environmental Sustainability* **3**, 321-327.

Baggs, E.M., Rees, R.M., Smith, K.A. and Vinten, A.J.A. (2000) Nitrous oxide emission from soils after incorporating crop residues. *Soil use and management* **16**, 82-87.

Barnard R.L., Blazewicz, S.J. and Firestone, M.K. (2020) Rewetting of soil: Revisiting the origin of soil CO_2 emissions. *Soil Biology and Biochemistry* **147**, 107819.

Batjes, N.H. (1996) Total carbon and nitrogen in the soils of the world. *European journal of soil science* **47**, 151-163.

Batson, J., Noe, G.B., Hupp, C.R., Krauss, K.W., Rybicki, N.B. and Schenk, E.R. (2015) Soil greenhouse gas emissions and carbon budgeting in a short-hydroperiod floodplain wetland. *Journal of Geophysical Research: Biogeosciences* **120**, 77-95.

Bhaumik, H.D. and Clark, F.E. (1948) Soil moisture tension and microbiological activity. *Soil Science Society of America Journal* **12**, 234-238.

Bogena, H. (2019) Monitoring soil moisture pattern with wireless sensor networks-Technologies, applications and future perspectives. Habilitation thesis, University of Bonn, 138 p.

Bogena, H., Kunkel, R., Krüger, E., Zacharias, S., and Pütz, T. (2012) TERENO: Long-term monitoring network for terrestrial research. *Hydrologie und Wasserwirtschaft* **56**,138-143.

Bogena, H.R., Huisman, J.A., Schilling, B., Weuthen, A. and Vereecken, H. (2017) Effective calibration of low-cost soil water content sensors. *Sensors* **17**, 208.

Bogena, H.R., Montzka, C., Huisman, J.A., Graf, A, Schmidt, M., Stockinger, M., Von Hebel, C., Hendricks-Franssen, H.J., Van der Kruk, J., Tappe, W., Lücke, A., Baatz, R., Bol, A., Groh, J., Pütz, T., Jakobia, J., Kunkel, R., Sorg, J. and Vereecken, H. (2018) The TERENO-Rur Hydrological Observatory: A Multiscale Multi-Compartment Research Platform for the Advancement of Hydrological Science. *Vadose Zone Journal* **17**, 1-22.

Bohn, H.L. (1971) Redox potentials. *Soil Science* **112**, 39-45.

Bond-Lamberty, B. and Thomson, A. (2010) Temperature-associated increases in the global soil respiration record. *Nature* **464**, 579-582.

Braker, G. and Conrad, R. (2011) Diversity, structure, and size of N_2O-producing microbial communities in soils—what matters for their functioning? *Advances in applied microbiology* **75**, 33-70.

Bremner, J.M. (1997) Sources of nitrous oxide in soils. *Nutrient cycling in Agroecosystems* **49**, 7-16.

Brettar, I., Sanchez-Perez, J.M. and Trémolieres, M. (2002) Nitrate elimination by denitrification in hardwood forest soils of the Upper Rhine floodplain-correlation with redox potential and organic matter. *Hydrobiologia* **469**, 11-21.

Bruce, J.P., Frome, M., Haites, E., Janzen, H., Lal, R. and Paustian, K. (1999) Carbon sequestration in soils. *Journal of Soil and Water Conservation* **54**, 382-389.

Brümmer, C., Brüggemann, N., Butterbach-Bahl, K., Falk, U., Szarzynski, J., Vielhauer, K., Wassmann, R. and Papen, H. (2008) Soil-atmosphere exchange of N_2O and NO in near-natural savanna and agricultural land in Burkina Faso (W. Africa). *Ecosystems* **11**, 582-600.

Brzezinska M. (2004) Aeration status of soil and enzyme activity. (Eds J. Gliński, G. Józefaciuk, K. Stahr) Soil-plant-atmosphere aeration and environmental problems. Agrophysics/Hohenheim University/Institure of Agrophysics Polish Academy of Science, Lubli-Stuttgart. pp. 55-59.

Buresh, R.J. and Patrick Jr, W.H. (1978) Nitrate reduction to ammonium in anaerobic soil. *Soil Science Society of America Journal* **42**, 913-918.

Buresh, R.J. and Patrick Jr, W.H. (1981). Nitrate reduction to ammonium and organic nitrogen in an estuarine sediment. *Soil Biology and Biochemistry* **13**, 279-283.

Burgin, A.J., Yang, W.H., Hamilton, S.K. and Silver, W.L. (2011) Beyond carbon and nitrogen: how the microbial energy economy couples elemental cycles in diverse ecosystems. *Frontiers in Ecology and the Environment* **9**, 44-52.

Butterbach-Bahl, K. and Dannenmann, M. (2011) Denitrification and associated soil N_2O emissions due to agricultural activities in a changing climate. *Current Opinion in Environmental Sustainability* **3**, 389-395.

Butterbach-Bahl, K., Baggs, E.M., Dannenmann, M., Kiese, R. and Zechmeister-Boltenstern, S. (2013) Nitrous oxide emissions from soils: how well do we understand the processes and their controls? *Philosophical Transactions of the Royal Society B: Biological Sciences* **368**, 20130122.

Chang, C.T., Sabaté, S., Sperlich, D., Poblador, S., Sabater, F. and Gracia, C. (2014) Does soil moisture overrule temperature dependence of soil respiration in Mediterranean riparian forests? *Biogeosciences* **11**, 6173-6185.

Chapuis-Lardy, L., Wrage, N., Metay, A., Chotte, J.L. and Bernoux, M. (2007) Soils, a sink for N_2O? A review. *Global Change Biology* **13**, 1-17.

Cheng, Y., Zhang, J.B., Wang, J., Cai, Z.C. and Wang, S.Q. (2015) Soil pH is a good predictor of the dominating N_2O production processes under aerobic conditions. *Journal of Plant Nutrition and Soil Science* **178**, 370-373.

Cicerone R.J. and Oremland R.S. (1988) Biogeochemical aspects of atmospheric methane. *Global Biogeochemical Cycles* **2**, 299-327.

Clément, J.C., Pinay, G. and Marmonier, P. (2002) Seasonal dynamics of denitrification along topohydrosequences in three different riparian wetlands. *Journal of Environmental Quality* **31**, 1025-1037.

Cogger, C.G., Kennedy, P.E. and Carlson, D. (1992) Seasonally saturated soils in the Puget Lowland II. Measuring and interpreting redox potentials. *Soil Science* **154**, 50-58.

Collier, S.M., Ruark, M.D., Oates, L.G., Jokela, W.E. and Dell, C.J. (2014) Measurement of greenhouse gas flux from agricultural soils using static chambers. *Journal of Visualized Experiments* **90**, e52110.

Comerford, N.B., Jerez, A., Freitas, A.A. and Montgomery, J. (1996) Soil water table, reducing conditions, and hydrologic regime in a Florida flatwood landscape. *Soil Science* **161**, 194-199.

Comfort, S.D., Kelling, K.A., Keeney, D.R. and Converse, J.C. (1990) Nitrous oxide production from injected liquid dairy manure. *Soil Science Society of America Journal* **54**, 421-427.

Dalal, R.C., Wang, W., Robertson, G.P. and Parton, W.J. (2003) Nitrous oxide emission from Australian agricultural lands and mitigation options: A review. *Australian Journal of Soil Research* **41**,165-195.

Davidson, E.A. (2009) The contribution of manure and fertilizer nitrogen to atmospheric nitrous oxide since 1860. *Nature Geoscience* **2**, 659-662.

De Carlo, N.D., Oelbermann, M. and Gordon, A.M. (2019) Carbon dioxide emissions: Spatiotemporal variation in a young and mature riparian forest. *Ecological Engineering* **138**, 353-361.

De Klein, C., Novoa, R.S., Ogle, S., Smith, K.A., Rochette, P., Wirth, T., McConkey, B., Mosier, A., Rypdal, K. and Williams, S.A. (2006) N_2O emissions from managed soils, and CO_2 emissions from lime and urea application. In *IPCC guidelines for National greenhouse gas inventories, prepared by the National greenhouse gas inventories programme, 4,* Institute for Global Environmental Strategies, Hayama, Japan, pp. 1-54.

De Klein, C.A. and Monaghan, R.M. (2011) The effect of farm and catchment management on nitrogen transformations and N_2O losses from pastoral systems—can we offset the effects of future intensification? *Current Opinion in Environmental Sustainability* **3**, 396-406.

Decock, C., and Six, J. (2013) How reliable is the intramolecular distribution of ^{15}N in N_2O to source partition N_2O emitted from soil? *Soil Biology and Biochemistry* **65**,114-127.

Del Prado, A., Merino, P., Estavillo, J., Pinto, M., and González-Murua, C. (2006) N_2O and NO emissions from different N sources and under a range of soil water contents. *Nutrient Cycling in Agroecosystems* **74,** 229-243.

DeLaune, R.D. and Reddy, K.R. (2005) Redox potential. In *Encyclopedia of Soils in the Environment (Vol. 3)*. Amsterdam, Elsevier. pp. 366-371.

Dilustro, J.J., Collins, B., Duncan, L., Crawford, C. (2005) Moisture and soil texture effects on soil CO_2 efflux components in southeastern mixed pine forests. *Forest Ecology and Management* **204**, 87-97.

Dorau, K., Eickmeier, M. and Mansfeldt, T. (2016) Comparison of manganese and iron oxide-coated redox bars for characterization of the redox status in wetland soils. *Wetlands* **36**, 133-141.

Dorau, K., Luster, J. and Mansfeldt, T. (2018) Soil aeration: the relation between air-filled pore volume and redox potential. *European Journal of Soil Science* **69**, 1035-1043.

Durner, W. and Or, D. (2006) Soil water potential measurement. Encyclopedia of hydrological sciences.

Dutaur, L. and Verchot, L.V. (2007) A global inventory of the soil CH_4 sink. *Global biogeochemical cycles* **21**.

Dwire, K.A., Kauffman, J.B. and Baham, J.E. (2006) Plant species distribution in relation to water-table depth and soil redox potential in montane riparian meadows. *Wetlands* **26**, 131-146.

Fang, C. and Moncrieff, J. (2001) The dependence of soil CO_2 efflux on temperature. *Soil Biology and Biochemestry* **33**,155-165.

FAO, E. (2017) Food and Agriculture Organization of the United Nations: Rome.

Farrell, R., Swerhone, G.D.W. and van Kessel, C. (1991) Construction and evaluation of a reference electrode assembly for use in monitoring in situ soil redox potentials. *Soil Science and Plant Analysis* **22**, 1059-1068.

Fenchel T, King G.M. and Blackburn T.H. (1998) Bacterial biogeochemistry: The ecophysiology of mineral cycling. Academic press, San Diego.

Fiedler, S., Höll, B.S. and Jungkunst H.F. (2005) Methane emissions, groundwater levels, and redox potentials of common wetland soils in a temperate-humid clime. *Global Biogeochemical Cycles* **76**, 1–20.

Fiedler, S., Vepraskas, M.J. and Richardson, J.L. (2007) Soil redox potential: importance, field measurements, and observations. *Advances in agronomy* **94**, 1-54.

Fierer, N., Schimel, J.P. and Holden, P.A. (2003) Variations in microbial community composition through two soil depth profiles. *Soil Biology and Biochemistry* **35**, 167-176.

Flessa, H. and Beese, F. (1995) Effects of sugarbeet residues on soil redox potential and nitrous oxide emission. *Soil Science Society of America Journal* **59**, 1044-1051.

Flessa, H. and Fischer, W.R. (1992) Plant-induced changes in the redox potentials of rice rhizospheres. *Plant and soil* **143**, 55-60.

Galloway, J.N., Townsend, A.R., Erisman, J.W., Bekunda, M., Cai, Z., Freney, J.R., Martinelli, L.A., Seitzinger, S.P. and Sutton, M.A. (2008) Transformation of the nitrogen cycle: recent trends, questions, and potential solutions. *Science* **320**, 889-892.

Gardner, C.M.K., Laryea, K.B. and Unger, P.W. (1999) Soil physical constraints to plant growth and crop production. In *Land and Water Development Division*, Rome.

Gebremichael, A.W., Osborne, B. and Orr, P. (2017) Flooding-related increases in CO_2 and N_2O emissions from a temperate coastal grassland ecosystem. *Biogeosciences* **14**, 2611-2626.

Gillespie, L.J. (1920) Reduction potentials of bacterial cultures and of water-logged soils. *Soil Science* **9**, 199-216.

Gilliam, J.W. (1994) Riparian wetlands and water quality. *Journal of Environmental Quality*, **23**.

Grosse, W., Frye, J. and Lattermann, S. (1992) Root aeration in wetland trees by pressurized gas transport. *Tree Physiology* **10**, 285-295.

Gu, J., Nicoullaud, B., Rochette, P., Grossel, A., Hénault, C., Cellier, P. and Richard, G. (2013) A regional experiment suggests that soil texture is a major control of N_2O emissions from tile-drained winter wheat fields during the fertilization period. *Soil Biology and Biochemistry* **60**, 134–141.

Guardia, G., Sanz-Cobena, A., Sanchez-Martín, L., Fuertes-Mendizábal, T., González-Murua, C., Álvarez, J.M., David, C. and Vallejo, A. (2018) Urea-based fertilization strategies to reduce yield-scaled N oxides and enhance bread-making quality in a rainfed Mediterranean wheat crop. *Agriculture, ecosystems and environment* **265**, 421-431.

Hansen, M., Clough, T.J. and Elberling, B. (2014) Flooding-induced N_2O emission bursts controlled by pH and nitrate in agricultural soils. *Soil Biology and Biochemistry* **69**, 17-24.

Heil, J., Liu, S., Vereecken, H. And Brueggemann, N. (2015) Abiotic nitrous oxide production from hydroxylamine in soils and their dependence on soil properties. *Soil Biology and Biochemistry* **84**, 107-115.

Heimann, M. and Reichstein, M. (2008) Terrestrial ecosystem carbon dynamics and climate feedbacks. *Nature* **451**, 289-292.

Henneberg, A., Brix, H. and B.K. Sorrell. 2016. The interactive effect of Juncus effusus and water table position on mesocosm methanogenesis and methane emissions. *Plant and Soil* **400**, 45-54.

Herbst, M., Hellebrand, H.J., Bauer, J., Huisman, J.A. and Šimůnek, J. (2008) Multiyear heterotrophic soil respiration: Evaluation of a coupled CO_2 transport and carbon turnover model. *Ecological Modelling* **214**, 271-283.

Hou, A.X., Chen, G.X., Wang, Z.P., Van Cleemput, O. and Patrick, W.H. (2000) Methane and nitrous oxide emissions from a rice field in relation to soil redox and microbiological processes. *Soil Science Society of America Journal* **64**, 2180-2186.

Huang, G., Li, Y., Chen, G., Yang, Y. and Zhao, C. (2001) Influence of environmental factors on CH_4 emission from reed wetland. *Huanjing Kexue* **22**, 1-5.

Huber, B., Bernasconi, S.M., Pannatier, E.G. and Luster, J. (2012) A simple method for the removal of dissolved organic matter and $\delta^{15}N$ analysis of NO_3^- from freshwater. *Rapid Communications in Mass Spectrometry* **26**, 1475-1480.

Hunting, E.R. and Kampfraath, A.A. (2013) Contribution of bacteria to redox potential (Eh) measurements in sediments. *International Journal of Environmental Science and Technology* **10**, 55-62.

Hunting, E.R. and Van der Geest, H.G. (2011) Predictability of bacterial activity and denitrification in aquatic sediments with continuous measurements of redox potential. *International Journal of Environmental Science and Technology* **8**, 553-560.

Husson, O. (2013) Redox potential (Eh) and pH as drivers of soil/plant/microorganism systems: a transdisciplinary overview pointing to integrative opportunities for agronomy. *Plant and Soil* **362**, 389-417.

Husson, O., Husson, B., Brunet, A., Babre, D., Alary, K., Sarthou, J. P., Hubert, C., Michel, D., Jaroslav, B. and Henry, M. (2016) Practical improvements in soil redox potential (Eh) measurement for characterisation of soil properties. Application for comparison of conventional and conservation agriculture cropping systems. *Analytica Chimica Acta* **906**, 98-109.

Ibraim, E., Wolf, B., Harris, E., Gasche, R., Wei, J., Yu, L., Kiese, R., Eggleston, S., Butterbach-Bahl, K., Zeeman, M., Tuzson, B., Emmenegger, L., Six, J., Henne, S. and Mohn, J. (2019) Attribution of N_2O sources in a grassland soil with laser spectroscopy based isotopocule analysis. *Biogeosciences* **16**, 3247-3266.

IPCC (2007) The Physical Science Basis. In *Contribution of Working Group I to the Fourth Assessment Report of the Intergovernmental Panel on Climate Change*, Cambridge University Press: Cambridge, UK; New York, NY, USA, pp. 468-479.

IPCC (2013) Climate change 2013: The physical science basis. In *Contribution of working group I to the fifth assessment report of the intergovernmental panel on climate change*, Cambridge University Press: Cambridge, UK; New York, NY, USA, pp. 1535.

IPCC (2014) Mitigation of Climate Change. Contribution of Working Group III to the Fifth Assessment Report of the Intergovernmental Panel on Climate Change, Cambridge University Press: Cambridge, UK; New York, NY, USA, pp. 154-196.

IPCC (2018) Summary for Policymakers. An IPCC Special Report on the impacts of global warming of 1.5°C above pre-industrial levels and related global greenhouse gas emission pathways, in the context of strengthening the global response to the threat of climate change, sustainable development, and efforts to eradicate poverty. In *World Meteorological Organization*, Geneva, Switzerland, pp. 1-32.

Itoh, M., Ohte, N., Koba, K., Katsuyama, M., Hayamizu, K. and Tani, M. (2007) Hydrologic effects on methane dynamics in riparian wetlands in a temperate forest catchment. *Journal of Geophysical Research: Biogeosciences* **112**.

Jacinthe, P.A. (2015) Carbon dioxide and methane fluxes in variably-flooded riparian forests. *Geoderma* **241**, 41-50.

Johnson, D.W. and Henderson, P. (1995) Effects of forest management and elevated carbon dioxide on soil carbon storage. In: Lal, R. et al., editors, *Soil management and the greenhouse effects*. Lewis Publ., Boca Raton, FL. pp. 137-145.

Karathanasis, A.D., Thompson, Y.L. and Barton, C.D. (2003) Long-term evaluations of seasonally saturated “wetlands” in western Kentucky. *Soil Science Society of America Journal* **67**, 662-673.

Krause, K., Niklaus, P.A. and Schleppi, P. (2013) Soil-atmosphere fluxes of the greenhouse gases CO_2, CH_4 and N_2O in a mountain spruce forest subjected to long-term N addition and to tree girdling. *Agricultural and Forest Meteorology* **181**, 61-68.

Kaurichev, I.S. and Tararina, L.F. (1972) Oxidation-reduction conditions inside and outside gray forest soil aggregates. *Pochvovedenie* **10**, 39-42.

Kitzler, B., Zechmeister-Boltenstern, S., Holtermann, C., Skiba, U. and Butterbach-Bahl, K. (2006) Controls over N_2O, NO_x and CO_2 fluxes in a calcareous mountain forest soil. *Biogeosciences, European Geosciences Union* **3**, 383-395.

Korres, W., Reichenau, T.G., Fiener, P., Koyama, C.N., Bogena, H.R., Cornelissen, T., Baatz, R., Herbst, M., Diekkrüger, B., Vereecken, H. and Schneidera, K. (2015) Spatio-temporal soil moisture patterns: A meta-analysis using plot to catchment scale data. *Journal of Hydrology* **520**, 326-341.

Kralov, M., Masscheleyn, P.H. and Patrick Jr, W.H. (1992) Redox potential as an indicator of electron availability for microbial activity and nitrogen transformations in aerobic soil. *Zentralblatt für Mikrobiologie* **147**, 388-399.

Kutsch, W.L., Bahn, M. and Heinemeyer, A. (2009) Soil carbon dynamics: An integrated methodology. Cambridge University Press, Cambridge, UK.

Le Mer, J. and Roger, P. (2001) Production, oxidation, emission and consumption of methane by soils: A review. *European Journal of Soil Biology* **37**, 25-50.

Lewicka-Szczebak, D., Augustin, J., Giesemann, A. and Well, R. (2017) Quantifying N_2O reduction to N_2 based on N_2O isotopocules: Validation with independent methods (helium incubation and ^{15}N gas flux method). *Biogeosciences* **14**, 711-732.

Li, C. (2007) Quantifying greenhouse gas emissions from soils: Scientific basis and modeling approach. *Soil Science and Plant Nutrition* **53**, 344-352.

Li, C., Aber, J., Stange, F., Butterbach-Bahl, K. and Papen, H. (2000) A process-oriented model of N_2O and NO emissions from forest soils: 1. Model development. *Journal of Geophysical Research* **105**, 4369-4384.

Li, C., Frolking, S. and Harriss, R. (1994) Modeling carbon biogeochemistry in agricultural soils. *Global Biogeochemistry Cycles* **8**, 237-254.

Li, N., Yao, S.H., You, M.Y., Zhang, Y.L., Qiao, Y.F., Zou, W.X. and Zhang, B. (2014) Contrasting development of soil microbial community structure under no-tilled perennial and tilled cropping during early pedogenesis of a Mollisol. *Soil Biology and Biochemistry* **77**, 221-232.

Li, P. and Lang, M. (2014) Gross nitrogen transformations and related N_2O emissions in uncultivated and cultivated black soil. *Biology and fertility of soils* **50**, 197-206.

Linn, D.M. and Doran, J.W. (1984) Effect of water-filled pore space on carbon dioxide and nitrous oxide production in tilled and nontilled soils. *Soil Science Society of America Journal* **48**, 1267-1272.

Linzmeier, W., Gutser, R. and Schmidhalter, U. (2001) Nitrous oxide emission from soil and from a nitrogen-15-labelled fertilizer with the new nitrification inhibitor 3, 4-dimethylpyrazole phosphate (DMPP). *Biology and Fertility of Soils* **34**, 103-108.

Ludwig, J., Meixner, F.X., Vogel, B. and Förstner, J. (2001) Soil-air exchange of nitric oxide: an overview of processes, environmental factors and modeling studies. *Biogeochemistry* **52**, 225–257.

Luo, J., Saggar, S., Bhandral, R., Bolan, N., Ledgard, S., Lindsey, S. and Sun, W. (2008) Effects of irrigating dairy-grazed grassland with farm dairy effluent on nitrous oxide emissions. *Plant and soil* **309**, 119-130.

Mander, Ü., Lohmus, K., Teiter, S. and Augustin, J. (2008) Gaseous nitrogen and carbon fluxes in riparian alder stands. *Environmental Research* **13**, 231-241.

Mansfeldt, T. (2003) In situ long-term redox potential measurements in a dyked marsh soil. Journal of Plant *Nutrition and Soil Science* **166**, 210-219.

Mansfeldt, T. (2004) Redox potential of bulk soil and soil solution concentration of nitrate, manganese, iron, and sulfate in two Gleysols. *Journal of Plant Nutrition and Soil Science* **167**, 7-16.

Marin, J.C.A., Caravelli, A.H. and Zaritzky, N.E. (2016) Nitrification and aerobic denitrification in anoxic–aerobic sequencing batch reactor. *Bioresource technology* **200**, 380-387.

Marín-Muñiz, J. L., Hernández, M. E. and Moreno-Casasola, P. (2015) Greenhouse gas emissions from coastal freshwater wetlands in Veracruz Mexico: Effect of plant community and seasonal dynamics. *Atmospheric Environment* **107**, 107-117.

Martikainen, P.J., Nykanen, H., Crill, P. and Silvola, J. (1993) Effect of a lowered water table on nitrous oxide fluxes from northern peatlands. *Nature* **366**, 51-53.

Masscheleyn, P.H., DeLaune, R.D. and Patrick Jr, W.H. (1993) Methane and nitrous oxide emissions from laboratory measurements of rice soil suspension: effect of soil oxidation-reduction status. *Chemosphere* **26**, 251-260.

McDaniel, P.A., Gabehart, R.W., Falen, A.L., Hammel, J.E. and Reuter, R.J. (2001) Perched water tables on Argixeroll and Fragixeralf hillslopes. *Soil Science Society of America Journal* **65**, 805-810.

Minamikawa, K. and Sakai, N. (2007) Soil carbon budget in a single-cropping paddy field with rice straw application and water management based on soil redox potential. *Soil science and plant nutrition* **53**, 657-667.

Minick, K.J., Pandey, C.B., Fox, T.R. and Subedi, S. (2016) Dissimilatory nitrate reduction to ammonium and N_2O flux: effect of soil redox potential and N fertilization in loblolly pine forests. *Biology and Fertility of Soils* **52**, 601-614.

Mitsch, W.J. and Gosselink, J.G. (2015) *Wetlands*, 5th ed. John Wiley and Sons, Hoboken, NJ, USA.

Mitsch, W.J. and Gosselink, J.G. (2007) *Wetlands*. 4th ed. John Wiley and Sons, Hoboken, NJ, USA.

Monson, R.K., Lipson, D.L., Burns, S.P., Turnipseed, A.A., Delany, A.C., Williams, M.W. and Schmidt, S.K. (2006) Winter forest soils respiration controlled by climate. *Nature* **439**, 711-714.

Moore, T. and Knowles, R. (1989) The influence of water table levels on methane and carbon dioxide emissions from peatland soils. *Canadian Journal of Soil Science* **69**, 33-38.

Morales-Olmedo, M., Ortiz, M. and Sellés, G. (2015) Effects of transient soil waterlogging and its importance for rootstock selection. *Chilean journal of agricultural research* **75**, 45-56.

Mulvaney, R.L., Khan, S.A., Stevens, W.B. and Mulvaney, C.S. (1997) Improved diffusion methods for determination of inorganic nitrogen in soil extracts and water. *Biology and Fertility of Soils* **24**, 413-420.

Naimanand R.J, Décamps H. (1997). The ecology of interfaces: Riparian Zones. *Annual Review of Ecology and Systematics* **28**, 621–658.

Nason, G.E. and Myrold, D.D. (1991) ^{15}N in soil research: appropriate application of rate estimation procedures. *Agriculture, Ecosystems and Environment* **34**, 427-441.

Nasta, P., Bogena, H.R., Sica, B., Weuthen, A., Vereecken, H. and Romano, N. (2020) Explaining the spatiotemporal variability of soil moisture under a seasonal Mediterranean-type climate. *Frontiers in Water* **2**, 26.

Nazaries, L., Murrell, J.C., Millard, P., Baggs, L. and Singh, B.K. (2013) Methane, microbes and models: fundamental understanding of the soil methane cycle for future predictions. *Environmental microbiology* **15**, 2395-2417.

Ney, P., Graf, A., Bogena, H., Diekkrüger, B., Drüe, C., Esser, O., Heinemann, G., Klosterhalfen, A., Pick, K., Pütz, T., Schmidt, M., Valler, V. and Vereecken, H. (2019) CO_2 fluxes before and after partial deforestation of a Central European spruce forest. *Agricultural and forest meteorology* **274**, 61-74.

Nieder, R. and Benbi, D.K. (2008) Carbon and nitrogen in the terrestrial environment. *Springer*, Berlin and Heidelberg.

Nygaard, B. and Ejrnæs, R. (2009) The impact of hydrology and nutrients on species composition and richness: Evidence from a microcosm experiment. *Wetlands* **29**, 187-195.

Oertel, C., Matschullat, J., Zurba, K., Zimmermann, F. and Erasmi, S. (2016) Greenhouse gas emissions from soils-A review. *Chemie der Erde-Geochemistry* **76**, 327-352.

Olivier, J. and Janssens-Maenhout, G. (2012) CO_2 emissions from fuel combustion (2012 edition): Part III: greenhouse-gas emissions. In *CO_2 emissions from fuel combustion (2012 edition)*, International Energy Agency. Paris.

Pachauri, R.K., Meyer, L., Plattner, G.K. and T. Stocker. (2014) Synthesis report. In *Contribution of Working Groups I, II and III to the Fifth Assessment Report of the Intergovernmental Panel on Climate Change*. IPCC, Geneva, Switzerland.

Papen, H. and Butterbach-Bahl, K. (1999) A 3-year continuous record of nitrogen trace gas fluxes from untreated and limed soil of a N-saturated spruce and beech forest ecosystem in Germany: 1. N_2O emissions. *Journal of Geophysical Research: Atmospheres* **104**, 18487-18503.

Parkin, T.B., Venterea, R.T. and Follett, R.F. (2010) Chamber-based trace gas flux measurements. *Sampling protocols* **3**, 3-39.

Pärn, J., Verhoeven, J.T., Butterbach-Bahl, K., Dise, N.B., Ullah, S., Aasa, A., Egorov, S., Espenberg, M., Järveoja, J., Jauhiainen, J., Kasak, K., Klemedtsson, L., Kull, A., Laggoun-Défarge, F., Lapshina, E.D., Lohila, A., Lõhmus, K., Maddison, M., Mitsch, W.J., Müller, C., Niinemets, Ü., Osborne, B., Pae, T., Salm, J., Sgouridis, F., Sohar, K., Soosaar, K., Storey, K., Teemusk, A., Tenywa, M.M., Tournebize, J., Truu, J., Veber, G., Villa, J.A., Zaw, S.S. and Kasak, K. (2018) Nitrogen-rich organic soils under warm well-drained conditions are global nitrous oxide emission hotspots. *Nature communications* **9**, 1-8.

Patrick, W.H. and Jugsujinda, A. (1992) Sequential reduction and oxidation of inorganic nitrogen, manganese, and iron in flooded soil. *Soil Science Society of America Journal* **56**, 1071-1073.

Pattey, E., Edwards, G.C., Desjardins, R.L., Pennock, D.J. and Smith, W. (2007) Tools for quantifying N_2O emissions from agroecosystems. *Agricultural and Forest Meteorology* **142**, 103-119.

Peralta, A.L., Ludmer, S., Matthews, J.W. and Kent, A.D. (2014) Bacterial community response to changes in soil redox potential along a moisture gradient in restored wetlands. *Ecological Engineering* **73**, 246-253.

Pezeshki, S.R. (2001) Wetland plant responses to soil flooding. *Environmental and Experimental Botany*, **46**, 299-312.

Pezeshki, S.R. and DeLaune, R.D. (2012) Soil oxidation-reduction in wetlands and its impact on plant functioning. *Biology* **1**, 196-221.

Pfeifer-Meister, L., Gayton, L.G., Roy, B.A., Johnson, B.R., and Bridgham, S.D. (2018) Greenhouse gas emissions limited by low nitrogen and carbon availability in natural, restored, and agricultural Oregon seasonal wetlands. *PeerJ* **6**.

Phillips, C.L. and Nickerson, N. (2015) Soil Respiration. In *Reference module in earth systems and environmental* sciences. Elsevier Amsterdam.

Phillips, R. and Beeri, O. (2008) The role of hydropedologic vegetation zones in greenhouse gas emissions for agricultural wetland landscapes. *Catena* **72**, 386-394.

Picek, T., Šimek, M. and Šantrůčková, H. (2000) Microbial responses to fluctuation of soil aeration status and redox conditions. *Biology and fertility of soils* **31**, 315-322.

Pilegaard, K., Skiba, U., Ambus, P., Beier, C., Brüggemann, N., Butterbach-Bahl, K., Dick, J., Dorsey, J., Duyzer, J., Gallagher, M., Gasche, R., Horvath, L., Kitzler, B., Leip, A., Pihlatie, M.K., Rosenkranz, P., Seufert, G., Vesala, T., Westrate, H. and Zechmeister-Boltenstern, S. (2006) Factors controlling regional differences in forest soil emission of nitrogen oxides (NO and N_2O). *Biogeosciences* **3**, 651–661.

Poblador, S., Lupon, A., Sabaté, S. and Sabater, F. (2017) Soil water content drives spatiotemporal patterns of CO_2 and N_2O emissions from a Mediterranean riparian forest soil. *Biogeosciences* **14**, 4195-4208.

Poeplau, C. and Don, A. (2013) Sensitivity of soil organic carbon stocks and fractions to different land-use changes across Europe. *Geoderma* **192**, 189-201.

Ponnamporuma, F.N. (1972) The chemistry of submerged soils. *Advances in Agronomy* **24**, 29-96.

Popenda, A. (2014) Effect of redox potential on heavy metals and as behavior in dredged sediments. *Desalination and water treatment* **52**, 3918-3927.

Porter, G., Bajita-Locke, J., Hue, N. and Strand, D. (2004) Manganese solubility and phytotoxicity affected by soil moisture, oxygen levels, and green manure additions. *Communications in Soil Science and Plant Analysis* **35**, 99-116.

Post, W.M., Pastor, J., Zinke, P.J. and Stangenberger, A.G. (1985) Global patterns of soil nitrogen storage. *Nature* **317**, 613-616.

Ramaswamy, V. Boucher, O., Haigh, J., Hauglustaine, D., Haywood, J., Myhre, G., Nakajima, T., Shi, G.Y. and S. Solomon (2001) Radiative forcing of climate change, in Climate Change 2001: The Scientific Basis—Contribution of Working Group I to the Third Assessment Report of the Intergovernmental Panel on Climate Change, , Cambridge University Press, New York, pp. 239-287.

Reay, D., Davidson, E.A., Smith, K.A., Smith, P., Melillo, J.M., Dentener, F. and Crutzen, P.J. (2012) Global agriculture and nitrous oxide emissions. *Nature Climate Change* **2**, 410-416.

Reddy, K.R., Patrick Jr, W.H. and Lindau, C.W. (1989) Nitrification-denitrification at the plant root-sediment interface in wetlands. *Limnology and oceanography* **34**, 1004-1013.

Regina, K., Nykänen, H., Silvola, J. and Martikainen, P.J. (1996) Fluxes of nitrous oxide from boreal peatlands as affected by peatland type, water table level and nitrification capacity. *Biogeochemistry* **35**, 401-418.

Reth, S., Graf, W., Gefke, O., Schilling, R., Seidlitz, H.K. and Munch, J.C. (2008) Whole-year-round observation of N 2 O profiles in soil: a lysimeter study. *Water, Air, and Soil Pollution: Focus* **8**, 129-137.

Rezanezhad, F., Couture, R.M., Kovac, R., O'Connell, D. and Van Cappellen, P. (2014) Water table fluctuations and soil biogeochemistry: An experimental approach using an automated soil column system. *Journal of hydrology* **509**, 245-256.

Rinklebe, J., Shaheen, S.M. and Frohne, T. (2016) Amendment of biochar reduces the release of toxic elements under dynamic redox conditions in a contaminated floodplain soil. *Chemosphere* **142**, 41-47.

Rogelj, J., Den Elzen, M., Höhne, N., Fransen, T., Fekete, H., Winkler, H., Schaeffer, R., Sha, F., Riahi, K. and Meinshausen, M. (2016) Paris Agreement climate proposals need a boost to keep warming well below 2 °C. *Nature* **534**, 631-639.

Rosenkranz, P., Bruggemann, N., Papen, H., Xu, Z., Seufert, G. and Butterbach-Bahl, K. (2006) N_2O, NO and CH_4 exchange, and microbial N turnover over a Mediterranean pine forest soil. *Biogeosciences* **3**, 121–133.

Rubol, S., Silver, W.L. and Bellin, A. (2012). Hydrologic control on redox and nitrogen dynamics in a peatland soil. *Science of the total environment* **432**, 37-46.

Ruser, R., Flessa, H., Russow, R., Schmidt, G., Buegger, F. and Munch, J. (2006) Emission of N_2O, N_2 and CO_2 from soil fertilized with nitrate: Effect of compaction, soil moisture and rewetting. *Soil Biology* **38**, 263-274.

Sainju, U. M., Jabro, J. D. and Stevens, W.B. (2008) Soil carbon dioxide emission and carbon content as affected by irrigation, tillage, cropping system, and nitrogen fertilization. *Journal of Environmental Quality* **37**, 98-106.

Sainju, U., Jabro, J. and Stevens, W. (2006) Soil carbon dioxide emission as influenced by irrigation, tillage, cropping system, and nitrogen fertilization. In: Aneja, V.P. et al., editors, *Workshop on agricultural air quality: State of science*, North Carolina State University, Raleigh, pp. 1086-1098.

Schaufler, G., Kitzler, B., Schindlbacher, A., Skiba, U., Sutton, M.A. and Zechmeister-Boltenstern, S. (2010) Greenhouse gas emissions from European soils under different land use: effects of soil moisture and temperature. *European Journal of Soil Science* **61** 683-696.

Schindlbacher, A., Zechmeister-Boltenstern, S. and Butterbach-Bahl, K. (2004) Effects of soil moisture and temperature on NO, NO_2, and N_2O emissions from European forest soils. *Journal of Geophysical Research: Atmospheres* **109**.

Schlesinger, W.H. and Emily, S.B. (2013) Biogeochemistry: an analysis of global change, 3rd. Academic Press, Amsterdam.

Schlesinger, W.H. and Andrews, J.A. (2000) Soil respiration and the global carbon cycle. *Biogeochemistry* **48**, 7-20.

Seybold, C.A., Mersie, W., Huang, J. and McNamee, C. (2002) Soil redox, pH, temperature, and water-table patterns of a freshwater tidal wetland. *Wetlands* **22**, 149-158.

Shi, W.Y., Yan, M.J., Zhang, J.G., Guan, J.H. and Du, S. (2014) Soil CO_2 emissions from five different types of land use on the semiarid Loess Plateau of China, with emphasis on the contribution of winter soil respiration. *Atmospheric Environment* **88**, 74–82.

Shoemaker, C. and Kröger, R. (2017) Frequentist and Bayesian approaches to understanding changes in redox potential due to hydrology and vegetation in agricultural drainage ditches. *Wetlands* **37**, 705-714.

Signor, D. and Cerri, C. (2013) Nitrous oxide emissions in agricultural soils: a review. *Pesquisa Agropecuária Tropical* **43**, 322-338.

Šimůnek, J. and Suarez, D.L. (1993) Modeling of carbon dioxide transport and production in soil: 1. Model development. *Water Resource Research* **29**, 487-497.

Skiba, U., Sheppard, L., Pitcairn, C.E.R., Leith, I., Crossley, A., Van Dijk, S. and Fowler, D. (1998) Soil nitrous oxide and nitric oxide emissions as indicators of elevated atmospheric N deposition rates in seminatural ecosystems. *Environmental Pollution* 102, 457-461.

Smith, C.J. and DeLaune, R.D. (1984) Effect of rice plants on nitrification-denitrification loss of nitrogen under greenhouse conditions. *Plant and soil* **79**, 287-290.

Smith, K., Ball, T., Conen, F., Dobbie, K., Massheder, J. and Rey, A. (2003) Exchange of greenhouse gases between soil and atmosphere: Interactions of soil physical factors and biological processes. *Europe Journal of Soil Science*, **54**, 779-791.

Smith, M.S. and Tiedje, J.M. (1979) Phases of denitrification following oxygen depletion in soil. *Soil Biology and Biochemistry*, **11**, 261-267.

Smith, P., Bustamante, M., Ahammad, H., Clark, H., Dong, H., Elsiddig, E.A., Haberl, H., Harper, R., House, J. and Jafari, M. (2015) Agriculture, forestry, and other land use (AFOLU). Cambridge University Press: Cambridge, UK; New York, USA, pp. 816–886.

Smith, P., Martino, D., Cai, Z., Gwary, D., Janzen, H., Kumar, P., McCarl, B., Ogle, S., O'Mara, F., Rice, C., Scholes, B. and Sirotenko, O. (2007) Agriculture. In: Metz, B., Davidson, O.R., Bosch, P.R., Dav, R., Meyer, L.A. (Eds.), In *Climate Change 2007: Mitigation. Contribution of Working Group III to the Fourth Assessment Report of the Intergovernmental Panel on Climate Change*. Cambridge University Press, Cambridge, United Kingdom and New York, USA.

Suseela, V., Conant, R.T., Wallenstein, M.D. and Dukes, J.S. (2012) Effects of soil moisture on the temperature sensitivity of heterotrophic respiration vary seasonally in an old-field climate change experiment. *Global Change Biology* **18**, 336-348.

Sutka, R.L., Ostrom, N.E., Ostrom, P.H., Breznak, J.A., Gandhi, H., Pitt, A.J. and Li, F. (2006) Distinguishing nitrous oxide production from nitrification and denitrification on the basis of isotopomer abundances. *Applied and Environmental Microbiology* **72**, 638-644.

Sutka, R.L., Adams, G.C., Ostrom, N.E. and Ostrom, P.H. (2008) Isotopologue fractionation during N_2O production by fungal denitrification. *Rapid Communications in Mass Spectrometry* **22**, 3989-3996.

Tang, J., Baldocchi, D.D., Qi, Y. and Xu, L. (2003) Assessing soil CO_2 efflux using continuous measurements of CO_2 profiles in soils with small solid-state sensors. *Agricultural and Forest Meteorology* **118**, 207-220.

Teiter, S. and Mander, Ü. (2005) Emission of N_2O, N_2, CH_4, and CO_2 from constructed wetlands for wastewater treatment and from riparian buffer zones. *Ecological Engineering* **25**, 528-541.

Theng, B. and Orchard, V.A. (1995) Interactions of clays with microorganisms and bacterial survival in soil: a physicochemical perspective. *Environmental impact of soil component interactions* **2**, 123-143.

Thomas, C.R., Miao, S. and Sindhoj, E. (2009) Environmental factors affecting temporal and spatial patterns of soil redox potential in Florida Everglades wetlands. *Wetlands* **29**, 1133-1145.

Thompson, R.L., Lassaletta, L., Patra, P.K., Wilson, C., Wells, K.C., Gressent, A., Koffi, E.N., Chipperfield., M.P., Winiwarter, W., Davidson, E.A. , Tian, H. and Canadell, J.G. (2019) Acceleration of global N_2O emissions seen from two decades of atmospheric inversion. *Nature Climate Change* **9**, 993-998.

Thomson, A.J., Giannopoulos, G., Pretty, J., Baggs, E.M. and Richardson, D.J. (2012) Biological sources and sinks of nitrous oxide and strategies to mitigate emissions. *Philosophical Transactions of the Royal Society of London. Series B, Biological Sciences* **367**, 1157-1168.

Tokarz, E. and Urban, D. (2015) Soil redox potential and its impact on microorganisms and plants of wetlands. *Journal of Ecological Engineering* **16**, 20-30.

Toyoda, S., Yoshida, N. and Koba, K. (2017) Isotopocule analysis of biologically produced nitrous oxide in various environments. *Mass Spectrometry Reviews* **36**, 135-160.

Toyoda, S., Yoshida, O., Yamagishi, H., Fujii, A., Yoshida, N. and Watanabe, S. (2019) Identifying the origin of nitrous oxide dissolved in deep ocean by concentration and isotopocule analyses. *Scientific Reports* **9**, 1-9.

Toyoda, S., Mutobe, H., Yamagishi, H., Yoshida, N. and Tanji, Y. (2005) Fractionation of N_2O isotopomers during production by denitrifier. *Soil Biology and Biochemistry* **37**, 1535-1545.

Van Bochove, E., Beauchemin, S. and Thériault, G. (2002) Continuous multiple measurement of soil redox potential using platinum microelectrodes. *Soil Science Society of America Journal* **66**, 1813-1820.

Vepraskas, M. J. and Wilding, L.P. (1983) Albic neoskeletans in argillic horizons as indices of seasonal saturation and iron reduction. *Soil Science Society of America Journal* **47**, 1202-1208.

Vereecken, H., Schnepf, A., Hopmans, J. W., Javaux, M., Or, D., Roose, T., Vanderborght, J., Young, M.H., Amelung, W., Aitkenhead, M., Allison, S.D., Assouline, S., Baveye, P., Berli, M., Brüggemann, N., Finke, P., Flury, M., Gaiser, T., Govers, G., Ghezzehei, T., Hallett, P., Hendricks Franssen, H.J., Heppell, Horn, R., Huisman, J.A., Jacques, D., Jonard, F., Kollet, S., Lafolie, F., Lamorski, K., Leitner, D., McBratney, A., Minasny, A., Minasny, B., Montzka, C., Nowak, W., Pachepsky, Y., Padarian, J., Romano, N., Roth, K., Rothfuss, Y., Rowe, E.C., Schwen, A., Šimůnek, J., Tiktat, A., Van Dam, J., van der Zee, S., Vogel, H.J., Vrugt, J.A., Wöhling, T. and Young, I.M. (2016) Modeling soil processes: review, key challenges, and new perspectives. *Vadose zone journal* **15**.

Verhoeven, E., Barthel, M., Yu, L., Celi, L., Said-Pullicino, D., Sleutel, S., Lewicka-Szczebak, D., Six, J. and Decock, C. (2019) Early season N_2O emissions under variable water management in rice systems: source-partitioning emissions using isotope ratios along a depth profile. *Biogeosciences* **16**, 383–408.

Vidon, P., Marchese, S., Welsh, M. and McMillan, S. (2016) Impact of precipitation intensity and riparian geomorphic characteristics on greenhouse gas emissions at the soil-atmosphere interface in a water-limited riparian zone. *Water, Air, and Soil Pollution* **227**.

Vorenhout, M., van der Geest, H. G., van Marum, D., Wattel, K. and Eijsackers, H.J. (2004) Automated and continuous redox potential measurements in soil. *Journal of environmental quality* **33**, 1562-1567.

Wagner, K. (2019) Impact assessment of land-use change and agricultural treatments on greenhouse gas emissions from wetlands of Uganda and Tanzania. Rheinische Friedrich-Wilhelms-Universit¨at Bonn. Doctoral dissertation.

Wang, J., Bogena, H.R., Vereecken, H. and Brüggemann, N. (2018) Characterizing redox potential effects on greenhouse gas emissions induced by water-level changes. *Vadose Zone Journal* **17**, 1-13.

Wang, J., Bogena, H.R., Vereecken, H. and Brüggemann, N. (2020) Stable-isotope-aided investigation of the effect of redox potential on nitrous oxide emissions as affected by water status and N fertilization. *Water* **12**, 2918.

Wang, Z., Zeng, D. and Patrick, W.H. (1996) Methane emissions from natural wetlands. *Environmental Monitoring and Assessment* **42**, 143-161.

Wang, Z.P., De Laune, R.D., Patrick, W.H. and Masscheleyn, P.H. (1993) Soil redox and pH effects on methane production in a flooded rice soil. *Soil Science Society of America Journal* **57**, 382-385.

Wanzek, T., Keiluweit, M., Baham, J., Dragila, M.I., Fendorf, S., Fiedler, S., Peter, S.N. and Kleber, M. (2018) Quantifying biogeochemical heterogeneity in soil systems. *Geoderma* **324**, 89-97.

Wei, J., Amelung, W., Lehndorff, E., Schloter, M., Vereecken, H. and Brüggemann, N. (2017) N_2O and NO_x emissions by reactions of nitrite with soil organic matter of a Norway spruce forest. *Biogeochemistry* **132**, 325-342.

Wei, J., Reichel, R., Islam, M.S., Wissel, H., Amelung, W. and Brüggemann, N. (2020) Chemical composition of high organic carbon soil amendments affects fertilizer-derived N_2O emission and nitrogen immobilization in an oxic sandy loam. *Frontiers in Environmental Science* **8**, 1-15.

Weigand, H., Mansfeldt, T., Baümler, R., Schneckenburger, D., Wessel-Bothe, S. and Marb, C (2010) Arsenic release and speciation in a degraded fen as affected by soil redox potential at varied moisture regime. *Geoderma* **159**, 371-378.

Weihermüller, L., Huisman, J., Graf, A., Herbst, M. and Sequaris, J.M. (2009) Multistep outflow experiments to determine soil physical and carbon dioxide production parameters. *Vadose Zone Journal* **8**, 772-782.

Weslien, P., Kasimir–Klemedtsson, Å., Börjesson, G. and Klemedtsson, L. (2009) Strong pH influence on N_2O and CH_4 fluxes from forested organic soils. *European Journal of Soil Science* **60**, 311–320.

Wiekenkamp, I., Huisman, J.A., Bogena, H.R., Graf, A., Lin, H.S., Drüe, C. and Vereecken, H. (2016) Changes in measured spatiotemporal patterns of hydrological response after partial deforestation in a headwater catchment. *Journal of hydrology* **542**, 648-661.

Włodarczyk, T., Stępniewski, W. and Brzezińska, M. (2002) Dehydrogenase activity, redox potential, and emissions of carbon dioxide and nitrous oxide from Cambisols under flooding conditions. *Biology and Fertility of Soils* **36**, 200-206.

Wolf, I. and Russow, R. (2000) Different pathways of formation of N_2O, N_2 and NO in black earth soil. *Soil Biology and Biochemistry* **32**, 229-239.

Wu, D., Senbayram, M., Well, R., Brüggemann, N., Pfeiffer, B., Loick, N., Stempfhuber., B., Dittert, K. and Bol, R. (2017) Nitrification inhibitors mitigate N_2O emissions more effectively under straw-induced conditions favoring denitrification. *Soil Biology and Biochemistry* **104**, 197-207.

Wu, X., Brüggemann, N., Gasche, R., Shen, Z., Wolf, B. and Butterbach-Bahl, K. (2010) Environmental controls over soil-atmosphere exchange of N_2O, NO, and CO_2 in a temperate Norway spruce forest. *Global Biogeochemical Cycles* **24**.

Xu, X., Han, L., Luo, X., Liu, Z. and Han, S. (2009) Effects of nitrogen addition on dissolved N_2O and CO_2, dissolved organic matter, and inorganic nitrogen in soil solution under a temperate old-growth forest. *Geoderma* **151**, 370-377.

Yaduvanshi, N., Setter, T.L., Sharma, S.K., Singh, K.N. and Kulshreshtha, N. (2010) Waterlogging effects on wheat yield, redox potantial, manganese and iron in different soils of India. In *19th World Congress of Soil Science*, Soil Solutions for a Changing World, 1-6 August 2010 Brisbane, Australia, pp. 45-48.

Yagi, K., Minami, K. and Ogawa, Y. (1998) Effects of water percolation on methane emission from rice paddies: a lysimeter experiment. *Plant and Soil* **198**, 193-200.

Yang, J., Hu, Y. and Bu, R. (2006) Microscale spatial variability of redox potential in surface soil. *Soil science* **171**, 747-753.

Ye, R. and Horwath, W.R. (2016) Nitrous oxide uptake in rewetted wetlands with contrasting soil organic carbon contents. *Soil Biology and Biochemistry* **100**, 110-117,

Yu, K. and Patrick, W.H. (2003) Redox range with minimum nitrous oxide and methane production in a rice soil under different pH. *Soil Science Society of America Journal* **67**, 1952-1958.

Yu, K. and Rinklebe, J. (2013) Soil redox potential and pH controllers. In *Methods in Biogeochemistry of Wetlands (methodsinbiogeo)*, Soil Science of America: USA, pp. 107-116.

Yu, K., Chen, G. and Patrick Jr, W.H. (2004) Reduction of global warming potential contribution from a rice field by irrigation, organic matter, and fertilizer management. *Global Biogeochemical Cycles* **18**.

Yu, K., Faulkner, S.P. and Baldwin, M.J. (2008) Effect of hydrological conditions on nitrous oxide, methane, and carbon dioxide dynamics in a bottomland hardwood forest and its implication for soil carbon sequestration. *Global Change Biology* **14**, 798-812.

Yu, K., Faulkner, S.P. and Patrick Jr, W.H. (2006) Redox potential characterization and soil greenhouse gas concentration across a hydrological gradient in a Gulf coast forest. *Chemosphere* **62**, 905-914.

Yu, K., Böhme, F., Rinklebe, J., Neue, H.U. and De Laune, R.D. (2007) Major biogeochemical processes in soils: A microcosm incubation from reducing to oxidizing conditions. *Soil Science Society of America Journal* **71**, 1406-1417.

Yu, K., Wang, Z., Vermoesen, A., Patrick, W.H. Jr and Van Cleemput, O. (2001) Nitrous oxide and methane emissions from different soil suspensions: Effect of soil redox status. *Biology and Fertility of Soils* **34**, 25-30.

Zou, Y., Hirono, Y., Yanai, Y., Hattori, S., Toyoda, S. and Yoshida, N. (2014) Isotopomer analysis of nitrous oxide accumulated in soil cultivated with tea (*Camellia sinensis*) in Shizuoka, central Japan. *Soil Biology and Biochemistry* **77**, 276-291.

Supplementary material

Table S1: Correlation values (Pearson's r) of the different variables and GHG fluxes , based on the daily Riparian site.

	CO_2	N_2O	CH_4	Eh 10	Eh 30	Eh 50	Air T.	Soil T. 10	Soil T. 30	Soil T. 50	SWC 10	SWC 30	SWC 50	SMP 10	SMP 20	SMP 50	WFPS 10	WFPS 30	WFPS 50	W. Table
CO_2	1	-0.08	0.08	0.22*	0.21*	0.20	-0.10	0.93**	0.90**	0.86**	-0.62**	-0.59**	-0.41**	-0.6**	-0.58**	-0.44**	0.48**	0.468**	0.254**	0.61**
N_2O		1	-0.17	-0.05	0.05	-0.09	0.00	-0.10	-0.10	-0.11	0.18	0.20	0.17	0.17	0.20	0.19	-0.13	-0.13	-0.14	-0.22*
CH_4			1	-0.21	-0.36*	-0.17	0.12	0.11	0.04	0.01	0.13	0.13	0.18	0.13	0.15	0.15	-0.17	-0.12	-0.21	-0.04
Eh 10				1	0.86**	0.62**	-0.70**	0.28**	0.43**	0.50**	-0.64**	-0.66**	-0.78**	-0.62**	-0.64**	-0.75**	0.36**	0.31**	0.25**	0.71**
Eh 30					1	0.77**	-0.58**	0.38**	0.50**	0.55**	-0.78**	-0.72**	-0.82**	-0.77**	-0.69**	-0.82**	0.50**	0.45**	0.36**	0.74**
Eh 50						1	-0.28**	0.36**	0.43**	0.45**	-0.8**	-0.68**	-0.71**	-0.79**	-0.58**	-0.82**	0.55**	0.52**	0.39**	0.70**
Air T.							1	-0.12	-0.27**	-0.35**	0.35**	0.33**	0.48**	0.34**	0.33**	0.43**	-0.12	-0.10	-0.09	-0.38**
Soil T. 10								1	0.97**	0.94**	-0.71**	-0.72**	-0.58**	-0.70**	-0.72**	-0.58**	0.52**	0.48**	0.34**	0.70**
Soil T. 30									1	0.99**	-0.78**	-0.79**	-0.68**	-0.77**	-0.79**	-0.66**	0.52**	0.47**	0.34**	0.78**
Soil T. 50										1	-0.78**	-0.81**	-0.72**	-0.77**	-0.81**	-0.69**	0.49**	0.43**	0.31**	0.80**
SWC 10											1	0.93**	0.91**	1.00**	0.89**	0.93**	-0.77**	-0.72**	-0.55**	-0.91**
SWC 30												1	0.94**	0.93**	0.99**	0.93**	-0.72**	-0.66**	-0.53**	-0.93**
SWC 50													1	0.91**	0.93**	0.97**	-0.71**	-0.65**	-0.54**	-0.92**
SMP 10														1	0.89**	0.93**	-0.76**	-0.71**	-0.54**	-0.91**
SMP 20															1	0.89**	-0.70**	-0.64**	-0.52**	-0.92**
SMP 50																1	-0.71**	-0.66**	-0.53**	-0.91**
WFPS 10																	1	0.99**	0.92**	0.61**
WFPS 30																		1	0.94**	0.54**
WFPS 50																			1	0.40**
W. Table																				1

Note: ** indicates signicant effects at $p < 0.001$, * at $p < 0.01$

Table S2: Stepwise regression output for different datasets with three GHGs

Data sets	$T_{10\ cm}$	$T_{30\ cm}$	$T_{50\ cm}$	T_{Air}	$WFPS_{10\ cm}$	$WFPS_{30\ cm}$	$WFPS_{50\ cm}$	W. table	$SMP_{10\ cm}$	$SMP_{30\ cm}$	$SMP_{50\ cm}$	$Eh_{10\ cm}$	$Eh_{30\ cm}$	$Eh_{50\ cm}$	Intercept	R^2
Model for soil CO_2																
Daily means	10.76	-3.97				1.06		0.73							-103.4	0.88
All stations	9	-3.6		1.40	0.64	-0.75	-0.64	0.3	-0.67		2.01		0.02	-0.02	75.2	0.66
Station 1		4.09		1.50	1.43		-1.28				0.31		-0.2	-0.16	245.6	0.87
Station 2	13.71				1.68			0.96		-0.31		0.16			-269.5	0.85
Station 3	9.41	-6.3		0.69	-3.78	2.98							-0.04		87.8	0.86
Station 4	11.89			1.1		16.55	-3.7	0.51						-0.23	-1189.1	0.83
Station 5	7.19						-0.45								37.36	0.86
Model for soil N_2O																
Station 2				0.56	1.23	-0.48								0.02	-61.21	0.28
Station 3			-6.98										-0.03	0.12	31.2	0.51
Model for soil CH_4																
Station 4					-0.27	-3.21			1.41	-4.39			-0.07	-0.09	333.99	0.45
Station 5	0.94					0.20						0.06	-0.03	-0.06	-42.59	0.33

Note: ** indicates signicant effects at $p < 0.001$, * at $p < 0.01$, - indicates non-available predictors for the specific dataset. For N_2O fluxes at Riparian Site only the Period Nov. 2018 to May 2019 was analysed. Hillslope Site based on daily data scale and Riparian Site based on sub-daily scale unless otherwise noted.

Table S3: Correlation values (Pearson's r) for different datasets with CO_2.

	Data sets	$T_{10\,cm}$	$T_{30\,cm}$	$T_{50\,cm}$	T_{Air}	$WFPS_{10\,cm}$	$WFPS_{30\,cm}$	$WFPS_{50\,cm}$	W. table	$SMP_{10\,cm}$	$SMP_{30\,cm}$	$SMP_{50\,cm}$	$Eh_{10\,cm}$	$Eh_{30\,cm}$	$Eh_{50\,cm}$
							Model for soil CO_2								
	Daily means	0.93**	0.90**	0.86**	0.85**	-0.62**	-0.60**	-0.42**	0.68**	0.48**	0.47**	0.25**	0.22*	0.21*	0.20
	All Stations	0.75**	0.71**	0.69**	0.70**	-0.19**	-0.38**	-0.28**	0.30**	0.12**	0.09	0.15**	0.08	0.07	0.00
	Station 1	0.78**	0.78**	0.76**	0.76**	-0.60**	-0.61**	-0.60**	0.43**	0.49**	0.48**	0.37**	0.07	0.15	0.37**
CO_2	Station 2	0.91**	0.86**	0.80**	0.83**	-0.48**	-0.52**	-0.22**	0.62**	0.14	0.13	0.08	0.21	0.38**	-0.31**
	Station 3	0.87**	0.77**	0.73**	0.81**	-0.15	0.10	-0.06	0.27**	0.14	0.06	-	0.15	-0.31**	-0.17
	Station 4	0.91**	0.88**	0.84**	0.82**	-0.50**	-0.21**	0.52**	0.39**	0.15	0.133	-	0.03	0.49**	0.53**
	Station 5	0.92**	0.90**	0.89**	0.81**	-0.40**	-0.43**	-0.37**	0.67**	0.36	0.18	0.07	-0.09	0.11	-0.31**

Note: ** indicates signicant effects at $p < 0.001$, * at $p < 0.01$

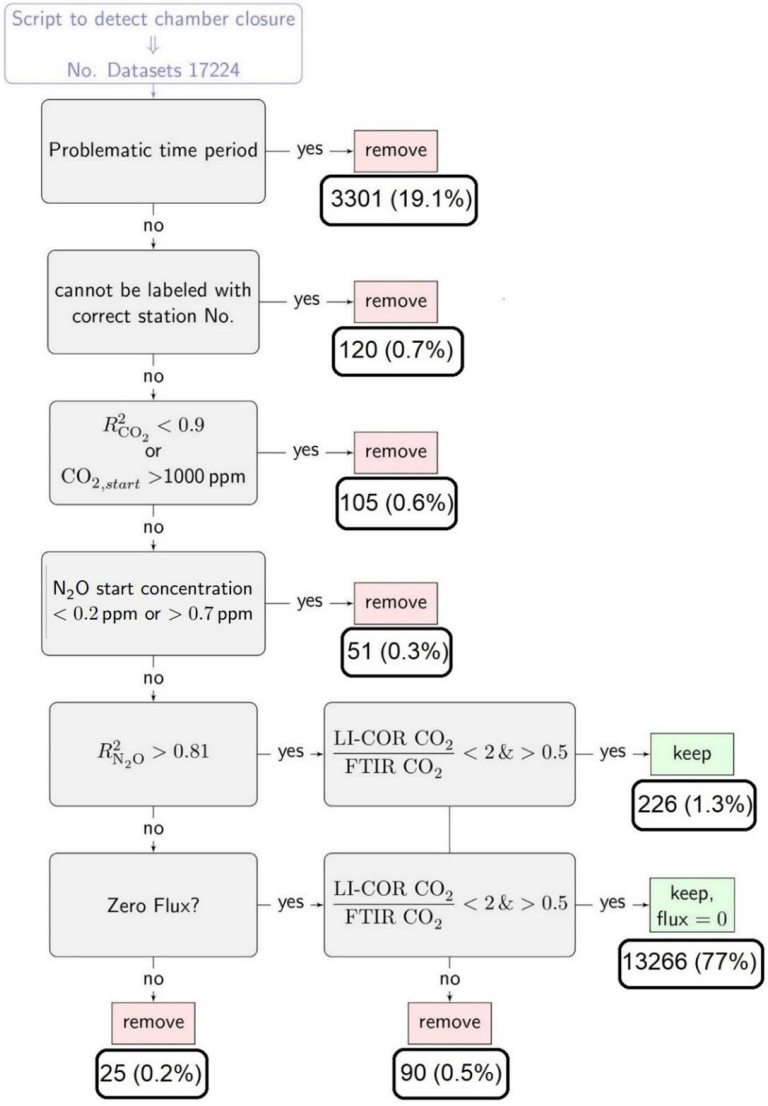

Figure S1. N_2O data quality management system. In the blue boxes the corresponding number of datasets is shown, and datasets of five stations were included.

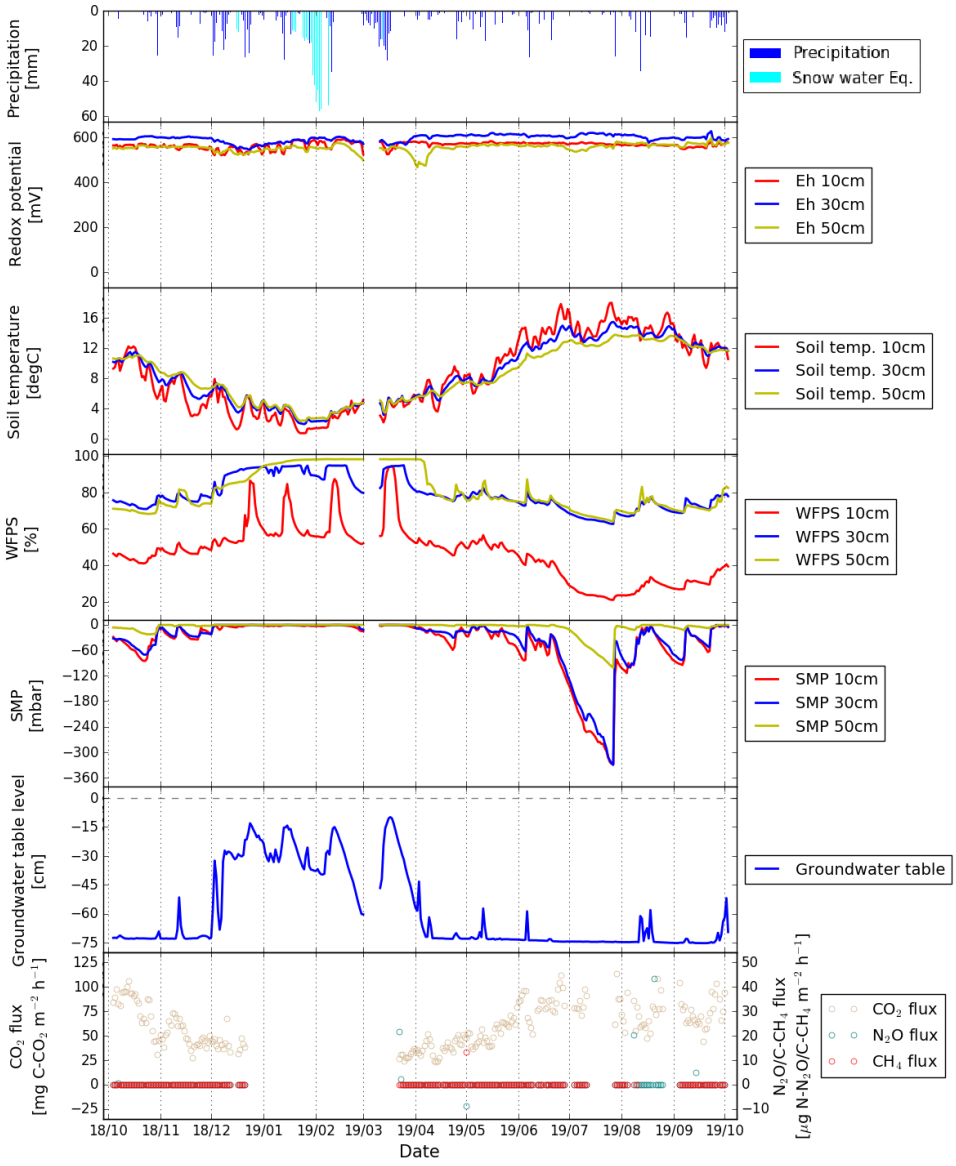

Figure S2. Time series of daily sums of precipitation, snow cover, and daily means of Eh, soil temperature, WFPS, SMP, groundwater table depth and GHG fluxes at Station 1.

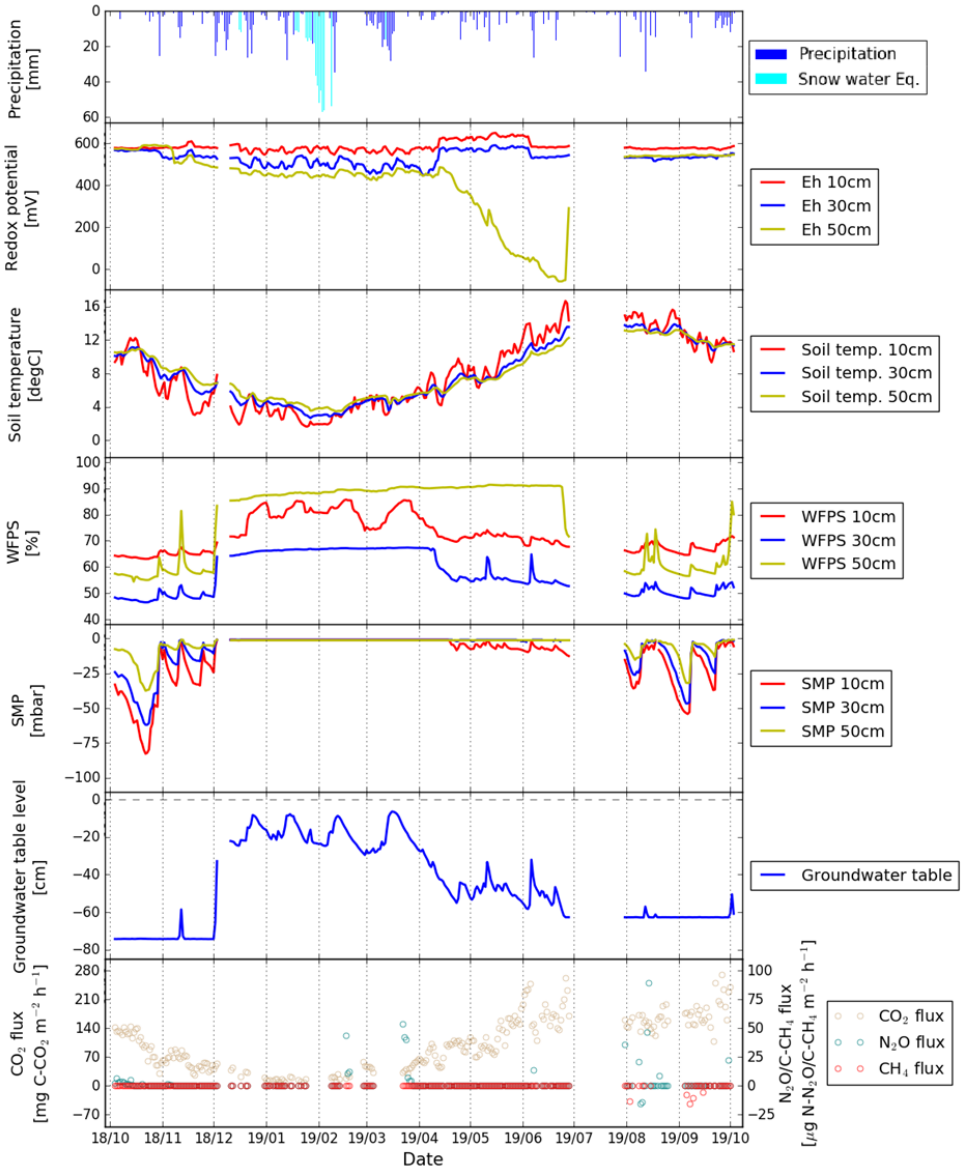

Figure S3. Time series of daily sums of precipitation, snow cover, and daily means of Eh, soil temperature, WFPS (water filled pore space), SMP (soil matrix potential), groundwater table depth and GHG fluxes at Station 2.

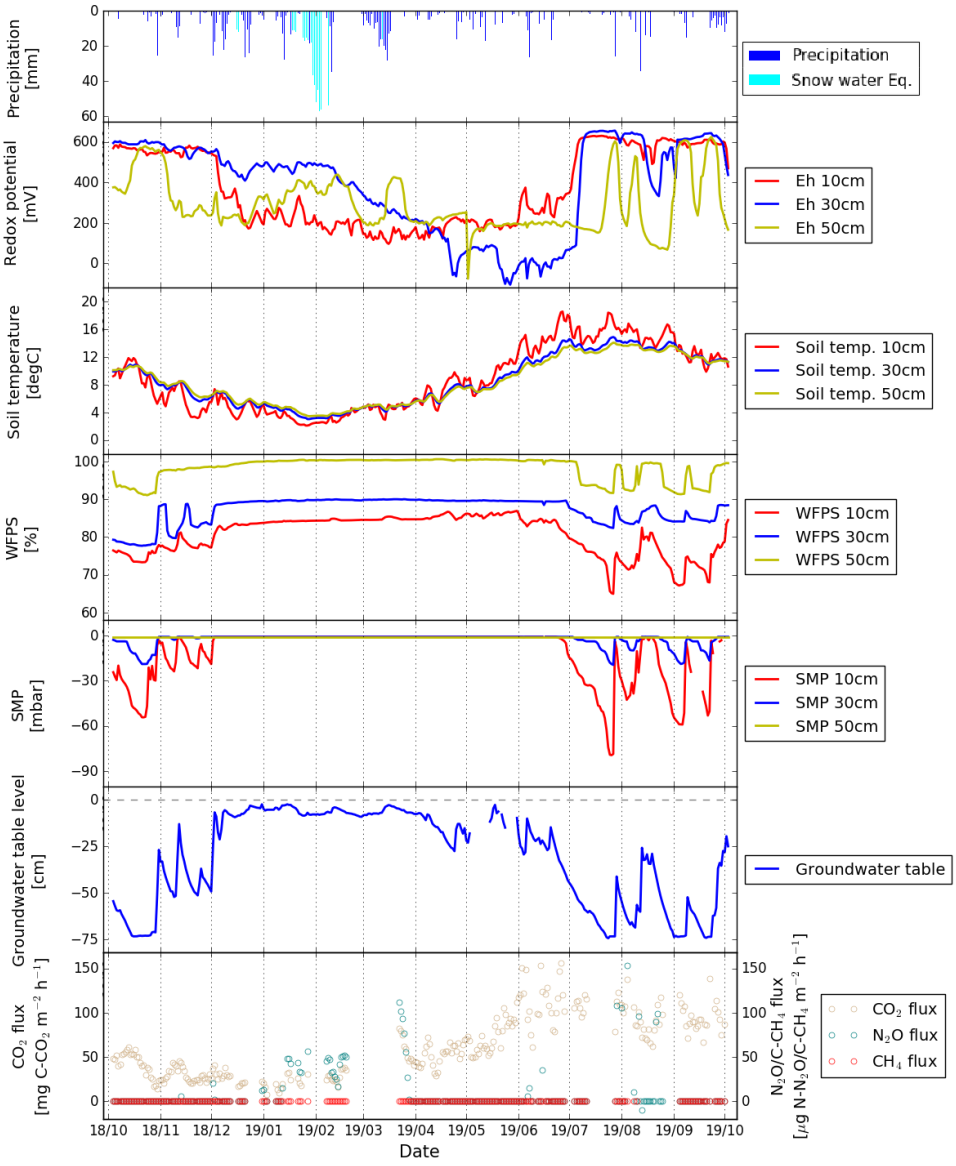

Figure S4. Time series of daily sums of precipitation, snow cover, and daily means of Eh, soil temperature, WFPS, SMP, groundwater table depth and GHG fluxes at Station 3.

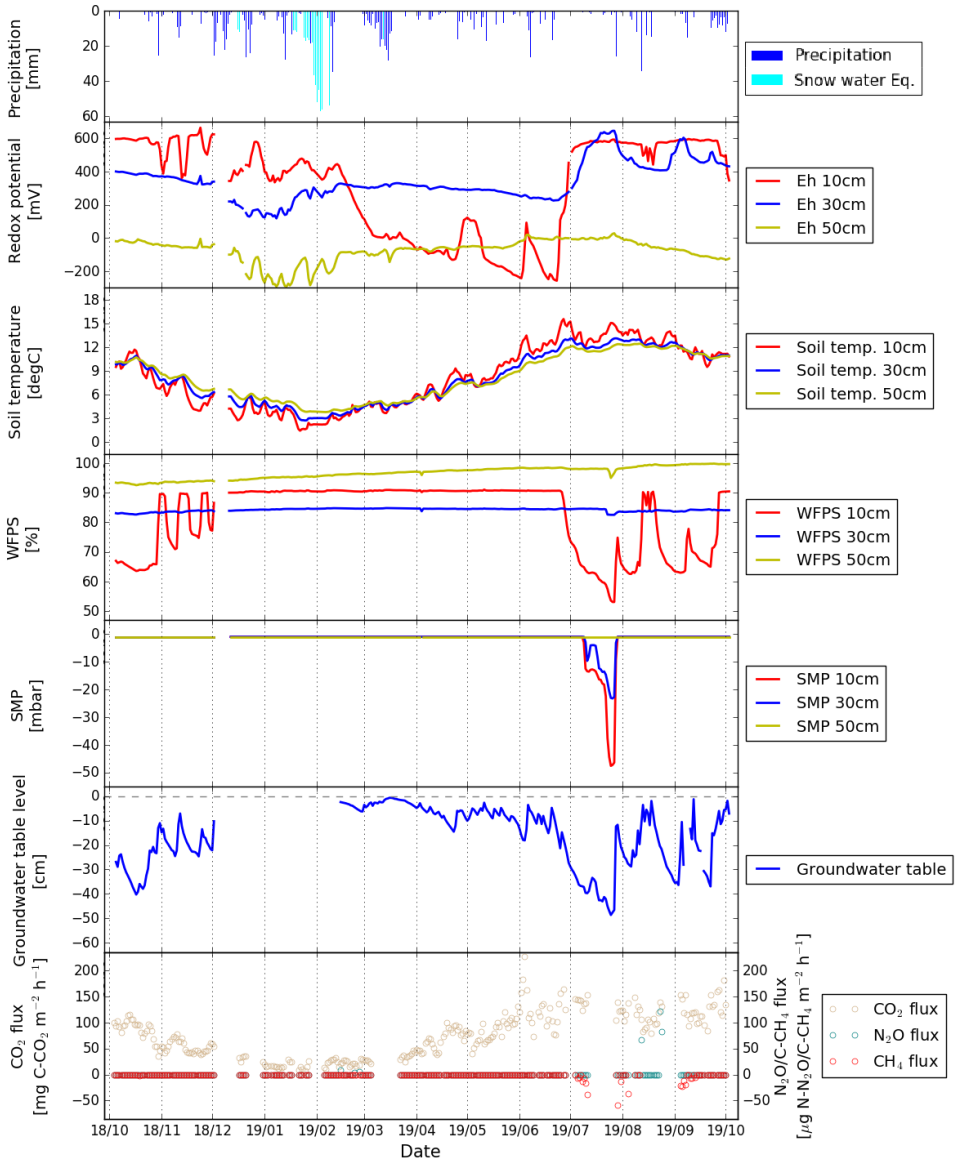

Figure S5. Time series of daily sums of precipitation, snow cover, and daily means of Eh, soil temperature, WFPS, SMP, groundwater table depth and GHG fluxes at Station 4.

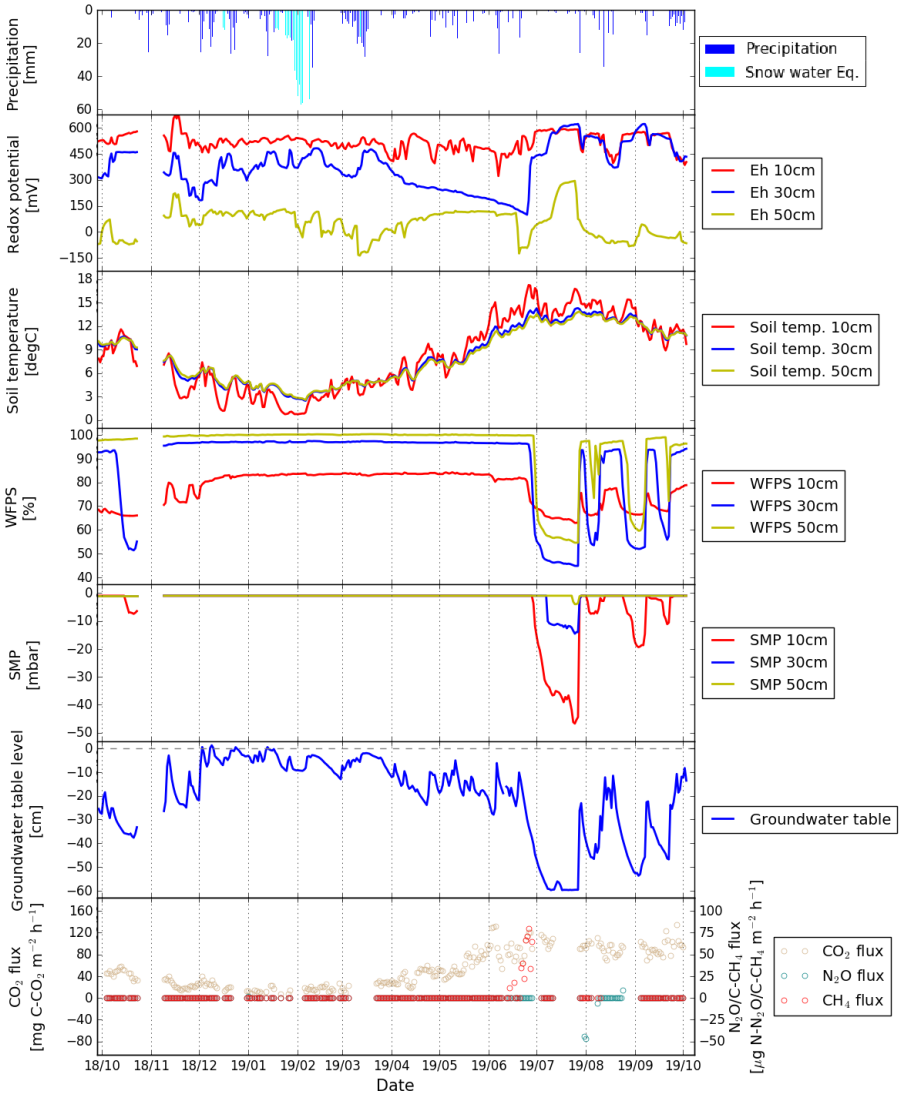

Figure S6. Time series of daily sums of precipitation, snow cover, and daily means of Eh, soil temperature, WFPS, SMP, groundwater table depth and GHG fluxes at Station 5.

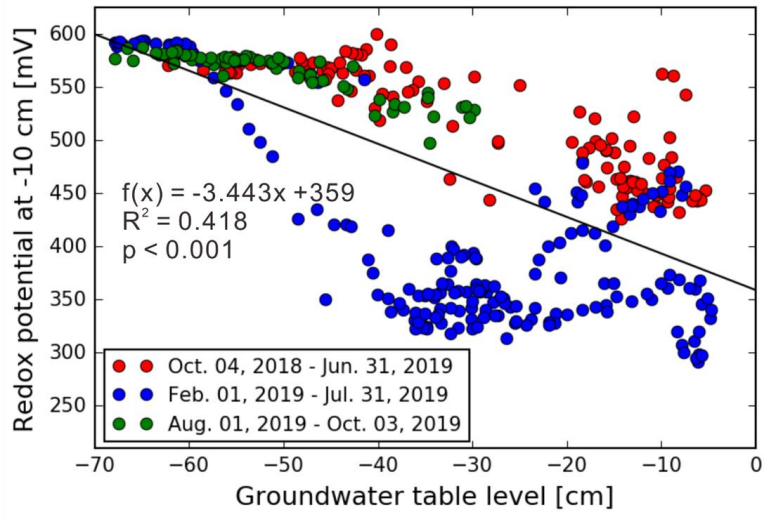

Figure S7. Redox potential at -10 cm with groundwater table level.

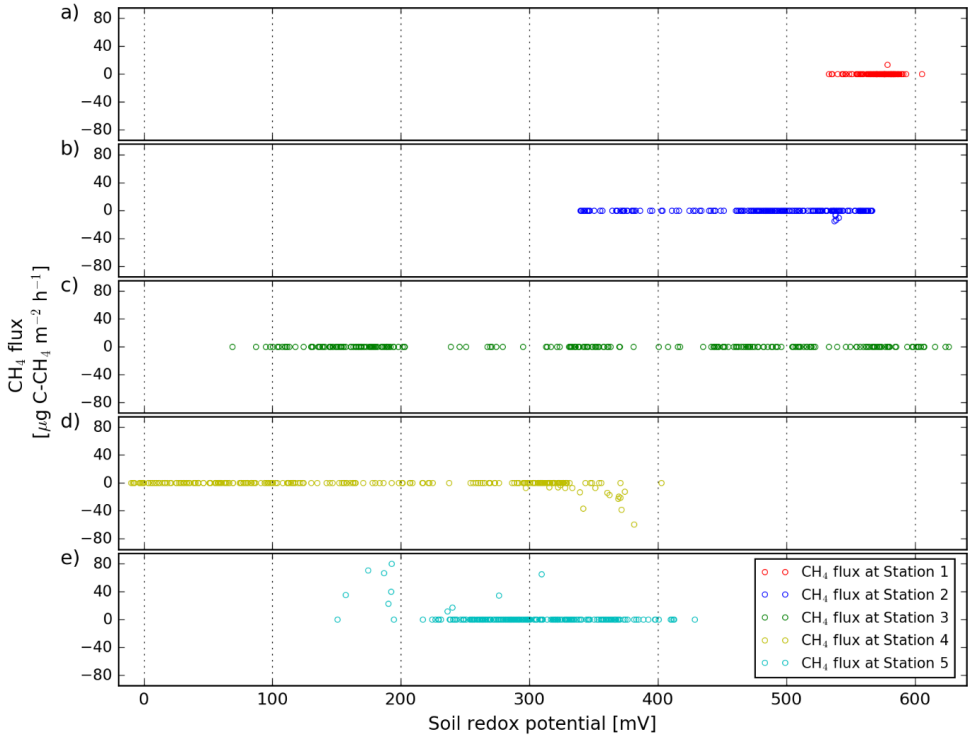

Figure S8. Mean redox potential versus CH_4 fluxes.

Band / Volume 540
Cyclotron Irradiation on Tungsten & Co-relation of Thermo-Mechanical Properties to Displacement and Transmutation Damage
R. Rayaprolu (2021), xiv, 211 pp
ISBN: 978-3-95806-552-9

Band / Volume 541
Smart Energy in Haushalten: Technologien, Geschäftsmodelle, Akzeptanz und Wirtschaftlichkeit
H. Shamon, T. Rehm, B. Helgeson, F. Große-Kreul, M. Gleue, U. Paukstadt, G. Aniello, T. Schneiders, C. Frings, A. Reichmann, A. Löschel, T. Gollhardt, W. Kuckshinrichs, K. Gruber, P. Overath, C. Baedeker, F. Chasin, K. Witte, J. Becker
(2021), VI, 142 pp
ISBN: 978-3-95806-554-3

Band / Volume 542
Deployment Status of Fuel Cells in Road Transport: 2021 Update
R. C. Samsun, L. Antoni, M. Rex, D. Stolten (2021), 37 pp
ISBN: 978-3-95806-556-7

Band / Volume 543
Processing and creep resistance of short SiC fiber containing Ti_3SiC_2 MAX phase composites
A. Dash (2021), vii, 125 pp
ISBN: 978-3-95806-558-1

Band / Volume 544
Synthese und Charakterisierung von Geopolymeren für die Entsorgung der Spaltprodukte ^{137}Cs und ^{90}Sr
S. K. Weigelt (2021), VI, 186 pp
ISBN: 978-3-95806-559-8

Band / Volume 545
Potential depletion of ozone in the mid-latitude lowermost stratosphere in summer under geoengineering conditions
S. Robrecht (2021), 185 pp
ISBN: 978-3-95806-563-5

Band / Volume 546
Two-phase Flow in Porous Transport Layers of Polymer Electrolyte Membrane Electrolysers
D. Borah (2021), xi, 196 pp
ISBN: 978-3-95806-564-2

Band / Volume 547
Effects of root temperature on food quality of horticultural crops
F. He (2021), V, 143 pp
ISBN: 978-3-95806-565-9

Band / Volume 548
Verhalten und Kontrolle von Schlacken des bioliq®-Vergasers
K. Mielke (2021), 162, XXXV pp
ISBN: 978-3-95806-566-6

Band / Volume 549
Gravity waves resolved in Numerical Weather Prediction products
C. Strube (2021), iii, 139 pp
ISBN: 978-3-95806-567-3

Band / Volume 550
Experimental study of the chemical degradation of biogenic volatile organic compounds by atmospheric OH radicals
M. Rolletter (2021), XIII, 199 pp
ISBN: 978-3-95806-568-0

Band / Volume 551
Infiltrated Positive Electrodes for All-Solid-State Sodium Batteries
T. Lan (2021), vi, 104 pp
ISBN: 978-3-95806-576-5

Band / Volume 552
Trajectory Analysis on the Asian Tropopause Aerosol Layer (ATAL) based on Balloon Measurements at the Foothills of the Himalayas
S. Hanumanthu (2021), xiv, 147 pp
ISBN: 978-3-95806-578-9

Band / Volume 553
Field assisted sintering of yttria ceramics for plasma etching applications
M. Kindelmann (2021), VI, 122, XXX pp
ISBN: 978-3-95806-579-6

Band / Volume 554
Characterisation of the effect of redox potential on the emission of greenhouse gases using wireless sensing techniques
J. Wang (2021), XIV, 104 pp
ISBN: 978-3-95806-581-9

Weitere ***Schriften des Verlags im Forschungszentrum Jülich*** unter
http://wwwzb1.fz-juelich.de/verlagextern1/index.asp

Energie & Umwelt / Energy & Environment
Band / Volume 554
ISBN 978-3-95806-581-9

Mitglied der Helmholtz-Gemeinschaft

JÜLICH
Forschungszentrum